PART I

LATENT HEAT OF VAPORIZATION OF N-DECANE

PART II

HEAT AND MASS TRANSFER FROM A CYLINDER PLACED IN A TURBULENT AIR STREAM - SHERWOOD AND FRÖSSLING NUMBERS AS A FUNCTION OF FREE STREAM TURBULENCE LEVEL AND REYNOLDS NUMBER

Thesis by

Harold Thompson Couch

In Partial Fulfillment of the Requirements

For the Degree of

Doctor of Philosophy

California Institute of Technology

Pasadena, California

1966

(Submitted April 19, 1966)

ACKNOWLEDGMENTS

The author wishes to express his gratitude to Professor B. H. Sage, under whose guidance this research was conducted, for his most helpful advice and counsel.

The author also wishes to express his appreciation for the encouragement and assistance given him by others in his research, and in the preparation of this manuscript.

Dr. William Kozicki assisted with the latent heat of vaporization measurements presented as Part I of this thesis. Henry E. Smith and H. Hollis Reamer cooperated in the experimentation leading to Part II of this thesis, and their care and continued interest has been greatly appreciated.

The cylinder used for the measurements considered in Part II was extremely successful, a tribute to the careful work and sound advice of William DeWitt and George Griffiths in the Instrument Machine Shop.

The assistance of Virginia Berry with the calculations, June Gray with the illustrations, and Alrae Tingley with the typing was gratefully received, and is hereby acknowledged. The faculty, staff, and fellow graduate students also willingly rendered assistance and helpful advice wherever possible.

Finally this work would not have been accomplished without the financial support rendered by the Standard Oil Company of California and the Peter E. Flour Foundation. The author acknowledges receipt of their fellowships and is most grateful for this necessary support.

ABSTRACT

Part I

The latent heat of vaporization of n-decane is measured calorimetrically at temperatures between 160° and 340°F. The internal energy change upon vaporization, and the specific volume of the vapor at its dew point are calculated from these data and are included in this work. The measurements are in excellent agreement with available data at 77° and also at 345°F, and are presented in graphical and tabular form.

Part II

Simultaneous material and energy transport from a one-inch adiabatic porous cylinder is studied as a function of free stream Reynolds Number and turbulence level. Experimental data is presented for Reynolds Numbers between 1600 and 15,000 based on the cylinder diameter, and for apparent turbulence levels between 1.3 and 25.0 per cent. n-heptane and n-octane are the evaporating fluids used in this investigation.

Gross Sherwood Numbers are calculated from the data and are in substantial agreement with existing correlations of the results of other workers. The Sherwood Numbers, characterizing mass transfer rates, increase approximately as the 0.55 power of the Reynolds Number. At a free stream Reynolds Number of 3700 the Sherwood Number showed a 40% increase as the apparent turbulence level of the free stream was raised from 1.3 to 25 per cent.

Within the uncertainties involved in the diffusion coefficients used for n-heptane and n-octane, the Sherwood Numbers are comparable for both materials. A dimensionless Frössling Number is computed which characterizes either heat or mass transfer rates for cylinders on a comparable basis. The calculated Frössling Numbers based on mass transfer measurements are in substantial agreement with Frössling Numbers calculated from the data of other workers in heat transfer.

TABLE OF CONTENTS

LIST OF FIGURES

LIST OF TABLES

Part I

LATENT HEAT OF VAPORIZATION OF n-DECANE[1]

[1] H. T. Couch, William Kozicki, and B. H. Sage, "Latent Heat of Vaporization at n-Decane," Journal of Chemical and Engineering Data, Vol. 8, No. 3, pp. 346-49, (1963).

Permission has been granted by the American Chemical Society to present this published article as Part I of the author's Ph.D. Thesis.

I. INTRODUCTION

Direct calorimetric measurements of the latent heat of vaporization of n-decane over a range of temperatures do not appear to be available. The volumetric behavior of the liquid phase of n-decane has been studied by Reamer and others (5). Likewise, the vapor pressure has been determined over a wide range of temperatures by Young (9), Reamer (5), and Willingham and co-workers (8). The volumetric data extend from a temperature of 40° to 460° F. and the vapor pressures cover a similar range of temperatures. Rossini (6) has also recorded several critically chosen values of the properties of n-decane at 77° F. As a result of the absence of directly measured values of the latent heat of vaporization of this paraffin hydrocarbon over a wide range of temperatures, the current investigation was initiated. This study involves measurements of the latent heat of vaporization of n-decane at temperatures between 160° and 340° F.

Page 3 is missing.

the essentially adiabatic jacket have been described (2). In the current measurements, the maximum deviations from ideal isobaric, isothermal conditions did not introduce corrections to the measured enthalpy change upon vaporization of more than 0.0054 fraction of the total change. The estimated uncertainty in each of the several variables associated with these measurements is set forth in Table I. These values are expressed in terms of the fraction of the measured enthalpy change upon vaporization of n-decane at a temperature of 340° F. Inspection of Equation 1 indicates that the volumetric correction factor, $(V_g - V_\ell)/V_g$, is necessary in order to relate the quantity of n-decane evaporated to that withdrawn. Experimental information concerning the volumetric behavior of the dew-point gas of n-decane is not available.

A combination of the Clapeyron equation with Equation 1 results in the following expression for the latent heat of vaporization of n-decane:

$$\ell = (H_g - H_\ell)_T = [Q]_{T,P} - V_\ell T(dP''/dT) \qquad (2)$$

It should be recognized that the quantity $[Q]_{T,P}$ in Equation (2) represents the thermal transfer required per unit weight of material withdrawn from the isochoric calorimeter under idealized conditions. It is necessary to apply the minor corrections that have been described (2) to account for the superheat of the liquid and the deviation from isobaric, isothermal conditions. As a result of the absence of volumetric data, the specific volume of the dew-point gas was

evaluated from

$$V_g = \left(\frac{\bar{\Omega}^*_{1,2}}{m_1 - m_2}\right)\left(\frac{1}{T(dP''/dT)}\right) \qquad (3)$$

III. MATERIALS

The n-decane employed was obtained as research grade from the Phillips Petroleum Company and was reported to contain not more than 0.0066 mole fraction of impurities. The specific weight of the material was 45.339 pounds per cubic foot at 77° F. as compared to 45.337 pounds per cubic foot reported by Rossini (6) for an air-saturated sample at the same temperature. The index of refraction relative to the D-lines of sodium at 77° F. was found to be 1.4097 as compared to a value of 1.40967 reported for an air-saturated sample at the same temperature (6). Review of these data leads the authors to believe that the sample of n-decane did not contain more than 0.0066 mole fraction of material other than n-decane. The probable impurities are the isomers of this hydrocarbon. The presence of small quantities of material other than n-decane does not influence the values of the latent heat of vaporization to the extent that such impurities might affect measurements of other properties such as vapor pressure.

IV. EXPERIMENTAL RESULTS

The experimental results of the measurements upon n-decane are reported in Table II. Values of the slope of the vapor pressure curve were obtained from the measurements of Reamer (5) and Willingham (8) by the use of residual methods. It should be recognized that a 2% uncertainty in the value of the slope of the vapor pressure curve does not introduce more than 0.00013 fraction uncertainty in the measured enthalpy change upon vaporization. The residual specific volume at dew point was calculated utilizing a molecular weight of n-decane of 142.276 and a value of the universal gas constant of $R = 10.73147$ (psi)(cu ft)/(lb-mol)(^{o}R).

Values of the volumetric correction factor used in the reduction of the calorimetric measurements have been included in Table II. The slight deviation of this factor from unity serves to illustrate the small effect of uncertainties in the slope of the vapor pressure curve upon the reported values of the latent heat of vaporization. The latent heats of vaporization recorded in Table II are depicted graphically in Figure 1. Values reported by Rossini (6) at 77^{o} and 345^{o} F. have been included for comparison.

In order to permit a more meaningful comparison of the precision of the experimental data and the agreement with the values recorded by Rossini (6), residual techniques have been employed. For present purposes the residual latent heat of vaporization of n-decane was established from

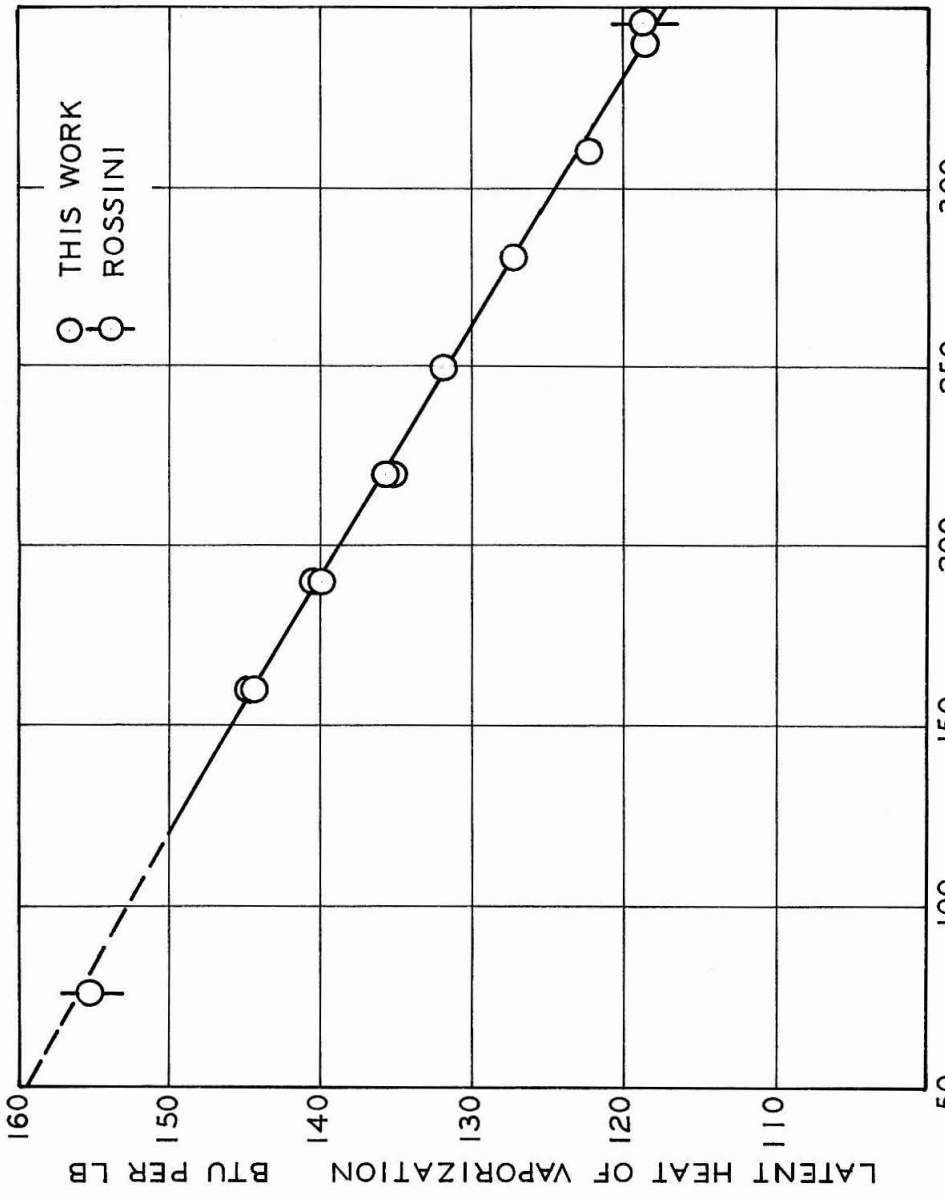

Fig. 1 Effect of Temperature on Latent Heat of Vaporization for n-Decane

$$\underset{\sim}{\ell} = \ell - (166.667 - 0.166667\,t) \qquad (4)$$

There is shown in Figure 2 values of the residual latent heat of vaporization of n-decane along with the values reported by Rossini (6). The standard error of estimate of the current latent heat of vaporization measurements from the smooth curves shown in Figures 1 and 2 is 0.03 Btu per pound.

Table III records the smooth values of the latent heat of vaporization as a function of temperature. The internal energy change upon vaporization and the specific volume at dew point are recorded in a part of Table III.

Values of the compressibility factor for the dew-point gas as a function of vapor pressure are shown in Figure 3. It is apparent that even at a vapor pressure of 13 p.s.i.a., corresponding to a temperature of 340° F., the dew-point gas of n-decane deviates only approximately 6.3% from the behavior of a perfect gas. At 160° F. additional uncertainty exists in evaluation of the slope of the vapor pressure-temperature relation. The standard error of estimate of the experimental values of the specific volume of the dew-point gas reported in Table II from the smooth curves drawn in Figure 3 is 0.27 cubic foot per pound, or 0.0025 when expressed in terms of the compressibility factor. This standard error corresponds to an uncertainty of approximately 0.26%.

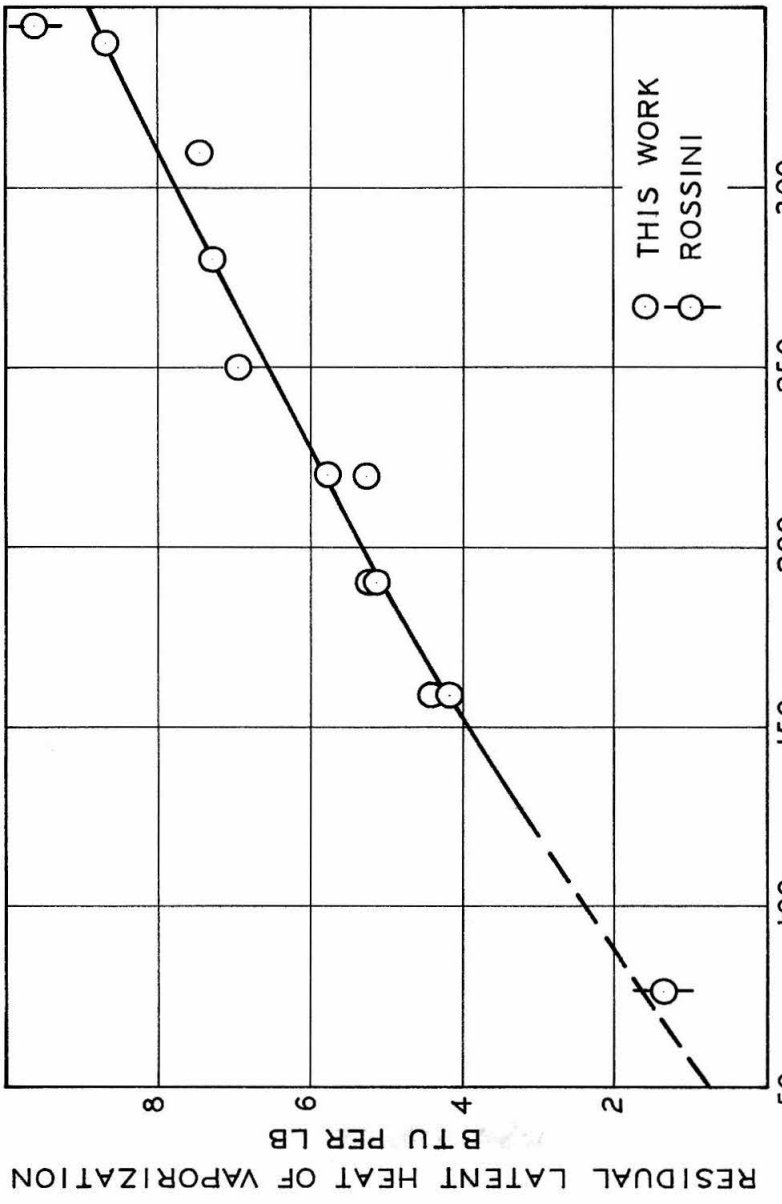

Fig. 2 Residual Latent Heat of Vaporization for n-Decane

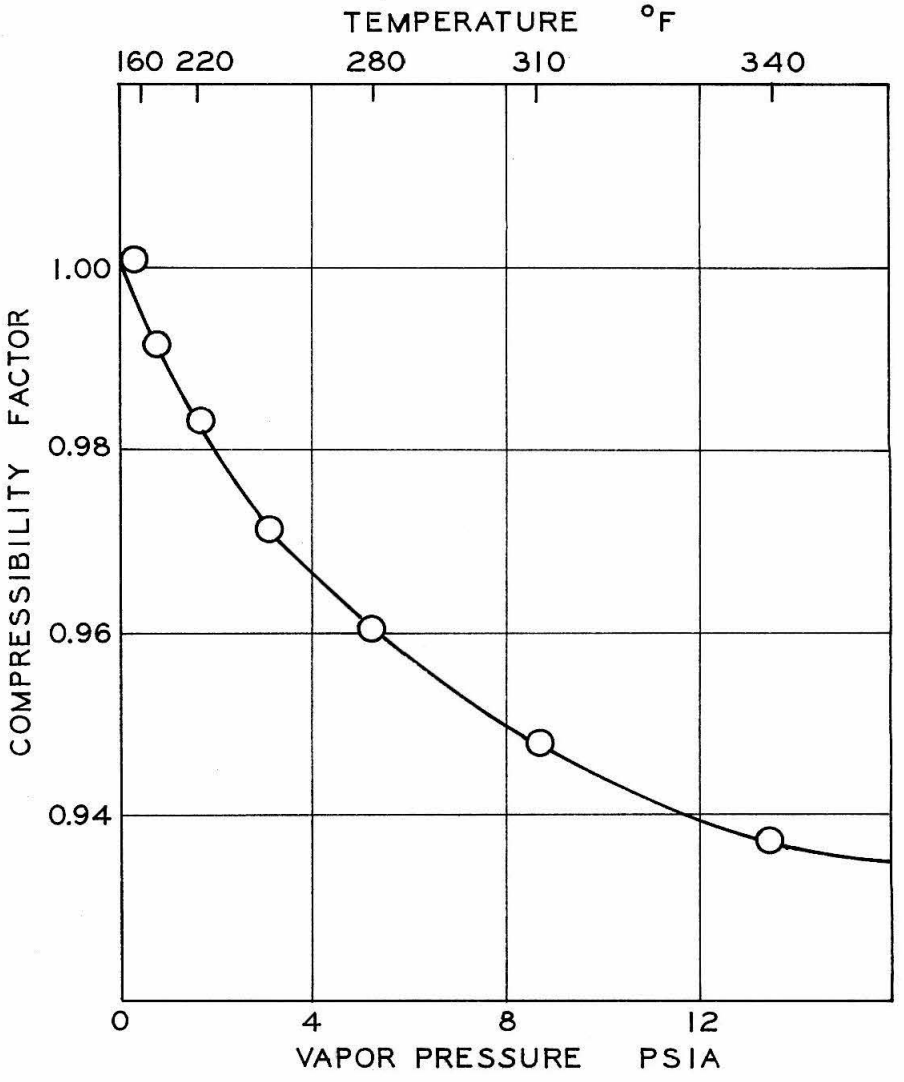

Fig. 3 Compressibility Factor for the Dew-Point Gas

REFERENCES

1. McKay, R. A., and Sage, B. H., Latent Heat of Vaporization for n-Octane, Am. Doc. Inst., Washington, D. C., Doc. No. 6072 (1959).

2. McKay, R. A. and Sage, B. H., "Latent Heat of Vaporization for n-Octane," J. Chem. Eng. Data, Vol. 5, pp. 21-24 (1960).

3. Osborne, N. S., Stimson, H. F., and Fiock, E. F., "A Calorimetric Determination of Thermal Properties of Saturated Water and Steam from 0° to 270 °C," Bur. Standards J. Research, Vol. 5, pp. 411-480 (1930).

4. Osborne, H. S., Stimson, H. F., and Ginnings, D. C., "Measurements of Heat Capacities and Heat of Vaporization of Water in the Range 0° to 100°C," J. Research Natl. Bur. Standards, Vol. 23, pp. 197-260 (1939).

5. Reamer, H. H., Olds, R. H., Sage, B. H., and Lacey, W. N., "Phase Equilibrium in Hydrocarbon Systems: Methane-Decane System," Ind. Eng. Chem., Vol. 34, pp. 1526-1531, (1942).

6. Rossini, F. D., et al., editors, Selected Values of Physical and Thermodynamic Properties of Hydrocarbons and Related Compounds, Carnegie Press, Pittsburgh, Pa., 1953.

7. Sage, B. H., and Hough, E. W., "Calorimeter for Some Corrosive Liquids," Anal. Chem., Vol. 22, pp. 1304-1309 (1950).

8. Willingham, C. B., Taylor, W. J., Pignocco, J., and Rossini, F. D., "Vapor Pressures and Boiling Points of Some Paraffin, Alkylcyclopentane, Alkylcyclohexane, and Alkylcyclobenzine Hydrocarbons," J. Research Natl. Bur. Standards, Vol. 35, p. 219 (1945).

9. Young, S., "Boiling Points of the Normal Paraffins at Different Pressures," Proc. Roy. Irish Acad., Vol. B38, pp. 65-92 (1928).

VI. NOMENCLATURE

A. Symbols

d	differential operator
H	enthalpy, Btu/lb
ℓ	latent heat of vaporization, Btu/lb
$\underset{\sim}{\ell}$	residual latent heat of vaporization, Btu/lb
m	weight of material, lb
P"	vapor pressure, psia
[Q]	heat added per unit weight of material withdrawn under idealized conditions, Btu/lb
$\underset{\sim}{Q}^{*}_{1,2}$	net energy added to calorimeter under ideal conditions, Btu
T	thermodynamic temperature, ^{o}R
t	temperature, ^{o}F
V	specific volume, cu ft/lb

B. Subscripts

g	gas phase
ℓ	liquid phase
P	pressure
T	temperature
1	initial state
2	final state

Table I

ESTIMATED UNCERTAINTIES OF MEASUREMENT

Quantity	Probable Uncertainty per cent
Energy added electrically	0.03
Energy added by agitation	0.18
Energy exchange between calorimeter and jacket	0.008
Change in temperature of liquid and vapor	0.05
Weight of material withdrawn	0.02
Volumetric correction factor	0.03
Superheat of liquid	0.07

Table II

EXPERIMENTAL RESULTS FOR n-DECANE

Identification	Temperature °F	Pressure[a] P.S.I.A.	Energy Added: Electrically Btu	Energy Added: By Agitation Btu	Energy Added: By Conduction and Radiation Btu	Weight of Material Withdrawn lb	Superheat of Liquid °F	dP"/dT psi/°R	Specific Volume: Dew Point cu ft/lb	Specific Volume: Bubble Point[b] cu ft/lb	Volumetric Correction Factor[c]	Latent Heat of Vaporization Btu/lb
367	160	0.40	3.8328	0.1248	-0.0027	0.027447	0.12	0.01060	116.4	0.02321	0.99980	144.12
368	160	0.40	3.3375	0.1092	-0.0028	0.023855	0.12	0.01060	116.4	0.02321	0.99980	144.39
371	190	0.84	4.7201	0.0828	0.0022	0.034306	0.00	0.02012	57.9	0.02370	0.99959	140.10
372	190	0.84	4.2639	0.0738	-0.0004	0.030939	0.20	0.02012	57.9	0.02370	0.99959	140.23
373	220	1.65	6.2177	0.0731	0.0030	0.046369	0.24	0.03540	30.5	0.02420	0.99921	135.74
374	220	1.65	5.9721	0.0706	0.0000	0.044687	0.27	0.03540	30.5	0.02420	0.99921	135.24
375	250	3.04	3.6583	0.0752	0.0000	0.028267	0.15	0.05867	17.1	0.02470	0.99856	131.96
376	280	5.27	4.2949	0.0762	-0.0012	0.034258	0.12	0.09171	10.2	0.02520	0.99752	127.30
377	310	8.66	2.7888	0.0832	0.0019	0.023374	0.05	0.13644	6.4	0.02573	0.99595	122.48
379	340	13.61	3.4606	0.0596	0.0022	0.029495	0.07	0.19423	4.2	0.02630	0.99367	118.71

[a]Based on Willingham (8) up to 220 °F and Reamer (5) up to 340 °F.

[b]Reamer et al. (5).

[c]Not used directly in evaluation of latent heat of vaporization.

Table III

CRITICALLY CHOSEN VALUES OF SOME PROPERTIES OF n-DECANE

Temp. °F	Specific Vol. at Dew Point cu ft/lb	Internal Energy Change on Vaporization Btu/lb	Latent Heat of Vaporization Btu/lb
100	578.0	144.60	152.40
110	434.0	143.10	151.04
120	329.0	141.62	149.70
130	251.0	140.12	148.34
140	193.0	138.61	146.96
150	149.1[a]	137.11	145.59[a]
160	116.4	135.60	144.21
170	91.5	134.07	142.82
180	72.6	132.56	141.43
190	57.9	131.05	140.04
200	46.5	129.54	138.64
210	37.5	128.03	137.25
220	30.5	126.52	135.84
230	25.0	125.00	134.43
240	20.6	123.49	133.02
250	17.1	121.98	131.60
260	14.3	120.47	130.18
270	12.0	118.96	128.76
280	10.2	117.44	127.33
290	8.6	115.91	125.89
310	6.4	112.88	123.03
320	5.5	111.36	121.58
330	4.8	109.83	120.15
340	4.2	108.30	118.70

[a]Values at this and lower temperatures extrapolated from data at higher temperatures.

Part II

HEAT AND MASS TRANSFER FROM A CYLINDER PLACED IN A TURBULENT AIR STREAM - SHERWOOD AND FRÖSSLING NUMBERS AS A FUNCTION OF FREE STREAM TURBULENCE LEVEL AND REYNOLDS NUMBER

I. INTRODUCTION

The transfer of matter to or from a cylinder placed normal to a fluid stream is an important phenomenon which, compared to energy transfer from a cylinder has received relatively little attention. Mass transfer operations are essential to the chemical industry, and with the concepts of ablative cooling and hypersonic velocities, situations involving simultaneous heat and mass transfer have found great importance in the aerospace industries.

Undoubtedly interest in the transport of material from cylinders has suffered because measurements of the related phenomenon of energy transport from cylinders are frequently associated with fewer experimental difficulties, and it has been anticipated that these results are directly applicable to the prediction of mass transfer rates through the Chilton Colburn analogy (8). The theory which forms the basis of this analogy has recently become suspect when flows involving a non-zero free stream turbulence level are involved (30, 46, 51), and the need for a systematic study of mass transport as opposed to energy transport for cylinders was indicated.

Winding and Cheney (59) studied the evaporation of cast napthalene cylinders as well as a variety of other shapes exposed to a current of warm air. They obtained local mass transfer rates by observing changes in the cylinder shape as a function of time. This information was used to predict local heat transfer rates for a cylinder using the Chilton Colburn analogy (8) between heat and

mass transfer. The results are interesting, but of somewhat limited value because the prevailing turbulence level or scale of turbulence of the air stream used in this study is uncertain. Also they had no provision for measuring local temperature variations as a function of angle from stagnation. In a study of energy and material transport from a sphere, Sato (45) determined that the surface temperature varied significantly with angular position, which introduces an additional complication into the study of local mass transfer rates.

Mendelson et al. (35) measured mass transfer rates at the stagnation point of a cylinder in an effort to predict the effect of interfacial resistance on evaporation rates. Again,uncertainties in the prevailing free stream turbulence limit the value of this work.

Comings, Clapp, and Taylor (10) studied the effects of free stream turbulence on heat and mass transfer from cylinders over a range of Reynolds numbers from 400 to 20,000 based on cylinder diameter. They determined that the effect of increasing free stream turbulence on heat transfer rates was greatest for low levels of turbulence. Specifically at a Reynolds Number of 5,800 they observed a 25 per cent increase in heat transfer rates as the turbulence level was increased from 1 to 7 per cent, and that a further increase in turbulence level up to 22 per cent had little additional effect on heat transfer rates. However, they used the Schubauer technique (50) for measuring the apparent level of turbulence, which is somewhat uncertain in this application. This is

true not only because of the high levels of turbulence studied, but also because of the nonuniformity of their turbulence grids. Their data on mass transfer scatter so badly as to be of little quantitative value.

Maisel and Sherwood (33) and Schnautz (49) studied mass transfer from a cylinder over a variety of conditions, and their results are compared with this work.

Energy transport from cylinders occurring as a result of a temperature gradient has received much additional attention from many other workers (20, 30, 39, 41, 42, 51, 56). Unfortunately, the importance of free stream turbulence level and scale in enhancing energy transfer rates has not been generally appreciated until rather recently (46, 51, 56) and one is confronted with large amounts of data from various sources in which the Reynolds number is well established, but for which the prevailing level or scale of turbulence is not documented. Some of the more recent data on energy transport from cylinders have been correlated by workers in this laboratory (18, 19) in terms of a Frössling Number which is a function of the free stream Reynolds Number and turbulence level. Richardson (41, 42) suggests a different correlation based on a cognizance of the basic differences in the transport mechanism before and aft of boundary layer separation. Geidt (20) measured skin friction and heat transfer rates from a cylinder placed normal to a free jet, and provided his cylinder with end plates to preserve the two dimensionality of the flow. He was interested in the

phenomenon attending transition from subcritical to supercritical flow causing the sharp decrease in the drag coefficient. His data differ substantially from those of Schmidt and Wenner (48) taken under similar conditions but without the end plates.

While most of the work referenced above was done at high Reynolds Numbers at or close to critical, several interesting aspects of transport from cylinders are well documented. Concerning energy transport from cylinders, the effect of free stream turbulence in enhancing transport is confined principally to the laminar boundary layer formed over the front half of the cylinder (30, 41, 42, 46, 55). The effect of turbulence is slight in influencing energy transport in the wake region of a cylinder, as well as in the turbulent boundary layer which can exist upstream of separation for supercritical Reynolds Numbers (46). Interestingly, the effect of free stream turbulence on skin friction from cylinders is an order of magnitude less than for heat transfer, a phenomenon measured by Geidt (20) and treated theoretically by Seban (51) and Sutera (55). In view of this defeat of the Chilton Colburn analogy between energy and momentum transport it has recently been felt that this analogy is a limiting case which has general validity only for vanishing turbulence levels (46, 51).

In view of these findings it would seem desirable to study mass transport from cylinders not only to determine the effects of the composition gradient on the formation and properties of the "blown" boundary layer, but to answer questions concerning the

applicability of an analogy between heat and mass transfer over a range of Reynolds Numbers and turbulence levels. It is the purpose of this research to provide quantitative information on mass transfer rates from cylinders over an intermediate range of Reynolds Numbers and turbulence levels.

II. THEORY

The mathematical description of transport from cylinders, whether it be momentum, material, or energy transport has proceeded on a semi-empirical basis. Transport from the front half of a cylinder placed in a moving fluid stream has been treated by many workers employing a variety of simplifying assumptions. This is especially true for subcritical flow where a laminar boundary layer persists up to the point of separation. However, an effective mathematical approach towards analyzing the effects of free stream turbulence on a laminar boundary layer has not been presented, and likewise, an effective mathematical approach to transport in the wake region of a cylinder seems still further removed.

In principle, mass transport from a cylinder can be described by a solution to the following equations. These are, respectively, the continuity equation, the momentum equations, (Navier Stokes equations of motion), in the x, y, and z Cartesian coordinate directions, the energy equation, and the continuity of k - 1 of the k chemical species.

Continuity: $$\frac{\partial}{\partial x}(\sigma u) + \frac{\partial}{\partial y}(\sigma v) + \frac{\partial}{\partial z}(\sigma w) + \frac{\partial \sigma}{\partial \theta} = 0 \qquad (1)$$

Momentum X: $$\frac{Du}{D\theta} = -\frac{g_o}{\sigma}\frac{\partial P}{\partial x} + \frac{g_o}{\sigma}\left\{\frac{\partial}{\partial x}\left[\eta\left(2\frac{\partial u}{\partial x} - \frac{2}{3}\vec{\nabla}\cdot\vec{q}\right)\right]\right.$$

$$\left. + \frac{\partial}{\partial y}\left[\eta\left(\frac{\partial u}{\partial y} + \frac{\partial v}{\partial x}\right)\right] + \frac{\partial}{\partial z}\left[\eta\left(\frac{\partial w}{\partial x} + \frac{\partial u}{\partial z}\right)\right]\right\} \qquad (2)$$

Momentum Y: $$\frac{Dv}{D\theta} = -\frac{g_o}{\sigma}\frac{\partial P}{\partial y} + \frac{g_o}{\sigma}\left\{\frac{\partial}{\partial y}\left[\eta\left(2\frac{\partial v}{\partial y} - \frac{2}{3}\vec{\nabla}\cdot\vec{q}\right)\right]\right.$$

$$\left. + \frac{\partial}{\partial x}\left[\eta\left(\frac{\partial u}{\partial y} + \frac{\partial v}{\partial x}\right)\right] + \frac{\partial}{\partial z}\left[\eta\left(\frac{\partial w}{\partial y} + \frac{\partial v}{\partial z}\right)\right]\right\} \quad (3)$$

Momentum Z: $$\frac{Dw}{D\theta} = -\frac{g_o}{\sigma}\frac{\partial P}{\partial z} + \frac{g_o}{\sigma}\left\{\frac{\partial}{\partial z}\left[\eta\left(2\frac{\partial w}{\partial z} - \frac{2}{3}\vec{\nabla}\cdot\vec{q}\right)\right]\right.$$

$$\left. + \frac{\partial}{\partial x}\left[\eta\left(\frac{\partial w}{\partial x} + \frac{\partial u}{\partial z}\right)\right] + \frac{\partial}{\partial y}\left[\eta\left(\frac{\partial w}{\partial y} + \frac{\partial v}{\partial z}\right)\right]\right\} \quad (4)$$

Energy: $$\frac{DT}{D\theta} = \frac{1}{\sigma c_P}\frac{DP}{D\theta} + \frac{1}{\sigma c_P}\vec{\nabla}\cdot(k\nabla T) + \eta\phi \quad (5)$$

and continuity of component k:

$$\frac{Dn_k}{D\theta} = \frac{1}{\sigma}\vec{\nabla}\cdot\left[\sigma D_{ckj}\nabla n_k\right] \quad (6)$$

In the equations above, u, v, and w are the velocity components, $\vec{\nabla}\cdot\vec{q}$ is the divergence of the velocity vector, ϕ is the frictional dissipation function described by Schlichting (46), and $\dot{m}_{dkx}$, $\dot{m}_{dky}$, and $\dot{m}_{dkj}$ are the diffusional mass fluxes of component k in the x, y, and z directions respectively. These last two quantities may be formulated as:

$$\phi = 2\left[\left(\frac{\partial u}{\partial x}\right)^2 + \left(\frac{\partial v}{\partial y}\right)^2 + \left(\frac{\partial w}{\partial z}\right)^2\right] + \left(\frac{\partial v}{\partial x} + \frac{\partial u}{\partial y}\right)^2 + \left(\frac{\partial w}{\partial x} + \frac{\partial u}{\partial z}\right)^2$$

$$+ \left(\frac{\partial w}{\partial y} + \frac{\partial v}{\partial z}\right)^2 - \frac{2}{3}\left(\frac{\partial u}{\partial x} + \frac{\partial v}{\partial y} + \frac{\partial w}{\partial z}\right)^2$$

and

$$\dot{m}_{dkx} = -\sigma D_{ckj} \frac{\partial n_k}{\partial x} = -\frac{\sigma \dot{V}^2}{R^2 T^2} \left[\frac{\partial f_x}{\partial n_k}\right]_{P,T} D'_{Mk} \frac{\partial n_k}{\partial x}$$

the latter definition coming from Longwell and Sage (32).

The necessity for a consideration of momentum in the z (axial) direction as well as axial variations in the continuity and energy equations is a consequence of local fluctuations in fluid properties in the axial direction due to the presence of turbulence. In this regard Sutera (55) demonstrated that it was necessary to consider turbulence in three dimensions even when the time averaged flow was two dimensional. Similarly the inclusion of a time dependence of the independent variables is also a necessity when random turbulent velocity components are considered.

The boundary conditions which are pertinent to the system of equations (1) to (6) above are:

at the cylinder surface:

$$x^2 + y^2 = r_o^2 \qquad u = v = w = 0$$

$$T = T_s(0)$$

$$n_k = n_{ks}$$

and at infinity:

$$u = U_\infty + u'(x,y,z,\theta)$$

$$v = v'(x,y,z,\theta)$$

$$w = w'(x,y,z,\theta)$$

$$T = T_o$$

$$n_k = n_{ko}$$

In practice, equations (1) to (6) are so complex that their general solution even for the simplest boundary conditions has thus far proven an impossible task. With the assumption of steady state with no turbulent fluctuations, which makes the problem two dimensional and eliminates the time dependent terms, a solution is still so difficult that in practice it is treated by considering separately the boundary layer flow within which all viscous effects are concentrated, and an external flow where the fluid is assumed to be inviscid. Such solutions have proved quite valuable in describing transport from the front half of the cylinder, up to the point of boundary layer separation, but have not shown much promise in describing either the flow or transport in the wake region. Beyond the point of separation, flow around a cylinder is inherently unsteady due to the alternate shedding of vortices from first one side then the other. This phenomenon is present whenever the Reynolds Number based on cylinder diameter lies above a certain range of transition, 60 - 200, a fact well documented by many investigators (1, 21, 52). These vortices which alternately build up and detach from the cylinder perturb the flow pattern about a cylinder enough so that a mathematical solution based on the premise of steady flow is severely limited. Surprisingly results obtained by this approach up to what is necessarily a time average point of separation are useful and will be discussed.

A. Two-Dimensional Steady Flow Around a Cylinder -- The Laminar Boundary Layer

For two-dimensional laminar steady flow around a solid object it may be shown that the appropriate boundary layer equations are (46):

Continuity:

$$\frac{\partial}{\partial x}(\sigma u) + \frac{\partial}{\partial y}(\sigma v) = 0 \tag{7}$$

Momentum along wall:

$$u\frac{\partial u}{\partial x} + v\frac{\partial u}{\partial y} = \frac{g_o}{\sigma}\frac{\partial}{\partial y}\left(\eta\frac{\partial u}{\partial y}\right) - \frac{g_o}{\sigma}\frac{\partial P}{\partial x} + g_x\left(\frac{\sigma_\infty}{\sigma} - 1\right) \tag{8}$$

Energy:

$$u\frac{\partial T}{\partial x} + v\frac{\partial T}{\partial y} = \frac{1}{\sigma c_P}\frac{\partial}{\partial y}\left(k\frac{\partial T}{\partial y}\right) + \frac{\eta}{\sigma c_P}\left(\frac{\partial u}{\partial y}\right)^2 + \frac{u}{\sigma c_P}\frac{\partial P}{\partial x} \tag{9}$$

Continuity component k:

$$u\frac{\partial n_k}{\partial x} + v\frac{\partial n_k}{\partial y} = \frac{1}{\sigma}\frac{\partial}{\partial y}\left\{\sigma D_{ckj}\frac{\partial n_k}{\partial y}\right\} \tag{10}$$

In deriving these equations momentum is considered only in the direction tangent to the wall because of the anticipated thinness of the boundary layer region. Similarly, all derivatives in the direction tangent to the wall are an order of magnitude smaller than the derivatives considered in a direction perpendicular to the wall, and in most cases may be dropped from further consideration.

Inspecting the boundary layer equations above, it can be

seen that aside from the effects of buoyancy apparent in the term $g_x\left(\frac{\sigma}{\sigma_\infty} - 1\right)$, the only influence of thermal and material transport on the solution of the momentum boundary layer equations (eqs. (7) and (8) above) is in causing a change in the fluid viscosity η, or the specific weight σ; or in the case of material transport, giving rise to a non-zero normal velocity component at the solid boundary. For Reynolds Numbers greater than 2500 the effects of natural convection on the momentum boundary layer are usually negligible, and the last term in equation (8) may be dropped from consideration (19). Finally in considering the boundary layer equations the derivatives of pressure in a direction normal to the surface are deleted, and a pressure which is determined either experimentally or from the potential flow solution about the body in question is assumed to be impressed on the boundary layer.

Laminar boundary layer solutions to equations (7) through (9) for the flow of an incompressible fluid with constant fluid properties are well known for the case of energy transport from flat plates and for cylinders up to the point of separation. Frössling (17) obtained numerical solutions for this case using a Prandtl Number of 0.7. His results are shown in Figure 4 where local values of the heat flux in terms of a Nusselt Number are shown plotted vs. the angle from stagnation. Squire (54) repeated these calculations in the vicinity of stagnation over a range of Prandtl Numbers and deduced that the Nusselt Number at stagnation was roughly proportional to the one-third power of the Prandtl Number and the one-half

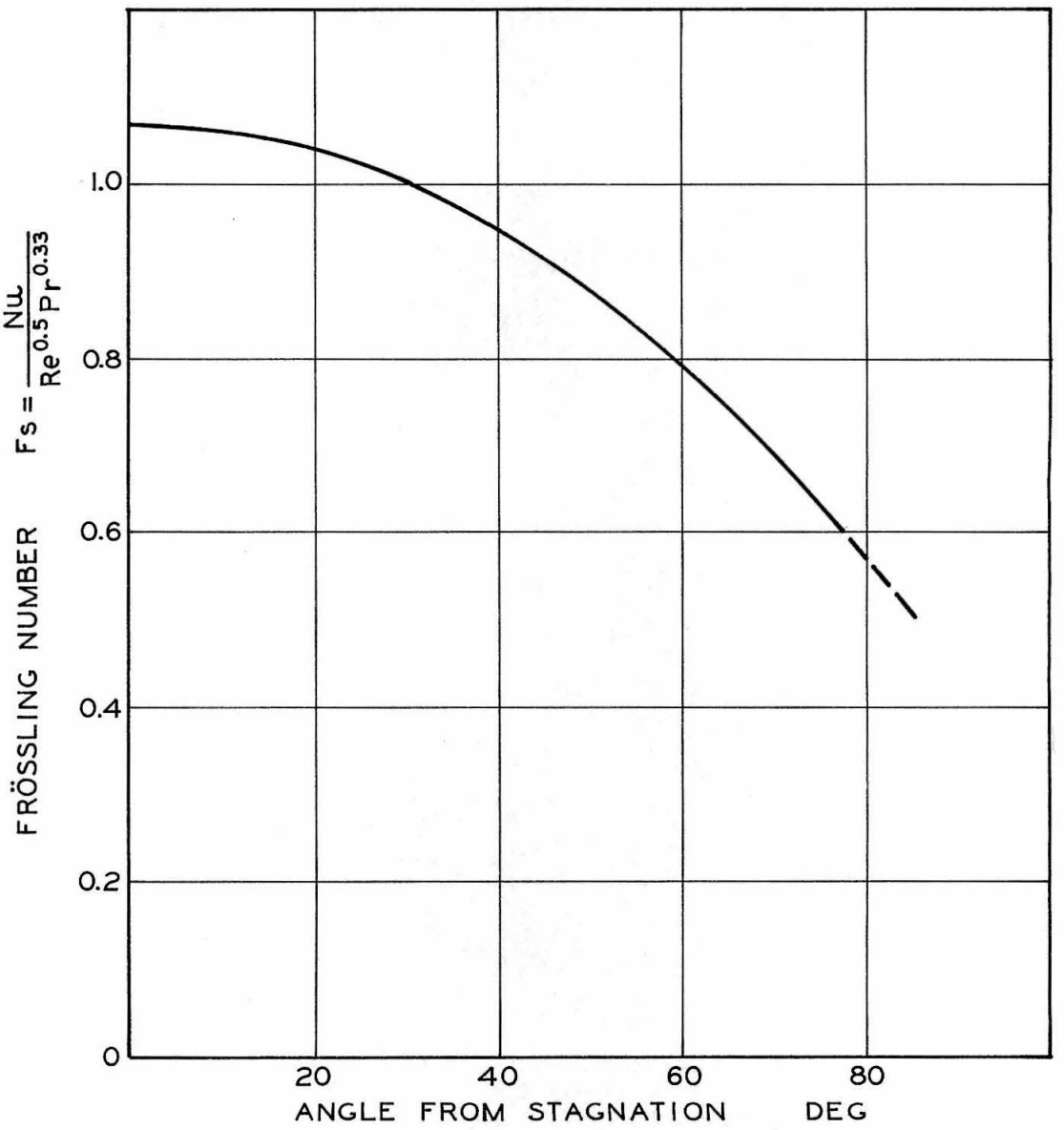

Fig. 4 Frössling Solution for Local Energy Transport Rates from Cylinders (17)

power of the Reynolds Number. Thus by neglecting viscous dissipation and assuming constant fluid properties at the stagnation point:

$$Nu = 1.14\ Re^{1/2} Pr^{1/3} \tag{11}$$

The results of Frössling (17) calculated for a Prandtl Number of 0.7 (air) correspond to a turbulence level of zero. In practice, the experimental values of other workers are somewhat higher due to the systematic effect of free stream turbulence.

However, it must be emphasized that even for the case of a laminar boundary layer with constant fluid properties and negligible viscous dissipation, the "theoretical" Nusselt Number dependence on the one-third power of the Prandtl Number is approximate only. It is obtained by smoothing the results of numerical calculations over a range of Prandtl Numbers, and noting that these results are correlated to within 5 to 6 per cent by the one-third power of the Prandtl group (6). In this regard it is noted that Korobkin (31) reviewed the results of Squire (54) at the stagnation point of a cylinder, and Homann (24) for a sphere, and deduces that the influence of the Prandtl group on stagnation point heat transfer is better correlated by the 0.4 power. These results are pertinent in this study, because, under the simplifying assumptions above, the boundary layer equation for energy transport becomes identical in form with the boundary layer equation for material transport except that the latter is a function of the Schmidt Number instead of Prandtl Number. Hence, except for the difference of a non-zero

normal velocity component at the boundary, material transfer is analogous to energy transfer, and one would expect the Schmidt dependence of the Sherwood Number to be comparable to the Prandtl dependence of the Nusselt Number.

B. The Frössling Number for Heat and Mass Transport

Referring again to the boundary layer equations (eq. 7 to 10), it is apparent that if the fluid properties are constant, buoyancy effects are negligible, and the effects of frictional dissipation and expansion work can be neglected, the momentum equation, (eq. 8), is independent of the energy and conservation of chemical species equations. Further, as mentioned above those latter equations are of identical mathematical form. Hence:

$$u \frac{\partial u}{\partial x} + v \frac{\partial u}{\partial y} = \nu \frac{\partial^2 u}{\partial y^2} - \frac{g_o}{\sigma} \frac{\partial P}{\partial x} \tag{8a}$$

and

$$u \frac{\partial T}{\partial x} + v \frac{\partial T}{\partial y} = K \frac{\partial^2 T}{\partial y^2} \tag{9a}$$

$$u \frac{\partial n_k}{\partial x} + v \frac{\partial n_k}{\partial y} = D_{ckj} \frac{\partial^2 n_k}{\partial y^2} \tag{10a}$$

It is apparent then, that if the "blown" velocity at the solid surface is negligible, (in the case of material transport), equations 9a and 10a will yield temperature and concentration distributions about the cylinder which are functions only of the Prandtl Number for the thermal boundary layer, or of the Schmidt Number for the material boundary layer. These solutions are well known for transport from a flat plate, and the following functional form is obtained:

$$Nu = C_o Re^{1/2} Pr^{1/3} \tag{12a}$$

$$Sh = C_o Re^{1/2} Sc^{1/3} \tag{12b}$$

Again, solutions for transport from the forward half of a cylinder also indicate that the Nusselt Number depends approximately to the one-third power of the Prandtl Number and the following functional forms have been used in this laboratory (19):

For thermal transport from cylinders:

$$Nu = C_1 Re^{1/2} Pr^{1/3} + C_2 \frac{Z_T}{Z_T + C_3} Re\ Pr^{1/2} \tag{13}$$

For material transport from cylinders:

$$Sh = C_1 Re^{1/2} Sc^{1/3} + C_2 \frac{Z_T}{Z_T + C} Re\ Sc^{1/2} \tag{14}$$

These equations suggest a new dimensionless group, the Frössling Number. The form of the Frössling Number would be identical for either energy or material transport for the following four conditions: (a) constant fluid properties; (b) negligible effect of a non-zero velocity component at the wall; (c) zero free stream turbulence; and (d) negligible frictional dissipation and compressive work. Hence:

$$\mathfrak{F}s_H = \frac{Nu}{Re^{1/2} Pr^{1/3}} = \mathfrak{F}s_D = \frac{Sh}{Re^{1/2} Sc^{1/3}} \tag{15}$$

C. Derivation of the Sherwood Number - The Modified Maxwell Diffusion Coefficient

Whereas the definition of the Nusselt Number for heat transfer has been completely standardized, the definition of a Sherwood Number is somewhat arbitrary since it has been dependent on the nature of the diffusion coefficient specified, and there are at least six diffusion coefficients in more or less common usage (32). Although the units most commonly encountered in the diffusion coefficient are those of length squared divided by time, there are variations (32, 37), and unlike the phenomenon of energy transport, the existence of a diffusion velocity caused by the bulk transport of material causes the actual rate of material transport in most instances to be somewhat different than that expressed by a diffusion coefficient multiplied by a concentration gradient (32, 37).

In this regard we can define the mass flux of a given component k from diffusion alone in any one of several ways (32);

Fick $$\dot{m}_{dk} = - D_{F,k} \nabla \sigma_k \qquad lb/ft^2 \cdot sec \qquad (16a)$$

Chapman Cowling $$\dot{m}_{dk} = - \sigma D_{ckj} \nabla n_k \qquad (16b)$$

Maxwell $$\dot{m}_{dk} = - \frac{P}{\sigma R^2 T^2} D_{Mkj} \nabla n_k \qquad (16c)$$

Modified Maxwell $$\dot{m}_{dk} = - \left(\frac{\partial f_k}{\partial n_k} \right)_{T,P} \frac{D'_{Mk}}{\sigma R^2 T^2} \nabla n_k \qquad (16d)$$

All of these diffusion coefficients have been used by workers

in this laboratory for some time, but some recent investigations have indicated that for gas phase diffusion the Modified Maxwell Diffusion coefficient shows only slight variations with composition (47), and because of this desirable characteristic it was selected in this work.

In analogy with the definition of the heat transfer coefficient, h, we can define a mass transfer coefficient, K_G, which yields material flux in pounds per second when differences in the mole fraction of the diffusing component are considered in the driving force:

$$\dot{\underline{m}}_k = K_G A \Delta \underset{\cdot}{n}_k \tag{17}$$

Similarly we can define the overall mass flux from a solid surface in terms of an "effective" diffusion coefficient which when employed with the mole fraction gradient of the diffusing species yields the correct mass flux for the case of one component stagnant. Hence also in analogy with the transport of energy we have:

$$\dot{\underline{m}}_k = - D_k^* A \left. \frac{d\underset{\cdot}{n}_k}{dy} \right|_{wall} \tag{18}$$

Combining these relations it is natural to define the Sherwood Number for a cylinder as

$$Sh = \frac{K_G D}{D_k^*} \tag{19}$$

which is, except for the various Reynolds analogy defeats discussed earlier, exactly comparable to the Nusselt Number for energy

transport. Therefore, if the Schmidt and Prandtl groups are equal, and the assumptions of negligible viscous dissipation or work of expansion in the energy equation (equation 9), constant fluid properties, and a negligible effect of the "blown" boundary layer, ($v \neq 0$ at the wall for material transport), are valid, the Sherwood Number defined in this manner should be identically equal to the Nusselt Number for heat transfer. Moreover, corresponding to the dependence of Nusselt Number on the one-third power of the Prandtl modules, the Sherwood Number should depend on the one-third power of the Schmidt group, again within the limitations of the assumptions cited above. At this point it is worth noting that the Sherwood Number defined by equation (19) is invariant whatever the choice of driving potential for the mass transfer coefficient, K_G, and effective diffusion coefficient, D_k^*, as long as this choice is consistent. It remains to evaluate the mass transfer coefficient in terms of laboratory data, and the effective diffusion coefficient, D_k^*, in terms of the Modified Maxwell diffusion coefficient for the case of one component stagnant.

It may be shown (32) that for the case of one component stagnant, the mass diffusion of component k may be written:

$$\dot{m}_k = - \frac{Z D'_{Mk}}{b_k T} \left(\frac{f_k^o}{P}\right) \frac{\partial \ln \dot{n}_j}{\partial x} \qquad (21)$$

where in this expression f_k^o is the fugacity of the pure component at the total pressure, P, of the diffusion process. For the vapors of volatile liquids this "standard state" is obtained by an extrapolation

of fugacity vs. pressure data up to the appropriate pressure, and Z is the compressibility factor of the mixture.

Finally if we consider the diffusion of component k over a distance Δx, through a stagnant second component, equation (21) may be integrated upon the assumption of a mean value for the ratio ZD'_{Mk}/T to give:

$$\dot{m}_k = \frac{ZD'_{Mk}}{b_k T \Delta x} \left(\frac{f_k^o}{P}\right) \ln \frac{n_{\cdot j,x}}{n_{\cdot j,o}} \tag{22}$$

If the gradient at the wall in equation (18) is expressed in terms of finite differences over the distance Δx, equation (18) may be compared with equation (22) to render an expression for the effective diffusion coefficient D_k^*.

$$D_k^* = \frac{ZD'_{Mk}}{b_k T} \left(\frac{f_k^o}{P}\right) \frac{1}{\Delta n_{\cdot k}} \ln \left[\frac{n_{\cdot j,\infty}}{n_{\cdot j,o}}\right] \tag{23}$$

Then since K_G is defined in terms of the mass flux of component k per unit area per unit mole fraction driving force, the Sherwood Number becomes for a cylinder:

$$Sh = \frac{\dot{m}_k b_k T}{LD'_{Mk} Z \left(\frac{f_k^o}{P}\right) \ln \left[\frac{n_{\cdot j,\infty}}{n_{\cdot j,o}}\right]} \tag{24}$$

an expression which is analogous to that for the Sherwood Number for a sphere presented by Sage (44).

III. EXPERIMENTAL APPARATUS

The object of this investigation is a one-inch adiabatic porous cylinder whose surface temperature was monitored, and which was fed with a liquid hydrocarbon (n-heptane or n-octane) which evaporated from the surface. Auxiliary equipment includes the air supply system,which was used to provide an air stream whose temperature and mass flowrate were held constant,and the liquid feed system,which was used to monitor liquid feed rates and to match them to the rate at which liquid was evaporating from the cylinder surface. In the subsequent discussion, the cylinder itself will be considered first,to be followed by a description of the air supply system, the liquid injection system, and the thermocouples in that order.

The direct measurements made are those of liquid vaporization rate as a function of the measured air stream velocity and temperature. The local temperature profiles of the cylinder surface during the vaporization process are also measured. These must be known to determine the driving force during the vaporization process.

A. The Porous Cylinder

The porous cylinder itself is one inch in diameter and features three 2-inch porous sections, each one of which can be fed independent of the other two sections. In practice, the center section was fed independently, first by gravity feed until a steady state was reached and then by the 3/8" injector which will be described later. During the course of experimentation, it was found possible to switch from gravity feed to the injector feed system without affecting the internal liquid pressure by more than 0.2 centimeters of the evaporating liquid (which could be determined by observing the action of various micromanometers associated with the feed system). The remaining two porous sections were used to reduce longitudinal temperature gradients, thereby reducing energy conducted to the center section from the brass core and to preserve the two dimensional nature of the flow field about the center section. Both guard sections were fed by gravity from the same source.

1. Construction

Figure A1 shows the porous cylinder during final stages of completion. Visible in this illustration are the three porous sections in the center, the vacuum jacket to the right, the spring-loaded compression sleeve to the left, and adjacent to it a screw adjustment nut, which was used to vary the spring loading on the compression sleeve. Also visible at the ends of the cylinder are the junction boxes, which were used in making connections to the liquid feed

systems for each section, and in making thermocouple connections. At this point in the construction, the thermocouple leads are visible, with their temporary labelling tags needed for future identification. The last thermocouple plug is waiting to be cemented in place. The support brackets are also shown which were designed to allow the cylinder to rotate freely by loosening the two Allen screws at the top. During the course of this investigation, the cylinder was rotated to allow temperature measurements to be made at various angles from stagnation.

Figure A2 is a close-up of the three porous sections taken at the same time as Figure A1. It clearly shows the four 0.020 inch soft lead gaskets used to isolate the porous sections from one another and details of the installation of surface thermocouples. Small amounts of #220 epoxy adhesive manufactured by Hughes Associates were used to cement the thermocouple plugs into place and to make a seal between the lead gaskets and the diatomaceous earth sections.

Figure A3 is another close-up of the center section taken during experimentation. The thermocouple junctions can be seen in the center of each diatomaceous earth plug, and the 0.003 inch leads can be seen where they are brought across the face of the plug to its edge and then down from the surface along the edge of the plug. Another interesting feature of this illustration is the formation of droplets which are located about 70^{o} from stagnation. It is apparent from this picture that the cylinder surface is quite saturated, and

the droplets have formed because a partial vacuum is created in this region as the air flows around the cylinder.

Figure A4 gives an exploded view of parts involved in the construction of the cylinder. Each diatomaceous earth sleeve (inside diameter 0.812 inches) slips over one of the three ribbed brass sections shown assembled in the center of the picture. Each brass core has threaded ends. These are joined after the diatomaceous earth sleeves are in place and a 0.002 inch lead gasket, A, has been bismuth soldered onto the end of each brass core. The liquid conduits, 0.072 inch stainless tubing, B, and the thermocouple conduits, 0.042 inch stainless tubing, C, appear at each end of the cylinder in this exploded view. Since the center and left-hand sections are fed from one side, and the appropriate thermocouple conduits are also brought out of this same side, there are six stainless conduit tubes appearing on the left of the cylinder in Figure A4, whereas there are only three emerging on the right-hand side of the cylinder. Also appearing in this figure are the openings in the brass cores, D, where the conduit tubes are brought to the surface and soldered in place.

The two junction boxes are equivalent in construction. The supporting plate, E, appears by itself and again installed on the right-hand half of the cylinder. The body of the junction boxes, F, differ only in that there is an additional union connection, G, for the liquid feed line to the center section. The junction box covers, H, are identical for both boxes.

Inside the junction boxes, a bakelite strip, I, gives support to the loose ends of the thermocouple conduits. The thermocouple leads are then tied to one of the junction posts, J, where they are eventually soldered in place. These junction posts were used in joining 0.003 inch thermocouple leads from the cylinder surface to 0.020 inch leads of the same material which led to a stirred ice bath.

The feed line union, G, is present both for support of the internal feed lines, and to facilitate the installation of the cylinder over the air duct. The lead gaskets shown at each end of the housing nut have proven very effective in making leak proof seals.

Also shown in Figure A4 are the support brackets, L, and the vacuum jacket, M. The seal between the cylinder and the vacuum jacket was made by tightening the end nuts to compress a neoprene ring at each end, the neoprene being compressed against the brass ends of the cylinder. The function of the vacuum jacket was to allow the complete evacuation of the evaporating sections through the associated feed lines. After a good vacuum was attained within the vacuum jacket the system could be filled with deaerated hydrocarbon sample with assurance that air bubbles would not be present between the brass cores and the outer diatomaceous earth sections. The vacuum jacket was also used between tests to prevent the evaporating sections from drying out. The vacuum jacket was constructed so that during operation it would slide off the evaporating sections into the position shown in Figure A1.

The compression sleeve, N, has the same inside diameter

as the brass cores and moved freely on an 0.812 inch inner support rod. It compressed the diatomaceous earth sections against the lead gaskets, A, to isolate each section from the liquid supply of the adjacent section, the compressing force coming from a spring contained within the spring housing, O. The compression could be adjusted by means of the compression nut, P.

Figure A5 shows the assembled cylinder with the vacuum jacket in place over the diatomaceous earth evaporating sections. It can be compared with Figure A1 showing the cylinder with the evaporating sections exposed.

B. Air Supply System

Figure A6 is a schematic diagram of the air supply system. The open-circuit air tunnel was originally designed by Sage (27) for studying the evaporation rates of drops, and later for heat and mass transfer work with spheres (25, 26, 45) and cylinders (13, 58).

The air supply system was fitted with a 3 × 12 inch exit area convergent section for this work, the same section employed by Short (53), Hsu (26), and Cuffel (13) in their investigations. With this convergent section the air supply system could produce average air velocities between 4 and 32 feet per second within ± 0.05% while maintaining a mean air temperature of 100 ^{o}F ± 0.2 ^{o}F.

After entering the air intake duct two blowers at A force the air past wire grid heaters, B, through the venturi meter V. The grid heater power is controlled by an electronic control system actuated by the temperature sensed by platinum resistance thermometer D. This type of temperature control system has been used with great success in this laboratory and is described by Corcoran et al. (12).

The air velocity is controlled by adjusting the blower speed, and then maintaining a constant RPM through the use of a preset counter monitored by a quartz oscillator. Since the measured phenomenon is a direct function of Reynolds Number, the blower speed was adjusted periodically to give a constant mass flow of air rather than constant velocity. The test velocities, namely 4, 8, 16, 24, and 32 feet per second are nominal only, and the actual

air velocities used were subject to small changes with changes in atmospheric pressure and in the humidity of the air drawn through the blower system. In practice, it was found that the air temperature was much easier to control if the intake air to the blower system was drawn from the same room as that in which the experimental work was carried out.

In continuing through the air system the air is turned by vanes at the elbow, passes over a high precision calibrated platinum resistance thermometer at E, and through a screen, F, used to provide a more uniform velocity distribution at the jet exit, and to reduce the free stream turbulence to a nominal level of 1.3% (13). For the higher turbulence levels used in some of the tests with n-heptane a turbulence grid was installed at the jet exit C, and a jet extension was added. The magnitude of the free stream turbulence is a strong function of distance downstream of the turbulence grid, and the cylinder was positioned accordingly. The temperature of the duct system downstream of the venturi was maintained within 1 ^{o}F of the air temperature by using external heaters.

The position of the cylinder over the jet exit can be seen in Figure A7. Also seen in this photograph, taken under test conditions, is the protractor used to determine the angular location relative to stagnation of surface thermocouples, and one of the liquid feed lines which was installed in such a way that the cylinder could be rotated through an angle of 360 degrees. This picture was taken during one of the low turbulence level tests.

C. The Liquid Feed System

The evaporation rate for the center section was measured directly by observing the displacement of the positive displacement piston, described by Chen (7), as part of the liquid injector system. Since the capacity of the injector system was small (approximately 20 cc), it was found necessary to achieve steady state operation by some other means until the laboratory conditions, air temperature and velocity, were those desired. It was necessary then to be able to switch over to the injector feed system to take vaporization rate data, and then back to the auxiliary feed system when the capacity of the injector was exhausted. It is imperative that the first switch be accomplished without appreciably disturbing the steady operation of the cylinder, whereas, for the second operation it was necessary only that the cylinder be kept from drying out since evacuating the cylinder and refilling it proved to be a very time consuming process. Since the injector itself provided the means for all vaporization rate measurements it will be described first.

1. The Injector

The liquid injector, originally developed by Reamer and Sage (40) contains fluid in a reservoir which is continuously displaced by the motion of a 3/8 inch plunger. The plunger is driven through a series of reduction gears by an electric motor. The motor's speed is controlled by a preset counter monitored by a quartz oscillator. The injector can be driven at almost any pre-

determined speed through the selection of the proper reduction gear ratio and motor speed. For details on the control circuit the reader is referred to the original paper by Reamer and Sage. The liquid in the injector was maintained at a constant temperature of 100 ^{o}F by means of a constant temperature oil bath surrounding the injector reservoir. Figure A8 is a photograph of the injector and some of the associated mechanisms.

2. The Injector Loading System

All operations involving the use of the 3/8 inch injector described above are controlled through a six-way manifold system. The manifold, and its relation to the injector, the vacuum system, the liquid loading system, and the cylinder are shown schematically in Figure A9.

The principle function of the liquid loading system is to deaerate the liquid sample. This function is essential to the use of injector as a volume metering device, since the formation of air bubbles within the injector system would destroy the simple relationship between volumetric displacement and weight flow to the cylinder. To accomplish the deaeration the sample was first loaded into boiler B_1 after which the top was sealed. The sample was then deaerated under vacuum until approximately 10% of the sample had evaporated. The next 80% of the sample was then trapped in B_2 by using liquid nitrogen as a coolant. Vacuum was continuously applied during this process so that after this step essentially all dissolved air had been

removed. Finally the sample ampule, A, which had been previously evacuated, was filled from the supply of liquid in B_2 by distillation. The reader will appreciate that this process resulted in some further purification of the sample used.

During the process of filling the sample ampule, A, the bottom was sealed against atmospheric pressure by freezing mercury which flowed between the mercury reservoir and the sample ampule at the glass "U" shown schematically in Figure A9. After loading, the sample ampule valve 2 was closed, mercury frozen in the freeze-off leg was allowed to thaw, and liquid hydrocarbon in A was forced up to the valve 2 by the weight of mercury in the reservoir and atmospheric pressure behind it. After evacuating the injector, hydrocarbon was forced into it through the opening of valves 2 and 5 with all other valves closed. Valve 2 was then closed, valve 4 opened, and the injector system was ready for use. Subsequent refillings of the injector were accomplished by closing valve 4, and opening valve 2 while the injector plunger was withdrawn in preparation for a run. This process was continued until the contents of the sample ampule, approximately 250 ml, had been exhausted.

3. The Auxiliary Feed System

Since the capacity of the injector, approximately 20 ml, was quickly exhausted during operation, some other source of liquid feed to the cylinder was necessary for the attainment of steady state

temperatures and evaporation rates from the cylinder prior to evaporation rate measurements made with the injector, and also for maintaining the cylinder feed while the injector was reloaded. This system is illustrated schematically in Figure A10.

Liquid hydrocarbon feed to the cylinder can reach the feed line in Figure A10 either from the injector, or from the large two liter reservoir, R, when the valve shown is opened. To force flow through the feed line when the injector system was inoperative the elevation of the liquid interface in R had to be from one to six inches above the elevation of the porous cylinder. Significantly, the resistance to fluid flow through the valve shown was so much less than that encountered in going through the feed line that the additional flow to the cylinder when the injector was operating with the shut off valve to the reservoir open was negligible. During the switch from gravity to injector feed this phenomenon proved very useful, and in practice the injector was always turned on before the gravity feed was shut off, and correspondingly the gravity feed system was opened to the cylinder before the injector was shut off. The readings of the micromanometers, M_1 and M_2, were independent of the feed source, and were very useful in determining how close to saturation the cylinder was actually operating, and in balancing the input liquid feed rate with the actual rate of vaporization from the cylinder.

The two guard sections were also supplied by a gravity feed system with one feed bottle supplying both sections. The feed to

these sections was split at the tee immediately below the shutoff valve so that the length of all feed lines from the reservoir bottles was approximately equal. The guard section feed lines also had micromanometers installed at the same relative distance from the feed bottles as micromanometer M_2 is located in the primary feed system.

Figure A11 is a photograph taken of the two reservoirs. The one on the left-hand side was used to feed the two guard sections, while the reservoir on the right-hand side of Figure A11 was used to feed the center section of the porous cylinder. To maintain a constant liquid level in the reservoirs the aluminum box housing the reservoirs could be moved in the vertical direction by a screw type traversing gear. In addition, the bottles themselves could be moved relative to each other since they were mounted on a channel section which slid up and down within the aluminum box, and were set in the desired position by tightening two wing nuts. Note that in Figure A11 the liquid levels in the feed bottles are approximately equal.

Towards the right-hand side of Figure A11, and closer to the observer the stationary micromanometer board can be seen. A closeup of the front side can be seen in Figure A12, a photograph taken during the operation of the cylinder. The micromanometers M_1 and M_2 shown schematically in Figure A10 are in the center of the manometer board, the outside one being the feed line manometer, M_2, and the inside one, M_1, indicating the actual internal pressure

of the cylinder. The two manometers on the right- and left-hand sides of the manometer board are feed line manometers for the guard sections, and their levels are approximately equal to the level of the line manometer of the primary feed line. All three liquid levels were significantly higher than the level of the central manometer indicating the internal pressure of the center section of the cylinder.

In practice the cylinder was operated very close to saturation which was an easily observed phenomenon. As an example, saturation occurred in the center section when the center manometer level in Figure A12 reached a height of 18.9 cm above the bottom of the manometer board. As can be seen in this figure the cylinder is being operated with an internal pressure which is less than one centimeter of heptane below atmospheric. The internal pressure in the guard sections while not known directly was adjusted by maintaining the line manometer levels of the guard sections approximately one half centimeter below that level which was observed to cause saturation of those sections.

D. Thermocouples

The thermocouples used to monitor the surface temperature of the cylinder during its operation were made from 0.003 inch copper, and 0.003 inch constantan. The copper was double glass covered electrolytic grade supplied by the Driver-Harris Corporation. The constantan used was also insulated with two layers of glass obtained from the same supplier under the trade name "Advance." Because of the high electrical resistivity of the 0.003 inch constantan, the thermocouple leads were brought out to one of the junction boxes located at the end of the cylinder and joined respectively to 0.020 inch copper and constant leads. The heavier gauge constantan was also supplied by the Driver-Harris Corporation, and was chosen because it gave rise to the same thermoelectric potential with copper to within 1 microvolt when the junctions were maintained at 32° and 100°F as did the smaller gauge constantan.

With this choice of thermocouple materials a thermoelectric potential of 1418.6 microvolts was generated when the two junctions were at 32° and 100 °F, and since the potential generated comes very close to being a linear function of the temperature difference between junctions, the error incurred by changing wire gauge, allowing for small differences in composition, was more than compensated for by the increased sensitivity of potential measurements. In this latter regard the deflection produced in a galvanometer by a small potential difference is inversely proportional to the line resistance of the thermocouple plus galvanometer circuit.

The junction itself was made by butt soldering the two 0.003 inch thermocouple leads with a small flake of silver solder. A micromanipulator used in conjunction with a microscope was used to align the leads. Figure A13 shows two photomicrographs of a typical diatomaceous earth plug with the thermocouple junction installed. This particular junction was discarded because of the inadvertent spread of epoxy resin over the junction itself. However, the two shots clearly show the junction on the top side, how epoxy resin was used to hold the junction flush against the cylinder surface, and how this resin supports the leads as they are brought around to the sides of the diatomaceous earth plug and then in to where they eventually re-emerged through a hole drilled through the bottom. The scale divisions in these photomicrographs are 0.01 inch apart. In practice the finished thermocouple plugs proved difficult to make, and several efforts were required to produce a plug in which the thermocouple junction lay flush against the diatomaceous earth surface, and was also free from the epoxy resin used to hold the ends in place. After a thermocouple plug was proven to be satisfactory the leads were drawn through the stainless thermocouple conduits, and the thermocouple plug was drawn and pushed into its final position. Before the final positioning a narrow band of epoxy resin was placed on the top edge of the plug both to hold the plug in place, and also to seal the center section from external air leaks. This latter requirement was quite important since the internal pressure within the outer diatomaceous earth sleeve was always less than atmospheric,

the evaporating fluid being drawn to the surface by capillary action. However, it was also necessary to ensure that the plug itself was not sealed off from the rest of the cylinder by an epoxy film. The fact that the surfaces of the plugs were evaporating surfaces can be seen by reference to Figure A3.

E. Materials Used

1. Evaporating Fluids

The volatile fluids used in this study are n-heptane and n-octane. These liquids were selected for three reasons: (1) The anticipated vaporization velocities would be high enough to significantly affect the boundary layer parameters from those found during fluid flow around a solid cylinder, but still low enough so that it was possible to measure the existing flow rates with great accuracy using the 3/8" injector apparatus described earlier. Also, (2) The boundary condition of zero concentration of the evaporating fluid in the free stream would not be affected by the atmospheric humidity. Finally, (3) The physical properties of the fluids are well known as a consequence of the large amount of experimental information available on those hydrocarbons (11, 34, 43, 47).

Both of these fluids used were supplied by the Phillips Petroleum Company. The "Pure" grades were used, which have a nominal purity of 99 mole per cent. The purity was checked by measuring the refractive index and comparing the measured values with those cited in reference (43) for the pure components at this temperature. The measured refractive index of n-heptane was 1.3850 which compares with a value of 1.38511 cited in the reference above. The measured value for the sample of n-octane used was 1.3950 which also agrees with the accepted standard of 1.39505 listed in the reference above.

The favorable comparisons with the accepted standard re-

fractive indices substantiate the stated minimum purity level of 99 mole per cent. Because of the method used by the manufacturer in preparing "Pure" grade examples, distillation, it is expected that the impurities would have volatilities very close to those of the hydrocarbon studies, and the probable error incurred by assuming the measured evaporation rates were equal to the evaporation rate of the pure component would be an order of magnitude less than the relative impurity level in the samples used.

2. Diatomaceous Earth Evaporating Sections

The porous sections of the cylinder were made from the "Fine Grade" diatomaceous earth known commercially as Allen Filter Material. The same material has been used in other studies of mass transport in this laboratory (7, 45), and has always worked well. Its main attributes are (1) it is easy to machine, (2) it has a very high porosity, and (3) a small cell size. In the latter regard it has been established experimentally that the capillary action of this material is sufficient to maintain a wet surface using water at room temperatures over an adverse pressure differential of 13 inches of water.

Also, during the course of this investigation it has been found that there was no detectable difference in observed evaporation rates during operation of the cylinder over an internal pressure range of from atmospheric minus two centimeters (heptane and octane at 100 ^{o}F) up to atmospheric. This observation is important

because it substantiates the implicit assumption that the air stream "sees" a wet surface or film of the evaporating fluid at all times.

IV. EXPERIMENTAL MEASUREMENTS

Discussions about the calibrations, measurements, calculations, and the anticipated uncertainties in the measurements or in the assumed physical properties of the system considered, are presented in this section.

A. Evaporation Rates

As discussed previously the vaporization rate measurements were made by adjusting the injection rate of the 3/8" injector until it matched the evaporation rate from the center section of the porous cylinder as evidenced by the observation of the two manometers indicating the line and cylinder (center section) pressures respectively. The uncertainties encountered with this method of evaporation rate measurement are very small, and will be discussed below.

The injector itself is surrounded by an oil bath which is maintained at 100 ^{o}F by using a platinum resistance thermometer in conjunction with an electronic control circuit used to control an oil bath heating element. The temperature excursions were very small, and since the specific volume of either n-heptane or n-octane at atmospheric pressure changes by less than 0.08% in going from 99.5 ^{o}F to 100.5 ^{o}F (43), the error incurred by assuming that the contents of the injector were expelled at the mean temperature of the injector bath during the duration of a run is completely negligible. Similarly the effect of variations in pressure of the ejected fluid may be assumed inconsequential, as it can be estimated from observing the

pressure drop encountered by the liquid feed between the "line" manometer and the cylinder internal pressure manometer that the pressure of the fluid leaving the injector ranged between atmospheric and atmospheric plus a four foot head of the ejected fluid for all runs.

The feed lines used were standard seamless stainless tubing with an internal diameter of 0.072 inches. The fluid leaving the injector must travel through approximately forty feet of tubing before reaching the cylinder of which approximately twenty feet are maintained at a constant temperature through an oil line trace. Oil recycles continuously through this "trace" using oil drawn from the isothermal injector oil bath. The unprotected length, about 20 feet, represents a total volume of about 16 cm^3 which is comparable to the volume of fluid displaced by the injector on any given run. If the mean temperature of the hydrocarbon in this line were to change by 3.0 ^{o}F between the start and completion of an injector run, which is a maximum figure, the error induced by assuming that the mass of hydrocarbon retained in the feed line was constant at the beginning and end of an injector run (so that a mass of fluid equal to that displaced from the injector reached the cylinder surface and evaporated) could amount to 0.25% of the total mass displaced by the injector.

Since the actual mass flow rates are obtained from an integrated average of the injector displacement rates during a run, and these rates are controlled to 1 part in 10,000 by use of a preset counter mechanism, described by Chen (7), the total uncertainty involved in measuring mass flow rates is essentially the same as

that due to changes in the specific volume of the residual hydrocarbon feed retained in the injector and in the feed lines during the completion of a run. This uncertainty for the average run is estimated to be on the order of 0.25%.

Uncertainties in evaluating the surface area of the evaporating center section arise principally from the use of an epoxy resin to bond the diatomaceous earth sleeves to the lead gaskets at each end, and to cement the thermocouple plugs in place. It was determined experimentally that the freshly mixed resin would penetrate approximately 0.008 inch into a fine grade diatomaceous earth sample of the material used in making the porous sleeves. It is presumed that the rapid polymerization rate of the setting resin prevented further diffusion into the diatomaceous earth sample. In constructing the cylinder a great effort was made to make the epoxy bonded seals between the evaporating sections and the lead gasket on the inner edge of the diatomaceous earth sleeve so that the outside surface would be unobstructed. Inspection of the finished cylinder (ref. Fig. A2 and A3) showed that these attempts were largely but not completely successful, a result which leads to an estimated 0.006 inch uncertainty concerning the effective length of a two inch porous section. In the case of the thermocouple plugs a ring of epoxy resin appears as a result of an endeavor to fill in the cavity between the cylinder surface and the plug to avoid creating irregularities in the resulting flow field. The surface area in question here is considerably less than that involved in bonding the end of each evaporating

section to the lead gaskets though, and is probably less than the error involved in estimating this loss of evaporating surface area.

Since each diatomaceous earth section is 2.000 ± 0.001 inches long by 1.000 ± 0.0005 inches in diameter, the uncertainty in the machined surface area is about 0.07% while the uncertainty in surface area due to not including that portion of the surface blocked by an epoxy film is on the order of 0.25%.

Combining the uncertainty in determining the liquid feed rate with the uncertainty involved in calculating the effective evaporating surface area the total uncertainty of the calculated evaporation rate per unit area is on the order of 0.35 per cent. In obtaining this estimate the square root of the sum of squares rule for random errors with no correlation between them was assumed.

B. Cylinder Surface Temperature

The surface temperature of the cylinder was measured by 0.003 inch copper constantan thermocouples mounted on each of two diatomaceous earth plugs per section. All thermocouples were made from the same materials and a representative sample of these materials was used for a calibration in this laboratory. A potential of 1418.6 microvolts was created at 100 ^{o}F when the cold junction was maintained at the ice point. It has been established in this laboratory that temperature measurements made with calibrated copper-constantan thermocouples are generally accurate to within $\pm$ 0.1 ^{o}F. However, as can be seen from Figure 5 point measurements of the cylinder surface temperature appear to have a standard deviation from the mean of approximately 0.5 ^{o}F when normal heptane was used as the evaporating fluid. This surprisingly large deviation was not observed with runs made with n-octane where the mean standard deviation of individual surface temperature measurements was 0.1 to 0.2 ^{o}F.

The only possible explanation for the observed deviations from a mean surface temperature is that the mean temperature of the cylinder was not constant during the course of a run, being influenced by the mean temperature of its surroundings. An approximate energy balance was made which indicated that radiant energy transferred from the cylinder surroundings could easily amount to ten per cent of the total energy required to affect the vaporization process. A more rigorous analysis was not possible

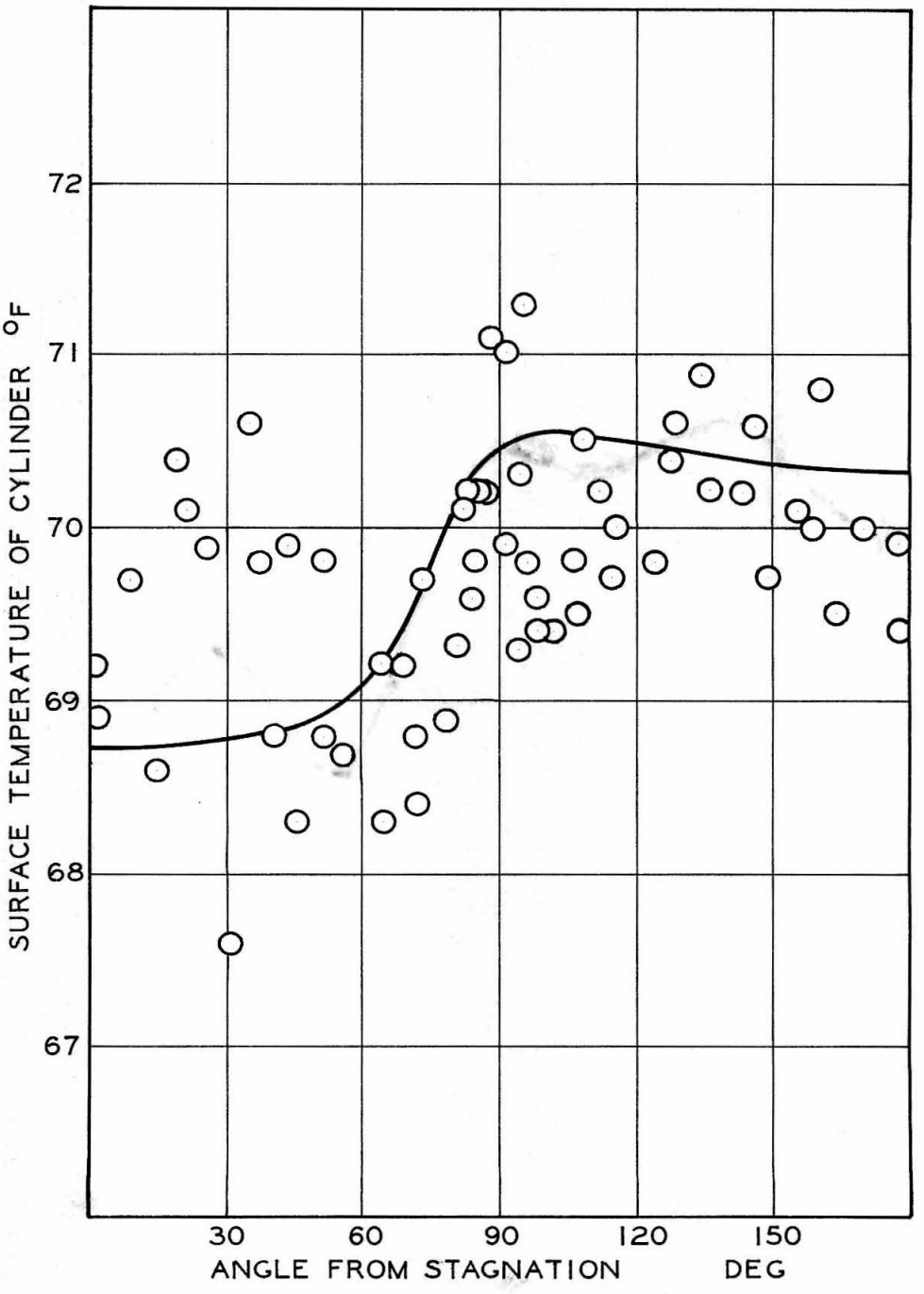

Fig. 5 Surface Temperature of Porous Cylinder Horizontal n-Heptane, U = 8 feet/second, $Z_t = 0.013$

because there were no temperature measurements made which would allow the evaluation of energy conducted to the center section from the exposed ends of the cylinder. Further such an analysis would still have required that the fluctuations in the temperature of the cylinder surroundings be documented. The desirability of these data was not anticipated.

However for purposes of evaluating the gross Sherwood Number the available surface temperature data indicate that, although the surface temperature of the cylinder was a function of time as well as angle from stagnation, the fluctuations did not amount to more than 0.5 ^{o}F, and by taking a statistical mean it is felt that the mean temperature at which the vaporization runs were made is known to within ± 0.2 ^{o}F in the case of n-heptane, and ± 0.1 ^{o}F for runs made using n-octane. The possible reasons for the greater stability of the observed surface temperature behavior with runs made using n-octane will be discussed in more detail later.

The effect of longitudinal temperature gradients is small as evidenced by the small differences in the mean surface temperatures of each of the three porous sections. The mean temperatures sensed by the guard section thermocouples at a point 9/16 inch away from the boundaries of the center section (the guard section thermocouples were not located at the center of the sections, c.f. Fig. A2) were never more than 2 ^{o}F higher than the mean temperature of the center

section. At this point it should be noted that the highest temperatures were always recorded by the thermocouples on the south guard section. Temperatures sensed by thermocouples on the north guard section were usually halfway between the temperatures recorded by the center section thermocouples and those of the south section. This lack of longitudinal surface temperature symmetry presumably occurs because the vacuum jacket, which fits around the north brass supporting rod during operation, shielded the north brass supporting rod from direct energy transfer. Because the vacuum jacket did not provide a low resistance thermal circuit to the north brass supporting rod less energy was conducted longitudinally to the north evaporating section through the brass core. To better appreciate the above discussion the reader is referred to Figure A1 showing the position of the vacuum jacket when the porous sections are exposed, and to Figure A7 taken looking south during a run.

Summarizing, the effect of longitudinal conduction in producing axial temperature gradients for the center evaporating section should not introduce an uncertainty of more than 0.1 ^{o}F in the determination of an overall mean temperature for the center section, and the estimated uncertainty involved in using a mean temperature is 0.25 ^{o}F for n-heptane and 0.1 ^{o}F for n-octane. The uncertainty in computing the mean temperature based on the various thermocouple readings is 0.2 ^{o}F for heptane, and 0.1 ^{o}F for octane. If these uncertainties are assumed to be independent of each other they may be combined according to a square root of the sum of squares law

for the total effect of randomly distributed uncertainties. Hence the total anticipated uncertainty in the cylinder surface temperature for this investigation is 0.35 ^{o}F for the measurements made with n-heptane, and 0.20 ^{o}F for measurements made with n-octane.

C. Sample Purity

The effect of impurities in the fluid investigation would be to introduce uncertainties into data derived from the measured mass evaporation rates and cylinder surface temperatures. Principally in deriving the Sherwood and Frössling groups which characterize mass transport rates, a vapor pressure is assumed which corresponds to that of the pure component at the measured mean temperature prevailing during the evaporation process. If the vapor pressure of the impurities did not correspond to that of the pure components such an assumption would be in error. Secondly, the diffusion coefficient which appears in the derivation of the mass transfer groups would also be subject to uncertainty with the addition of impurities. Fortunately, the method of preparation of pure grade samples tends to alleviate both of these objections, and the uncertainty introduced by sample impurities can be shown to be an order of magnitude less than the actual impurity level.

Concerning the effect of the supposed impurities on the vapor pressure of the sample, the n-heptane and n-octane obtained from the Phillips Petroleum Company are purified through fractionation in the manufacturing process. Hence, the impurities present would have vapor pressures very nearly equal to that of the pure component studied, and their effect in this regard would be minimal. The diffusion coefficient of the impurities when expressed in units of mass flowrate would increase approximately in proportion to the square root of the molecular weight. However, it is most probable

that the mean molecular weight of the impurities present is also very close to that of the hydrocarbon studied and certain that the effect on the over-all diffusion coefficient would be less than the actual impurity level.

D. The Free Stream Reynolds Number

The free stream Reynolds Number is computed from the measured weight flowrate of air, the diameter of the cylinder, and the viscosity of the air. The derived quantity which is based on a mean velocity through the jet exit is then increased by the factor 1.08 to account for differences between the average velocity seen by the horizontal cylinder and the mean velocity through the jet opening. The formula used for computing the free stream Reynolds Number is:

$$Re = 1.08 \frac{D\dot{m}_{air}}{g_o \eta_{air} A_{duct}}$$

where

$$u = 1.08U = -.08 \frac{\dot{m}}{\sigma A}$$

In the formula above, the cylinder diameter is known to 0.001 inch or 0.1%. The jet exit area was measured by Cuffel (13) to within an estimated accuracy of 0.1%. The uncertainty in the mass flowrate of air through the jet opening and the origin of the factor 1.08 merit some discussion and will be considered presently.

During operation the mass flowrate through the duct was maintained constant to within ±0.1 per cent. This was done by monitoring the blower RPM with a control system using a preset counter mechanism. The apparatus used to control the blower speed is comparable to that used to control the injector speed and was discussed earlier. Adjustments in the counter setting could be

made, if necessary.

The venturi meter discussed earlier in this work, shown schematically in Figure A6 was used to measure all air flowrates. In this work, either a 3- or a 6-inch throat diameter venturi was used, depending upon the weight flowrates desired. The design of the venturies and the calibrations for them are based on the research of Jorrison (29), who conducted an exhaustive investigation on the properties of venturi meters.

Jorrison (loc. cit.) published the results of test performed with over two hundred venturies. His results are expressed in terms of a venturi coefficient relating the actual pressure drop between the entrance and the throat of a venturi to the theoretical pressure drop which would prevail for the "one dimensional" flow of a perfect inviscid fluid. A sample of his results appear in Figure 6; from these it is judged that mass flowrates through the apparatus may be reproduced to within 0.1% in this laboratory and are known with an absolute accuracy of 0.5%.

The factor 1.08 is an estimate of the ratio of mean velocity in the center of the jet to the mean jet velocity. The velocity profile was measured by Venezian (58) and Cuffel (13) in the center region of the jet opening. These data, taken at a mean jet velocity of 7.8 feet per second, appear in Figure 7 where the velocity profile is extrapolated to the edge of the jet opening. The extrapolation conforms to the requirement that the area integral of the local velocities must equal the bulk velocity, as determined from the weight flow rate, multiplied by the duct area. It is anticipated that the *relative shape*

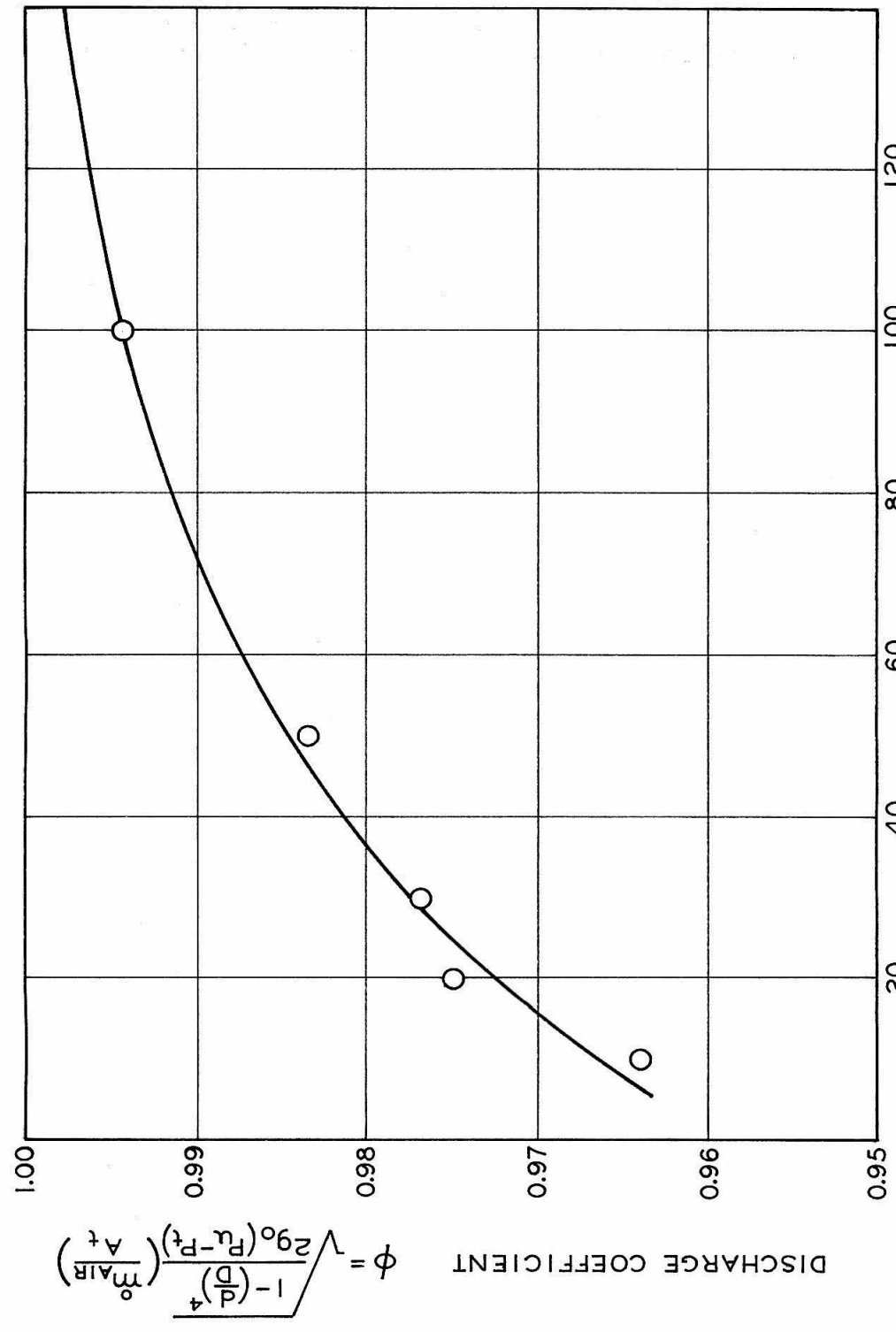

Fig. 6 Venturi Discharge Coefficients for Herschel Type Venturis (29)

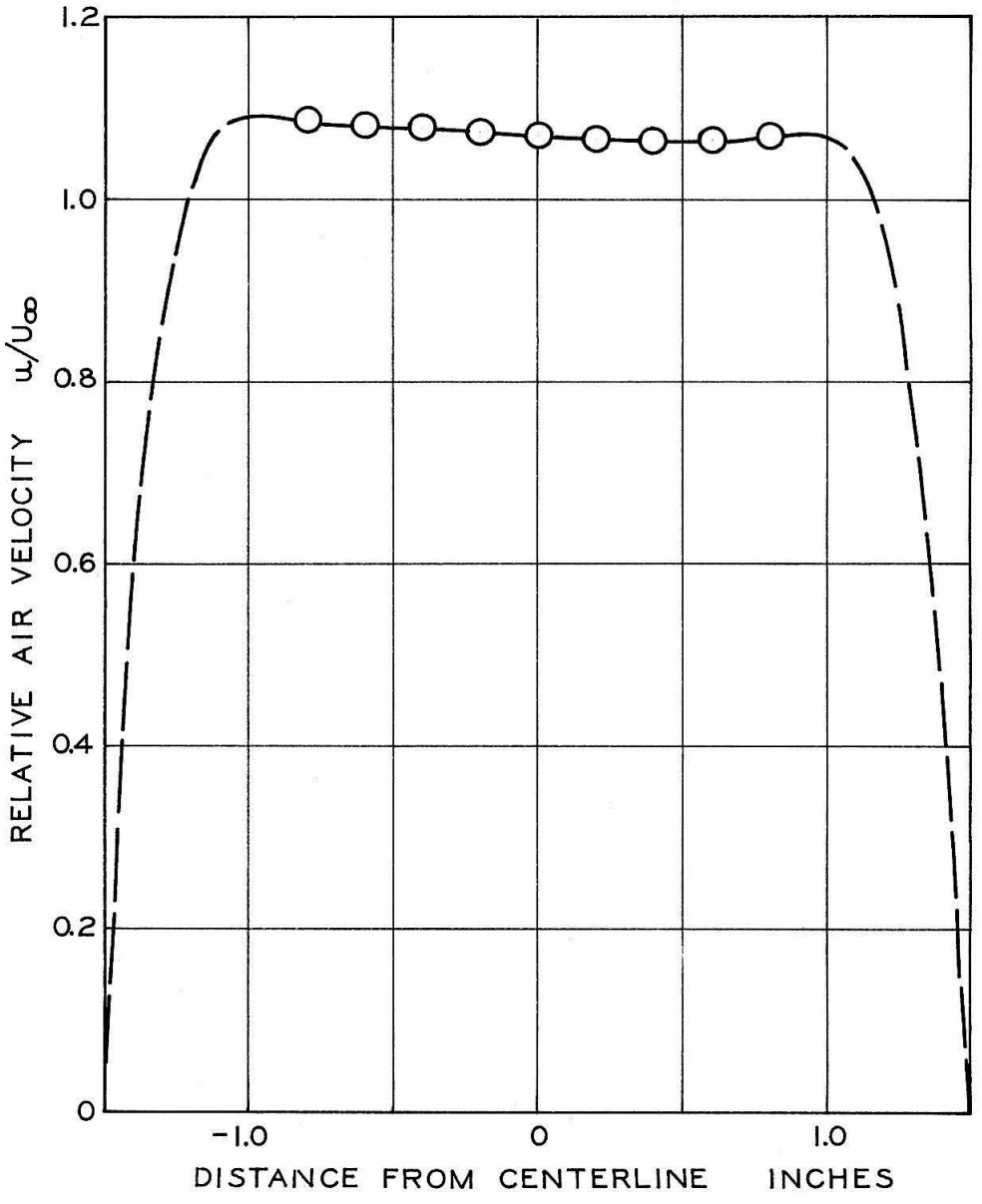

Fig. 7 Velocity Profile from 3 × 12 Inch Duct Used in This Study (13, 58)

of the velocity profile of the jet is a function of the mass flowrate. However in this regard the work of Venezian and Cuffel indicate that the velocity profile is quite flat over the center two-thirds of the jet width, and the ratio of peak to average velocity assumed above does not seem untoward. It is estimated that the relative velocity profile (for runs at different Reynolds Numbers) would not differ by more than 1 per cent on account of the short length downstream of the duct contraction, and that the absolute velocity in the center of the duct is known to within 1.5 per cent. Considering the factors above, it is estimated that the uncertainty in the free stream Reynolds Number is less than 2.0 per cent. Becuase the measured evaporation rates are approximately proportional to the square root of the Reynolds Number, this uncertainty would lead to a 1.4 per cent uncertainty in results presented as a function of Reynolds Number.

E. Free Stream Turbulence Level and Integral Scale of Turbulence

For all runs made without the turbulence grid and jet extension, the free stream turbulence level as measured by Cuffel (loc. cit.) was 1.3 per cent. The measurements were made using the Schubauer hot wire technique for measuring eddy conductivity, and the estimated uncertainty in the level of turbulence obtained from these measurements is $\pm$ 0.4, e.g., $0.9 \leq Z_T \leq 1.7$ per cent.

The higher turbulence levels were created by the use of a turbulence grid which consisted of a plate with 7/8 inch holes punched at 1-inch intervals on a square lattice. The turbulence created by such a grid is a strong function of the distance downstream of the grid and has been investigated by many workers (2, 3, 5, 14, 15, 22, 57). These workers reported that the high level of turbulence prevailing at downstream distances less than 10 hole diameters from the grid is non-isotropic so they correlate their results in terms of an "apparent" turbulence level defined as the ratio of the mean longitudinal fluctuating velocity component to the time average local velocity. Thus:

$$Z_T = \frac{1}{U} \left\{ \overline{u'^2} \right\}^{1/2}$$

Their results are in substantial agreement and indicate that the high apparent turbulence levels created in this laboratory can be predicted to within 10 per cent. Figure 8 shows the turbulence levels anticipated for various distances downstream of the turbulence grid used in this study. For details concerning the origin of this curve the reader is referred to Proposition 5 in the Appendix. The distance of the

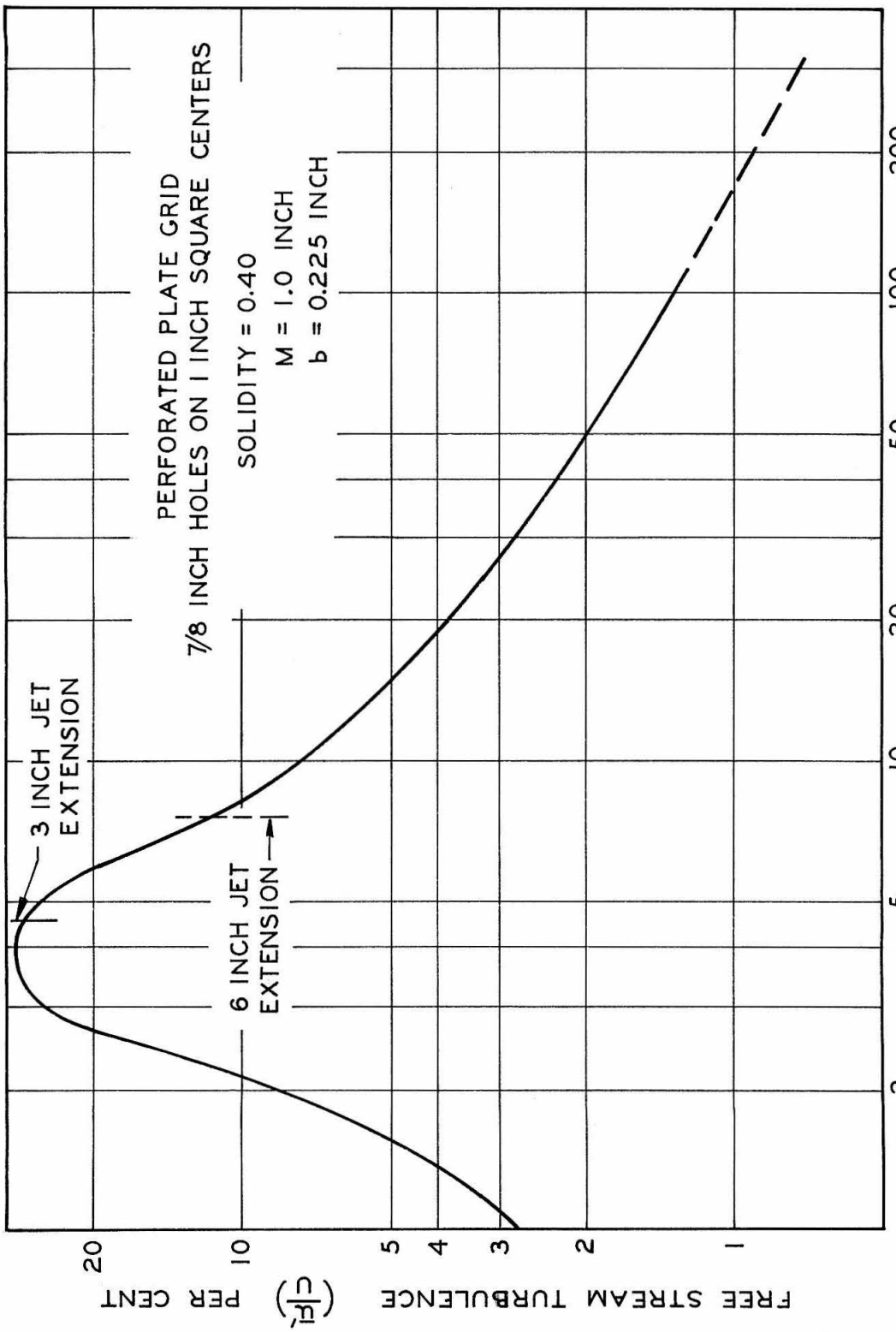

Fig. 8 Level of Turbulence Downstream of Perforated Plate Grid

cylinder stagnation point downstream of the turbulence grid was 4.512 inches for an estimated free stream turbulence level of 0.26% and 7.428 inches for an estimated turbulence level of 11%.

The scale of turbulence generated downstream of the turbulence grid is shown in Figure 9. As pointed out by Van der Hegge Zijnen (56) thermal transport from cylinders is a strong function of the scale of turbulence relative to the cylinders diameter. For details on the origin of Figure 9 the reader is again referred to Proposition 5 in the Appendix. The scale obtained from reference to Figure 9 is estimated to be accurate to within 10 per cent. It is 0.67 inches for the run at the high tubulence level, and 0.78 inches for the run at 11% turbulence.

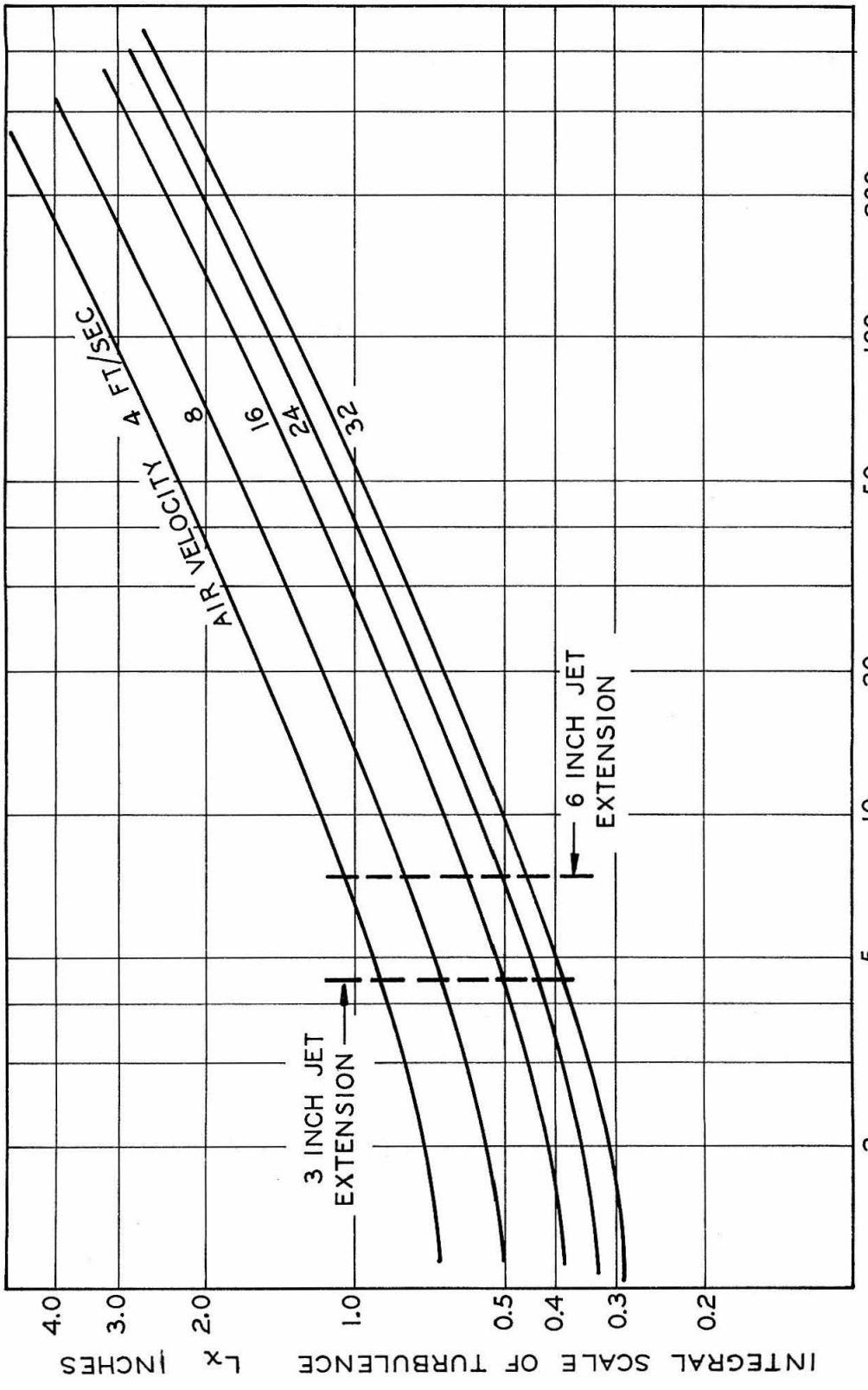

Fig. 9 Scale of Turbulence Downstream of Perforated Plate Grid

F. Effect of Finite Duct Width

Extrapolating test data taken in a finite jet to predict the behavior of a body placed in an "infinite" parallel stream has always caused workers some concern (20, 46). For objects tested in a wind tunnel, the "blockage ratio" is described as the ratio of blocked area to total area available for flow, and it is well known that blockage ratios greater than 0.20 significantly affect the flow around a cylindrical body (1, 21, 52). The effect of high blockage ratios in a tunnel is to compress the fluid streamlines in the region of maximum frontal area producing higher free stream velocities than would exist for the same object placed in an infinite air stream. Simultaneously, the sectional area occupied by the wake is reduced (21, 52).

In the case of a free jet one would anticipate the opposite effect wherein the streamlines would show a greater divergence at the point of maximum area, the wake cross section would be increased, and possibly, that separation would occur earlier than for the same object placed in an infinite air stream. Cuffel (13) predicts tangential velocity components in the vicinity of separation which are substantially less than those which would prevail for the same cylinder placed in an infinite air stream. His work is based on hot wire measurements made in the vicinity of the boundary layer, and he used the correlation of Collis and Williams (9) to transpose his hot wire Nusselt Numbers into local velocities. The results of his work in this area appear as Figure 10 of this thesis since he also worked with a one-inch cylinder using the same air jet with air velocities of 8 feet per second. Also presented in Figure 10 are the

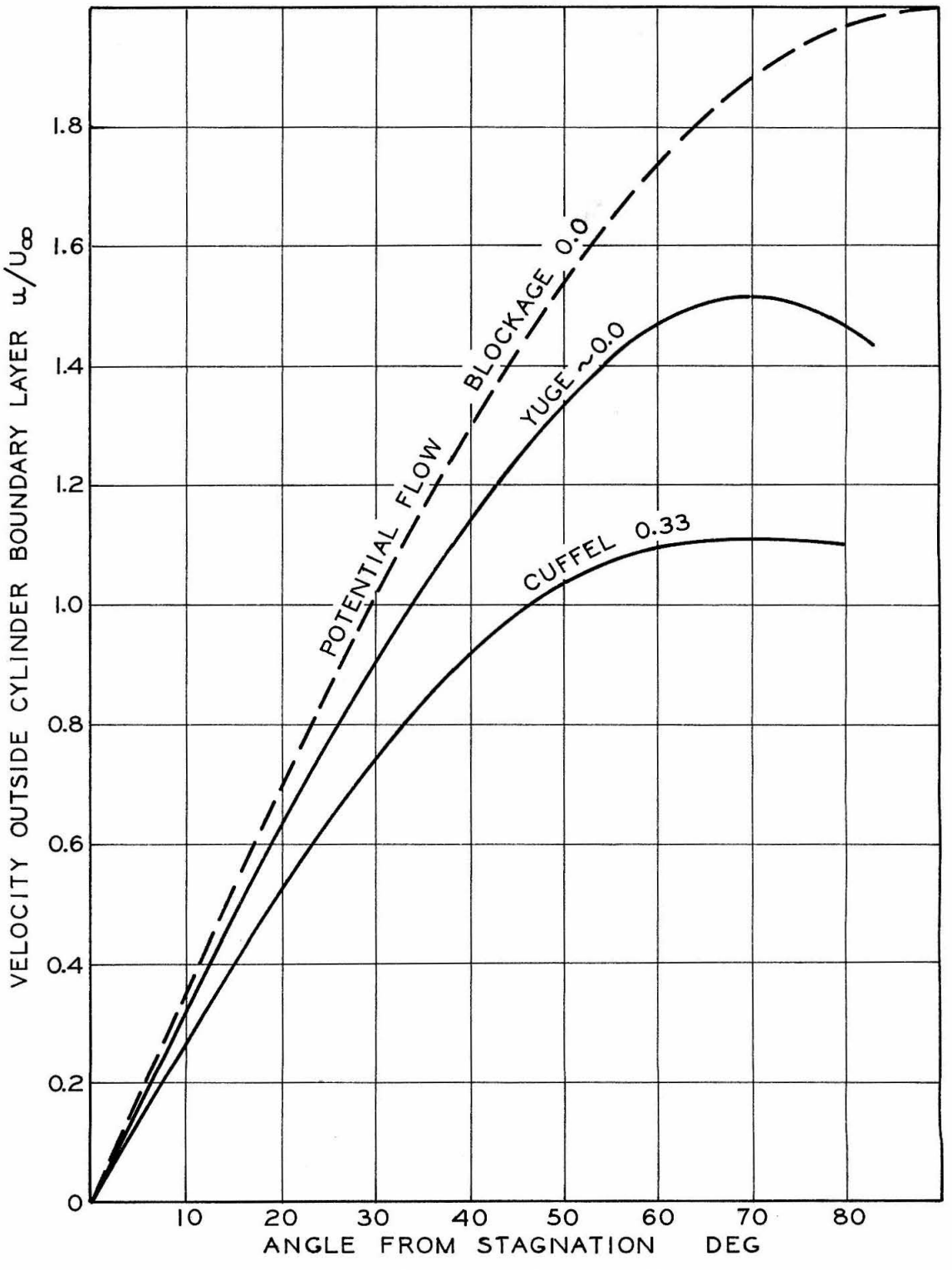

Fig. 10 Local Velocity Profile - Cylinder Placed in a Free Jet

results of Yuge (60) for a cylinder placed in a free jet or tunnel where the blockage ratio is negligible. It will be noted that even for this case local velocities are significantly lower than those predicted by potential flow theory due to the effect of the wake. Yuge's correlation is based on the experimental pressure distributions reported by several investigators, at Reynolds Numbers near 40,000. Regarding Figure 10, Cuffel reports that "the thickness of the boundary layer was not clearly defined beyond 60 degrees from stagnation," indicating possible separation at this point. This is in marked contrast with the observations of others working at lower blockage ratios who report laminar separation at approximately 81 degrees.

The effect of high blockage ratio, 0.33, for a cylinder placed in a free jet is still uncertain. It is hoped that future work will clarify this problem.

G. Air Temperature

The air temperature was measured at a point approximately three feet upstream of the jet exit. A high precision calibrated platinum resistance thermometer was used to measure the air temperature with an accuracy of ± 1 ^{o}F. During the course of this investigation the air temperature was always maintained between 99.8 and 101.1 ^{o}F. During the course of a run the air temperature cycled about 100 ^{o}F due to the action of the control circuit. The error introduced into the calculations by these air temperature excursions is completely negligible and may be disregarded.

H. Air Properties and the Boundary Layer Parameters

The derivation of the Sherwood Number in terms of the measured variables was discussed earlier. The final form shown is arrived at by assuming an isothermal diffusion process for an ideal solution where the mean modified Maxwell diffusion coefficient, $D_{Mk'}$, and the compressibility factor of the mixture, Z, are constant. However, if the mixture of heptane and air (or octane and air) is assumed to be an ideal solution, the differential form of the mass flux is rigorous, and the correct expression for the mass diffusion flux may be obtained by numerically evaluating the differential form through the boundary layer. Since in this work the simultaneous temperature and composition of the fluid in the boundary layer are not known the same results are approximated by evaluating all boundary layer parameters at a temperature halfway between the mean cylinder temperature and that of the air stream.

The diffusion coefficient for the diffusion of heptane into air has been measured in this laboratory (47). Values for the diffusion coefficient of n-octane into air were taken from the International Critical Tables (28). These data along with the data for n-heptane of reference (47) are presented in Figure 11. The Maxwell diffusion coefficient was selected for this work because it is relatively insensitive to composition changes. In the case of n-heptane the diffusion data were obtained at essentially the same temperature and composition as those encountered in this study, and the diffusion coefficient for this system was used with great confidence. The estimated uncertainty is $\pm 0.7\%$, the same uncertainty cited by the investigators (47).

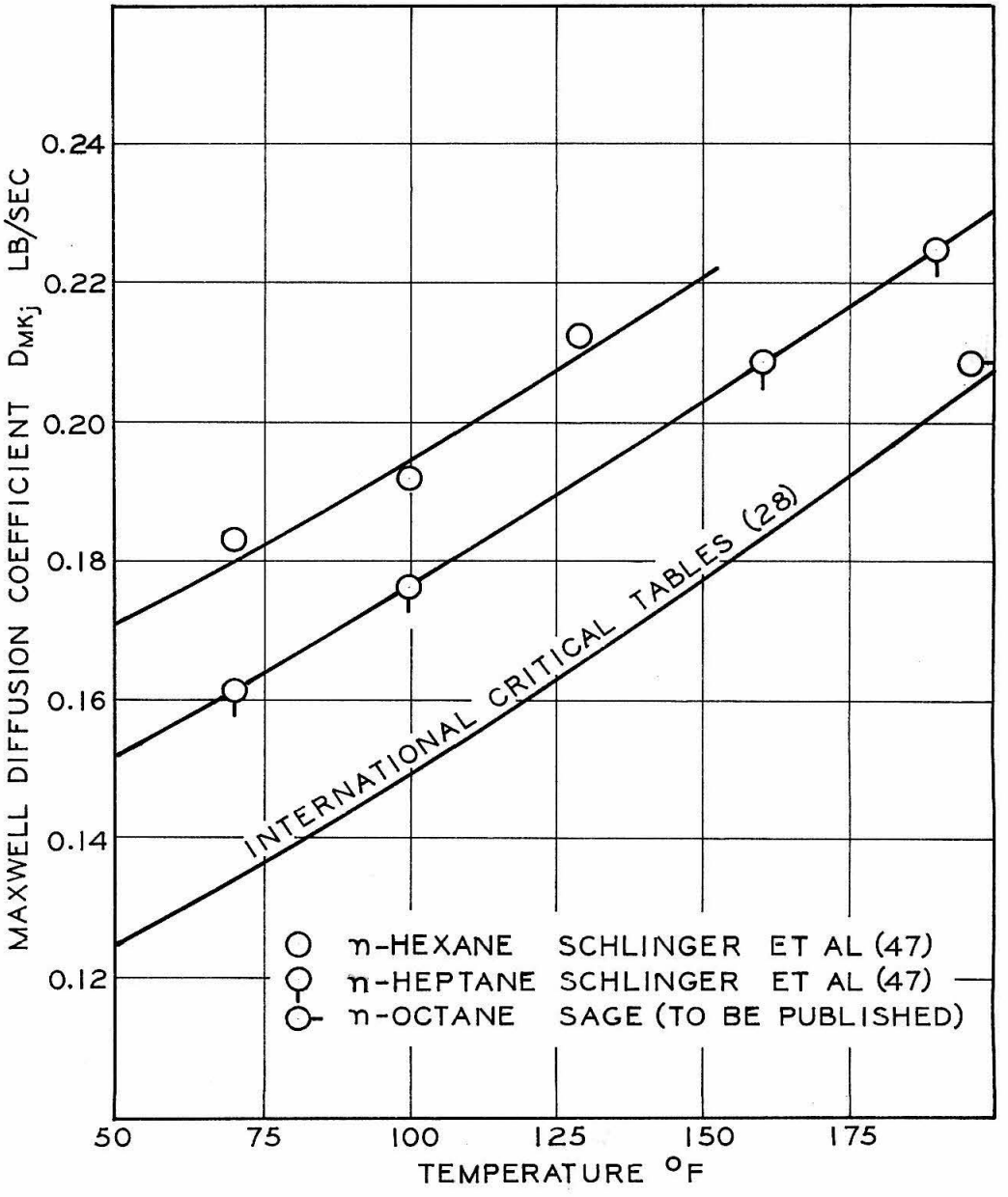

Fig. 11 Maxwell Diffusion Coefficients n-Heptane and n-Octane in Air

The uncertainty in the diffusion coefficient used for the n-octane air system is unknown. Reference to Figure 11 indicates that the reported diffusion coefficient for n-octane may be low. Also the effect of varying composition is unknown. Overall, the author estimates that uncertainty to be ± 3.0%. It is hoped that future work currently underway in this laboratory will improve this estimate.

The evaluation of the compressibility of the mixture can be approached in several ways. The method selected is based on the assumption of an ideal solution between the hydrocarbon and air giving:

$$Z_{mix} = n_{\cdot j} z_j^o + n_{\cdot k} z_k^o$$

In this expression the sub dots denote molar quantities and $n_{\cdot k}$ is the mole fraction of the hydrocarbon. The mole fraction hydrocarbon is never greater than 0.05, and the two phase compressibility factor for the vapor at the temperature and vapor pressure which prevailed during these tests was 0.995 or greater (34, 36). It is estimated that the uncertainty in the mean compressibility factor used is on the order of 0.01 per cent.

I. Standard State Fugacity

The evaluation of the standard state fugacity of the hydrocarbon vapor, f_k^o, when the ideal solution assumption is made regarding the fugacity of the hydrocarbon,

$$f_k = n_k f_k^o$$

requires that the "standard state" fugacity be obtained by a linear extrapolation of a graph at f_k/P vs. P up to one atmosphere of pressure. The validity of the extrapolation process requires that the fugacity of the hydrocarbon vapor be a function only of its partial pressure and temperature.

In this work the "standard state" fugacity of the hydrocarbon in atmospheres is evaluated at the mean temperature of the boundary layer. It will be recognized that the ordinary conception of a standard state fugacity as being the fugacity of the vapor at one atmosphere pressure does not have significance in this case, since the pure vapor does not exist at the temperature and pressure of the vaporization process.

V. EXPERIMENTAL RESULTS

The experimental results, the overall uncertainties, and the implications of these data are presented in this section and compared with the pertinent experimental results of other workers.

A. Sherwood and Frössling Numbers

The Sherwood Numbers characterizing mass transfer rates are plotted against the square root of the free stream Reynolds Number in Figure 12. These data are for an estimated free stream turbulence level of 1.3 per cent, taken without the turbulence grid in place. The choice of the one-half power of the Reynolds Number as the abscissa is a common one and is based on the theoretical considerations discussed earlier.

The data indicate an almost linear dependence on the one-half power of the Reynolds Number which, as indicated earlier, is in accord with "theory." The Sherwood Numbers for n-octane are significantly higher than those obtained with n-heptane, which is also anticipated since the Schmidt Number of n-octane in air at the mean temperature of the vaporization process, 2.39, is 26 per cent higher than the corresponding Schmidt Number for n-heptane, 1.89.

The Frössling Numbers are shown plotted against the square root of the Reynolds Number in Figure 13. These results are most interesting since they indicate that the Frössling Number for mass transfer from a cylinder is almost independent of the Reynolds Number for low free stream turbulence levels and Reynolds Numbers less

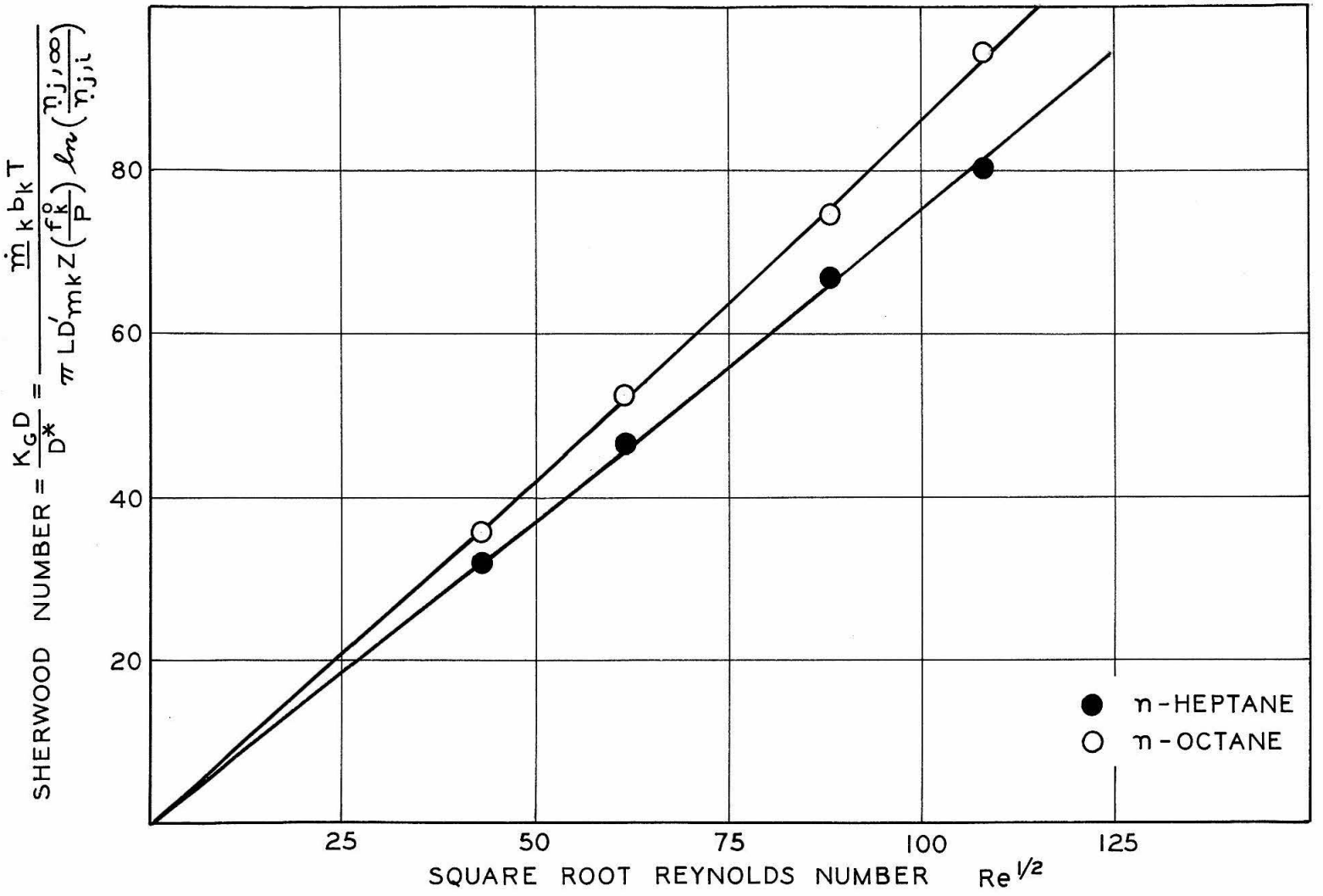

Fig. 12 Material Transport from Cylinders - Sherwood Numbers for Low Levels of Free Stream Turbulence ($Z_t = 0.013$)

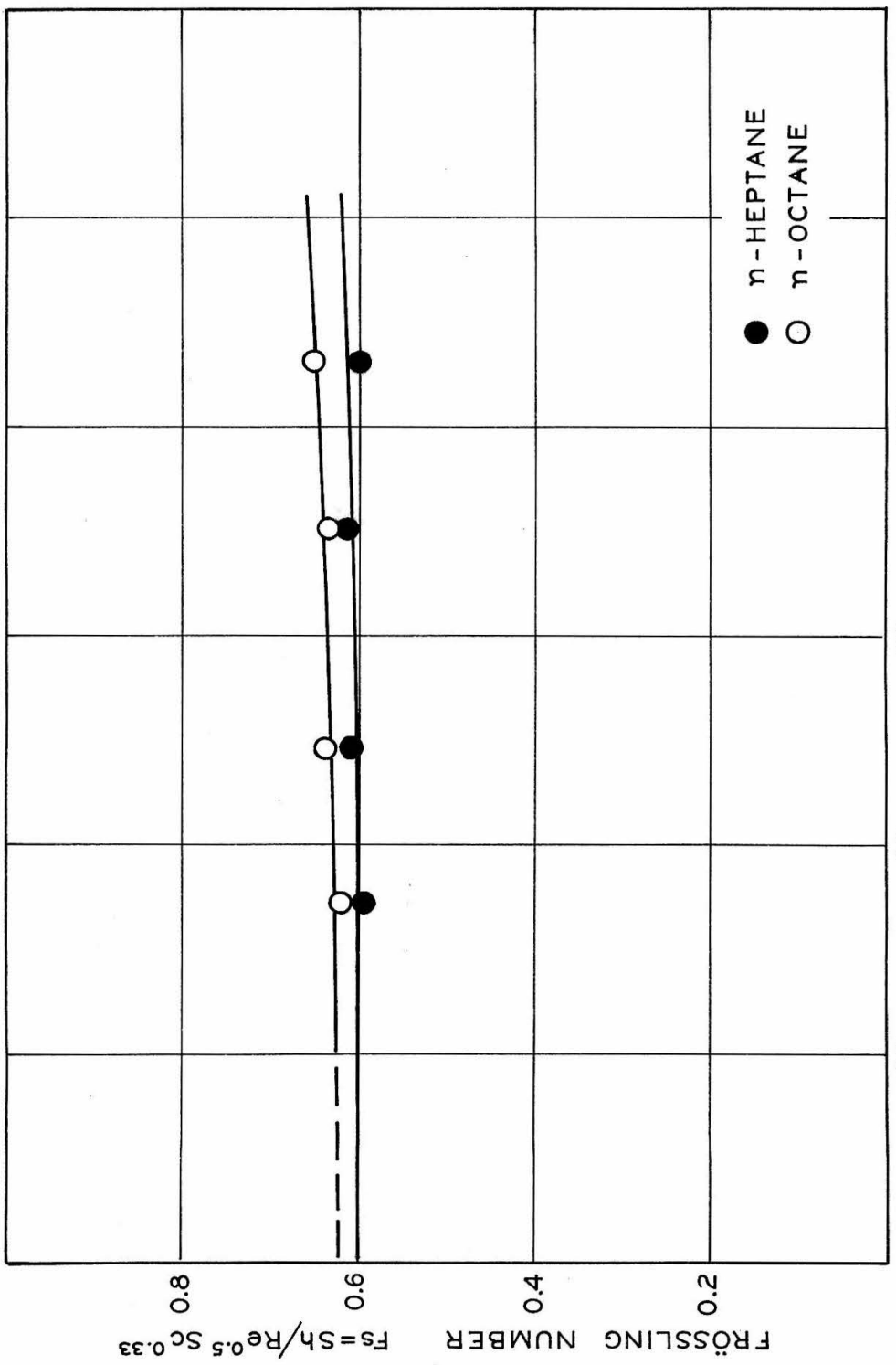

Fig. 13 Material Transport from Cylinders - Frössling Numbers for Low Levels of Free Stream Turbulence ($Z_t = 0.013$)

than 10,000. This is in marked contrast to the behavior of the Frössling Number for heat transfer at lower Reynolds Numbers as reported by this laboratory (19). Also the consistent difference between the observed Frössling Number obtained with n-octane as opposed to those observed with n-heptane would seem to indicate that the one-third power dependence of the Frössling Number on the Schmidt Number is not high enough. If instead of correlating a Frössling Number on the basis of an inverse one-third power of the Schmidt Number, an inverse 0.4 power dependence is assumed, the two curves in Figure 13 would coincide with an intercept of approximately 0.60 for the Frössling Number at vanishing Reynolds Numbers. This apparent dependence of the Sherwood Number on the 0.4 power of the Schmidt Number may be altered somewhat when a more accurate value of the diffusion coefficient of n-octane is available.

The Frössling Number taken at the higher turbulence levels with n-heptane are shown along with the data for the lowest level of turbulence in Figure 14. In constructing this figure it was assumed that the effect of free stream turbulence on mass transport rates diminishes with decreasing Reynolds Numbers until, in the limit as the Reynolds Number approaches zero, the effect of free stream turbulence disappears. This assumption has been made before in this laboratory for the case of energy transport (19) and is in accord with the "theory" presented earlier in all respects except for the indicated curvature. The increasing slope of the curves for the higher turbulence levels is anticipated from the indicated curvature

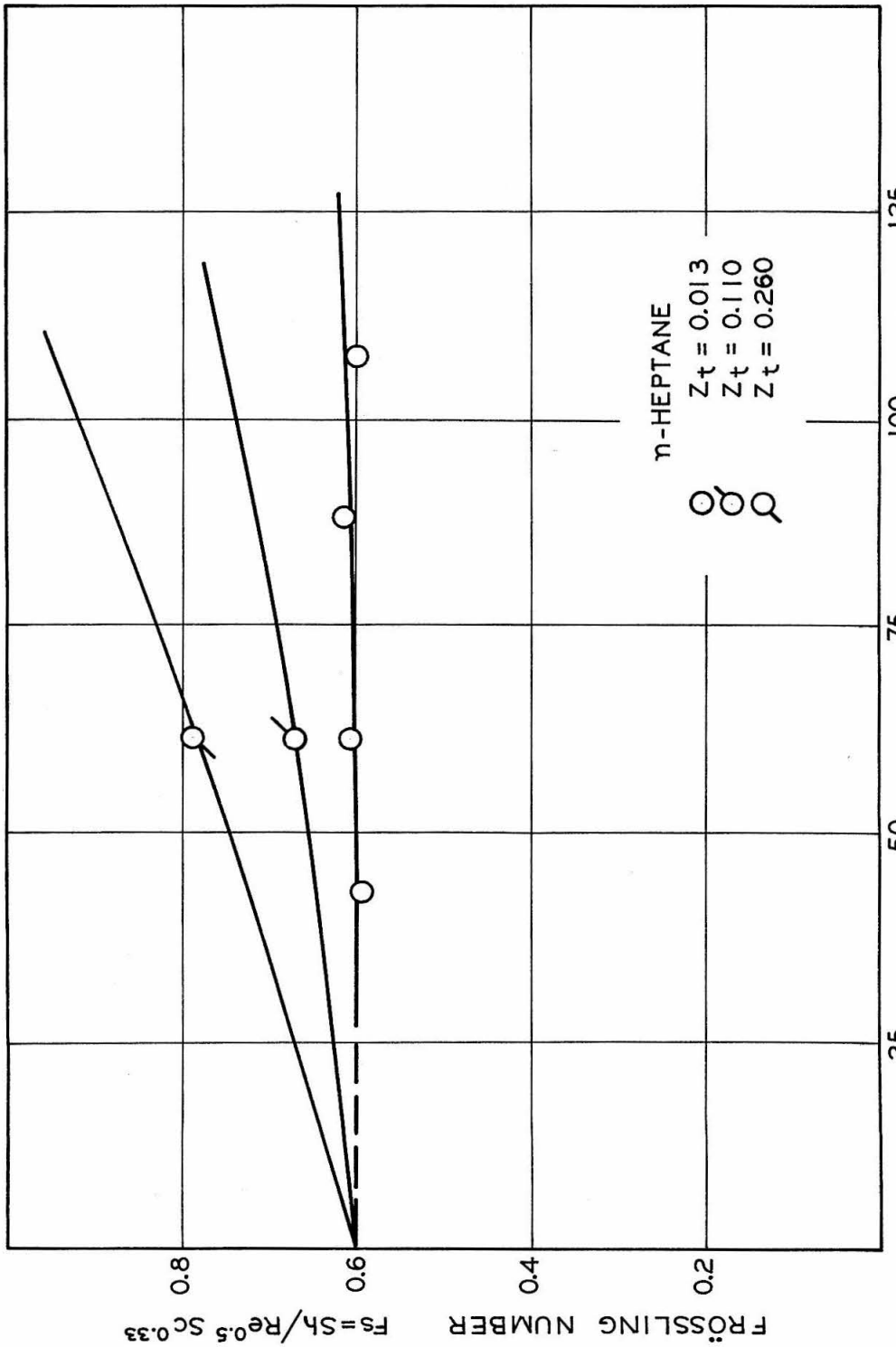

Fig. 14 Influence of Free Stream Turbulence on Transport of n-Heptane from Cylinders

of the data for the low turbulence level.

It will be recalled that the scale of turbulence downstream of a turbulence grid increases approximately as the square root of the downstream distance. The effect of the scale of turbulence on energy transport has been considered by Van der Hegge Zijnen (56), but the limited data available in this study do not warrant a similar comparison for the case of material transport.

B. Experimental Uncertainties

The measured data are tabulated along with the derived Sherwood and Frössling Numbers in Table I in the Appendix. In Table II the uncertainties in the measurements obtained and in the constants used in this study are tabulated. The uncertainties are those discussed in the previous section and are compared on the basis of relative and/or absolute uncertainties. In the case of n-octane the large uncertainty in the numerical value used for the diffusion coefficient causes the absolute uncertainty of the reduced data for this substance to be much greater than the uncertainty of the data for n-heptane. However it will be appreciated that the relative uncertainty, indicating the magnitude of anticipated scatter, is small. The observed trends of the Sherwood and Frössling Numbers obtained with this substance are felt to be fully as reliable as those indicated in the study of n-heptane.

The individual uncertainties are combined by taking the square root of the sum of the squares to obtain an overall uncertainty. This procedure is valid in this case since there is no reason to suspect a correlation between the individual uncertainties involved.

C. Cylinder Surface Temperature

During a run each of the six thermocouples which had been installed on the surface of the cylinder were read many times. In making these measurements the cylinder was rotated so that the surface temperature could be computed as a function of the angle from stagnation.

Upon the completion of this investigation there were over one thousand surface measurements made, and statistical methods were applied to the interpretation of results. A statistical approach was used principally to determine whether a rational explanation for the scatter of the individual points would be apparent, but it was also desired to establish surface temperature trends which could then be described as a function of the free stream Reynolds Number and turbulence level.

It was assumed that the cylinder surface temperature for a constant free stream Reynolds Number and turbulence level could be expressed by a Fourier Series in terms of cosines of even multiples of the angle from stagnation. Thus:

$$T(\phi) = A_o + A_1 \cos \phi + A_2 \cos 2\phi + \ldots + A_n \cos n\phi$$

The functional relationship above was selected because of an anticipated symmetry in the surface temperature about stagnation. It was further assumed that the temperatures of each of the three porous sections could be described by the same series with all coefficients

except the zeroth order term, denoting the average temperature of the section, being equal for each section during a given run.

The Fourier coefficients based on the data from each run were compared on this basis to determine the effect of Reynolds Number and turbulence level on the cylinder surface temperature. A further inspection of these results revealed a definite correlation between the zeroth and first order Fourier coefficients with the mean laboratory temperature which prevailed during a run. In this case the zeroth order Fourier coefficient is the average cylinder surface temperature, while the first order coefficient is indicative of the relative difference between the front and back halves of the cylinder surface during a run. The correlation observed between the first order coefficient and the prevailing laboratory temperature is significant because the front half of the cylinder "sees" the duct interior (and hence would be receiving radiation from an essentially constant temperature source, 100 ^{o}F, for all runs), while the back half of the cylinder faces the surroundings whose mean temperature varied from one run to the next, and presumably varied about the mean during a run. These observations are important because they demonstrate conclusively that the cylinder surface temperature is affected by the temperature of the laboratory surroundings.

This comparison is shown in Table III and also in Figures 15, 16, and 17 showing the variations in the mean cylinder temperature and the first order Fourier coefficient with laboratory temperature. These results for the evaporation of n-heptane at a turbulence level

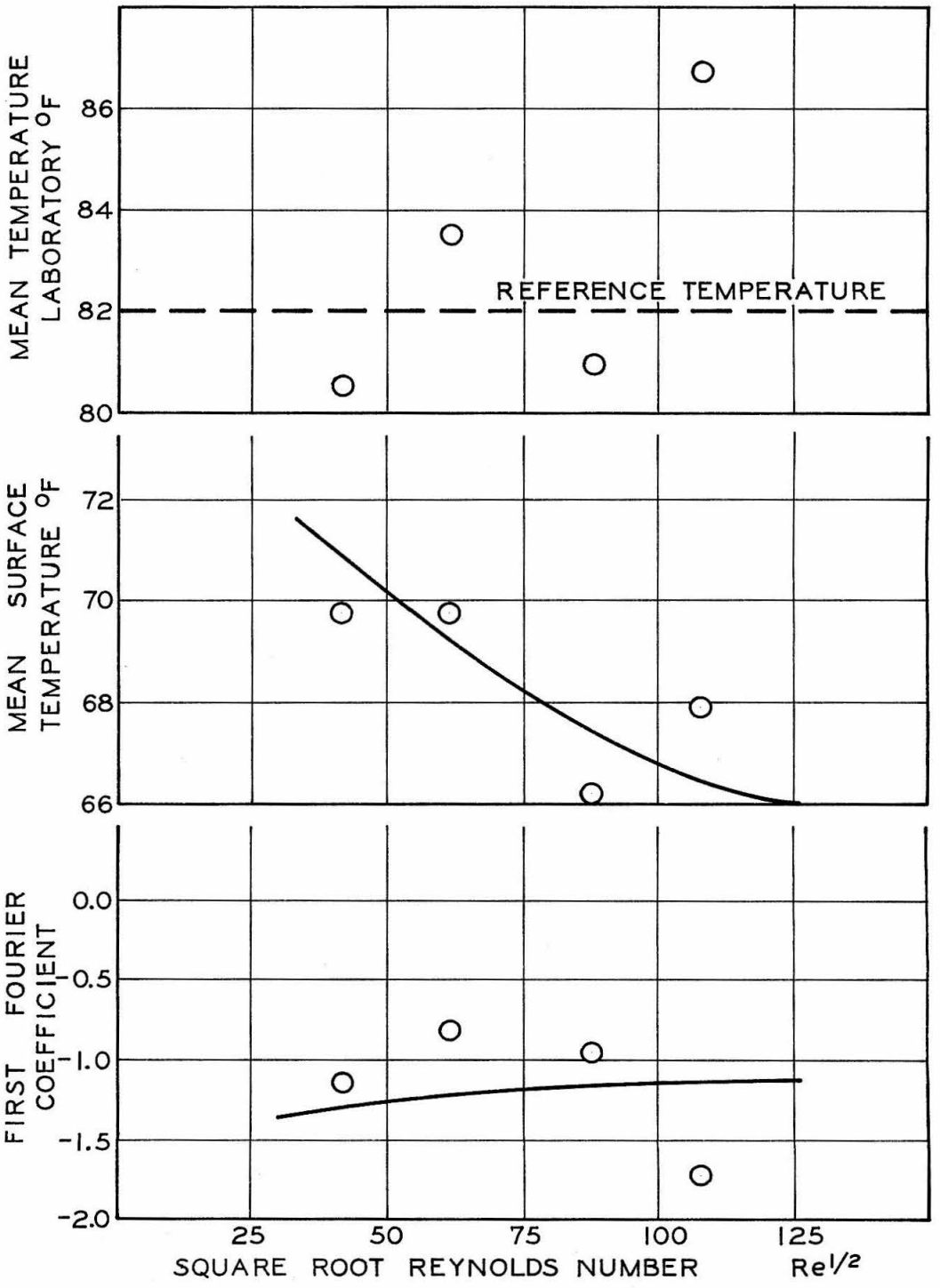

Fig. 15 Surface Temperature of Porous Cylinder - Variation of Mean Temperature and First Order Fourier Coefficient with Laboratory Temperature (n-Heptane, $Z_t = 0.013$)

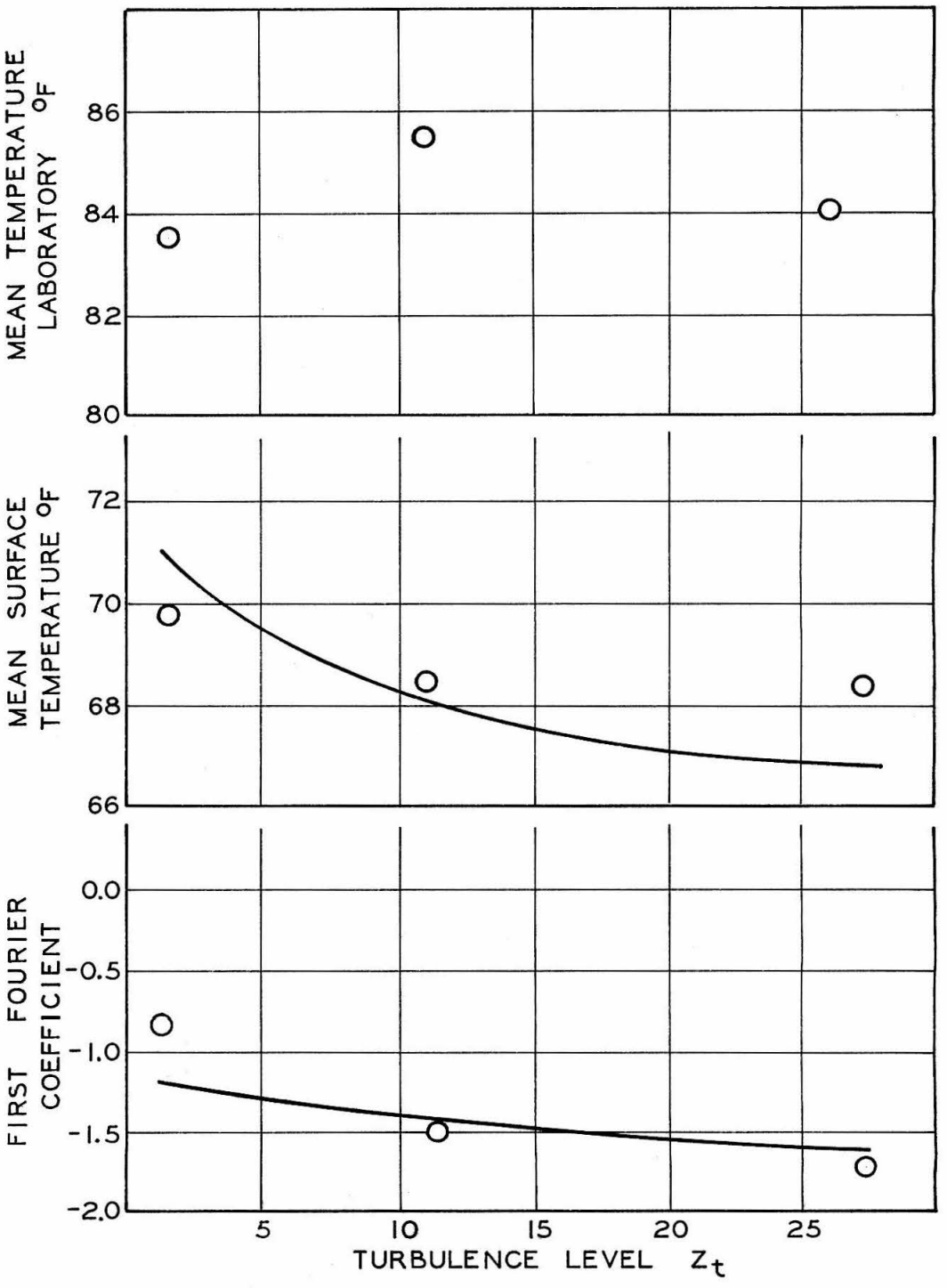

Fig. 16 Surface Temperature of Porous Cylinder - Variation of Mean Temperature and First Order Fourier Coefficient With Laboratory Temperature (n-Heptane, Re = 3780)

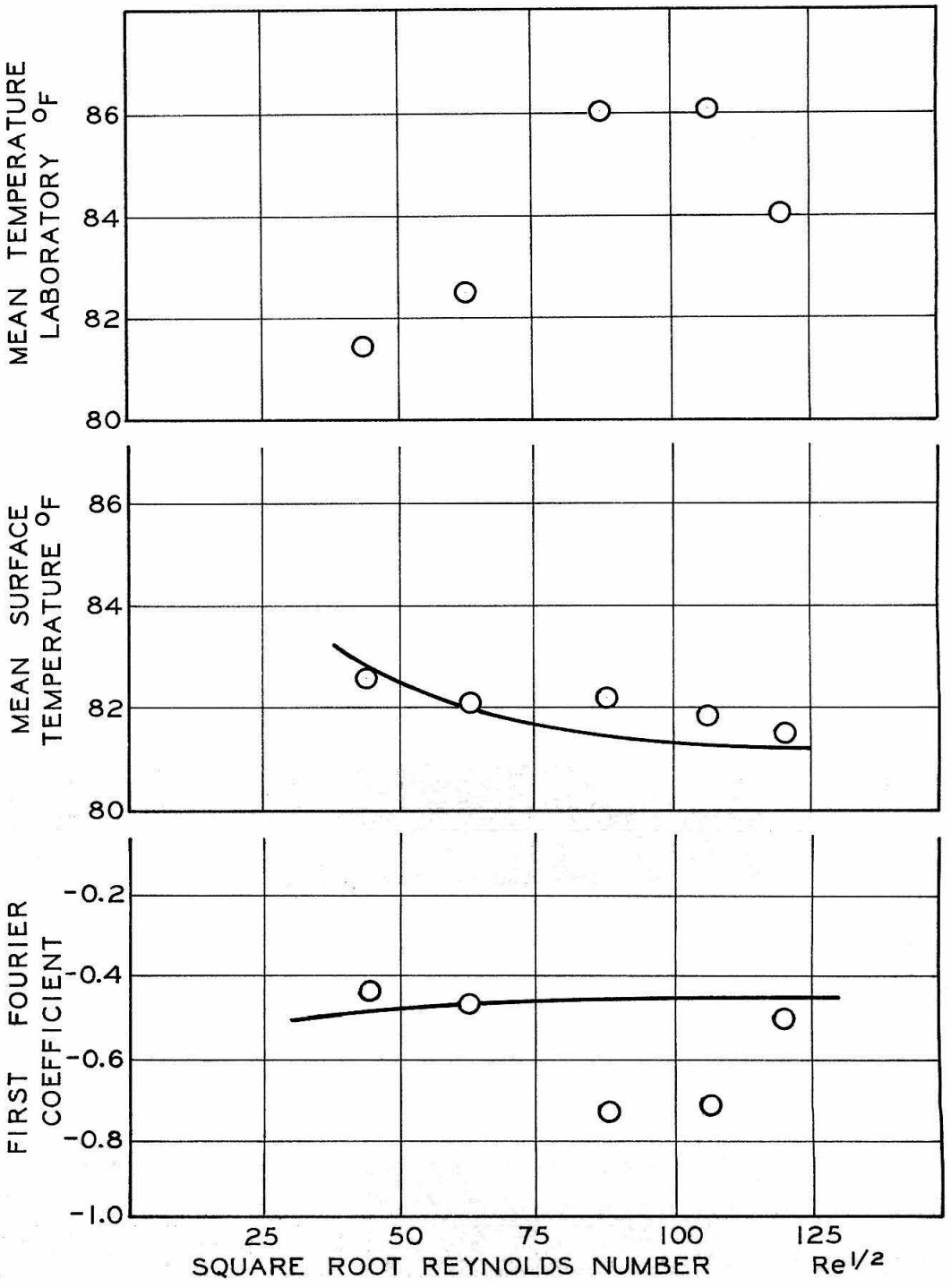

Fig. 17 Surface Temperature of Porous Cylinder - Variation of Mean Temperature and First Order Fourier Coefficient with Laboratory Temperature (n-Octane, $Z_t = 0.013$)

of 0.013 appear in Figure 15 plotted against the square root of the free stream Reynolds Number. In Figure 16 the data for various turbulence levels are plotted against the apparent free stream turbulence level for n-heptane at a constant free stream Reynolds Number of 3780. Figure 17 is comparable to Figure 15 except that the evaporating fluid is n-octane. In comparing Figures 15 through 17 it is apparent that the statistically determined first order coefficient for the evaporation of n-heptane at a Reynolds Number of 3780 and free stream turbulence level of 0.013 (Figure 15) is inconsistent with the trends observed in the surface temperature measurements for other runs. This is explained by the fact that tests were made over a three day period at these conditions, and the mean laboratory temperature varied from day to day (c.f. Table III). Alternatively it is possible that the measured laboratory temperatures do not represent a true mean temperature during the period the data were taken. In this regard it was not anticipated that the prevailing laboratory temperature was an important variable, and this variable was measured rather infrequently.

The higher order Fourier coefficients were calculated up to the seventh order for runs where more than forty surface temperature measurements per section were available, and up to the fifth order if fewer data points were available. The coefficients thus calculated for each run were smoothed according to the square root of the Reynolds Number for those tests made at a constant level of turbulence, and against the prevailing turbulence level when this parameter was varied. Further, the zeroth and first order coef-

ficients were adjusted to allow for the difference between the actual measured laboratory temperature and 82 °F, a representative average temperature for the cylinder surroundings. The smoothed curves in Figures 15 to 17 show this compensation. The results appear in Table IV and were used to calculate the cylinder surface temperature profiles as a function of local velocity, Figures 18 and 20, or of turbulence level, Figure 19. These are the surface temperatures anticipated if the laboratory temperature had been maintained at a constant 82 °F. However in the figure presented earlier, Figure 5, showing the results of point temperature measurements at 8 feet per second, the smoothed curve shown has not been adjusted for the difference between the laboratory temperature and 82 °F. The reader will recall the scatter apparent in this figure; again this is attributed to variations in the laboratory temperature during the course of a run. The analysis is not carried any further because it is known that there were fluctuations in the room temperature during the course of a run which were not sufficiently well monitored to justify a quantitative correlation between the prevailing temperature of a cylinder surroundings and the cylinder temperature. However the observed effect is substantial for room temperature changes of 3° to 5 °F (c.f. Figures 15, 16, 17), and is set forth as a possible explanation of the "random" deviations of individual surface temperature measurements from the general trend. In this regard there was no general sequence followed in obtaining the thermocouple measurements as a function of the angle from stagnation, and the

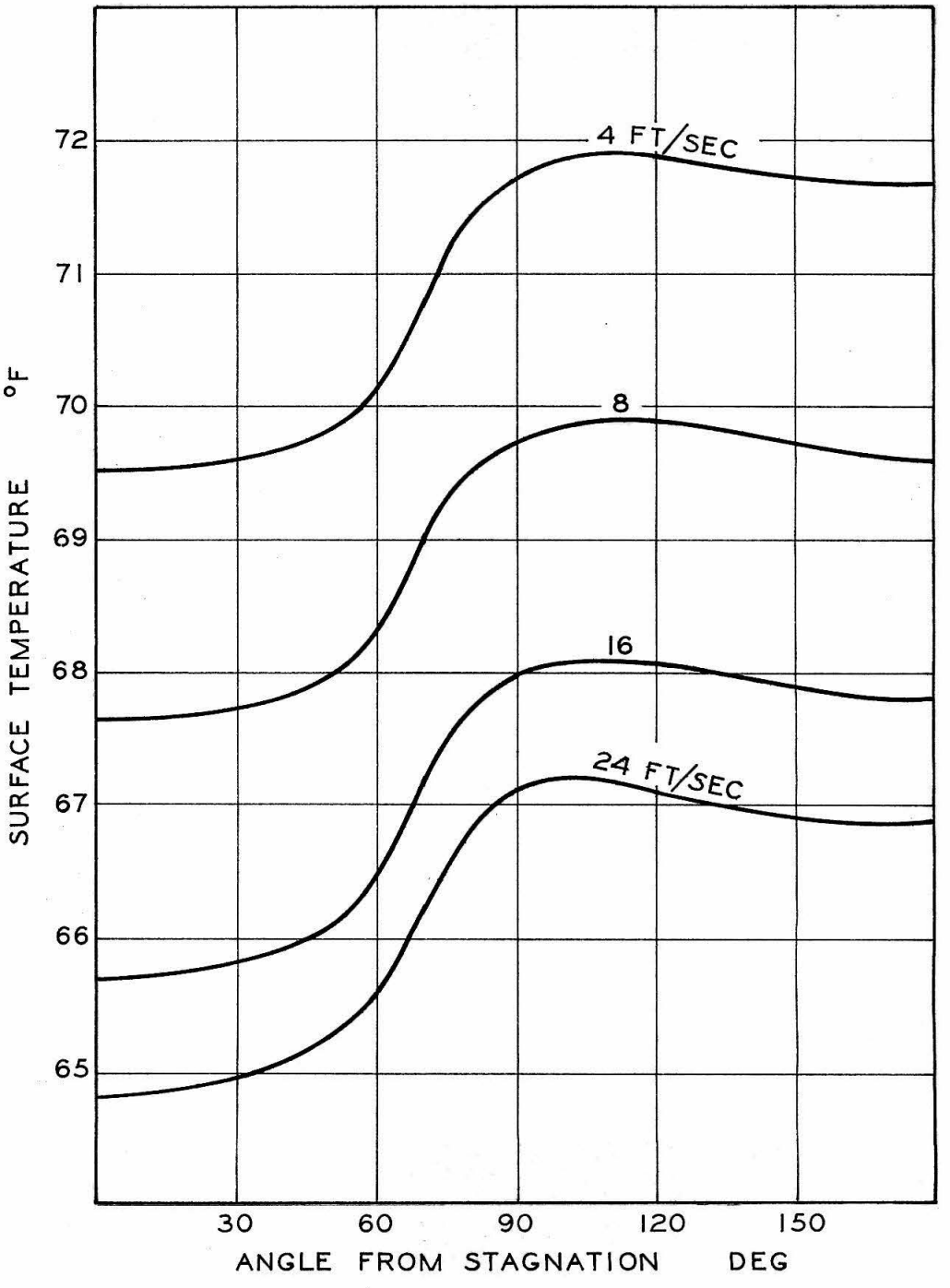

Fig. 18 Cylinder Surface Temperature with Surroundings at 82 °F; n-Heptane, $Z_t = 0.013$

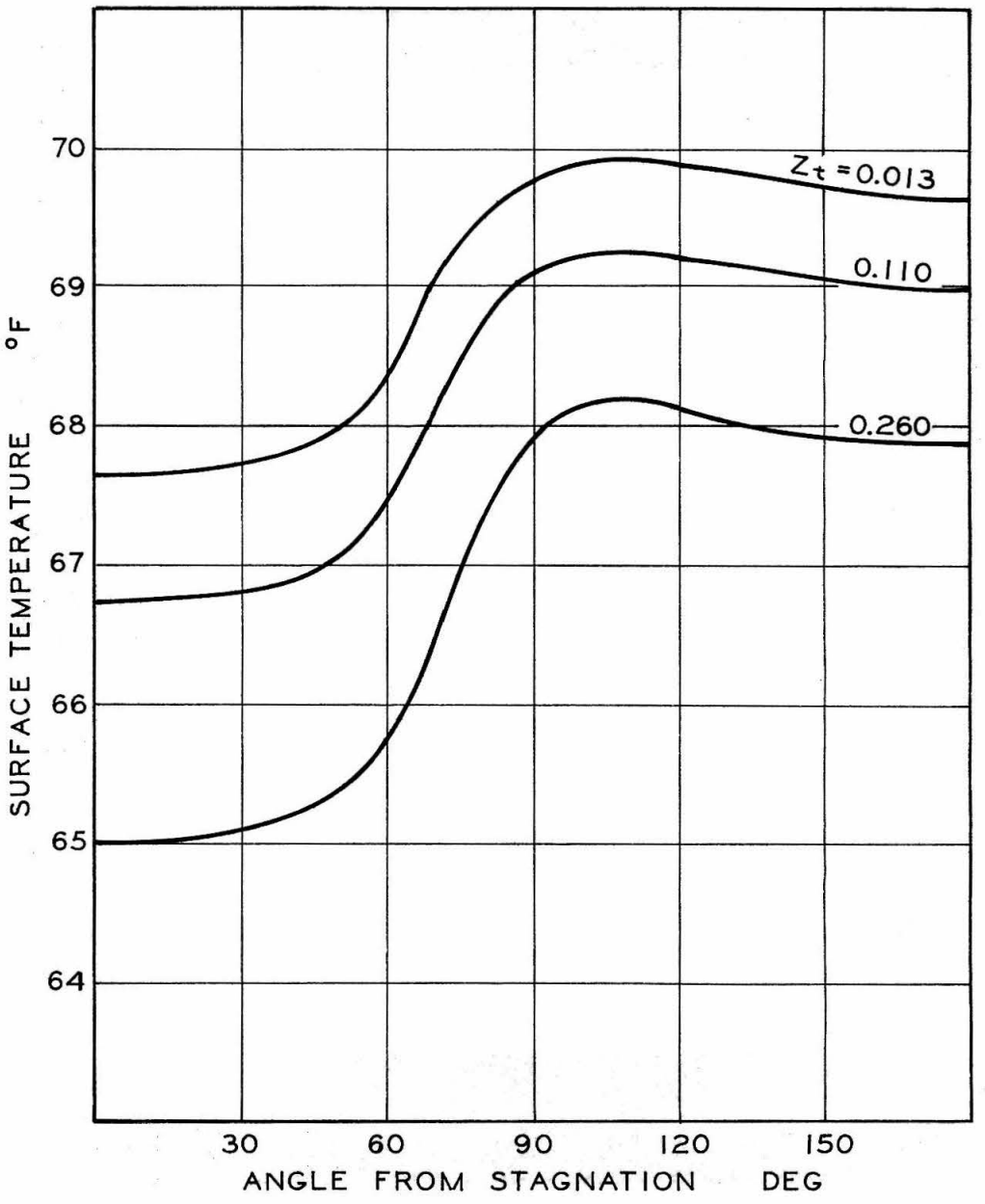

Fig. 19 Cylinder Surface Temperature with Surroundings at 82 °F; n-Heptane, Re = 3780

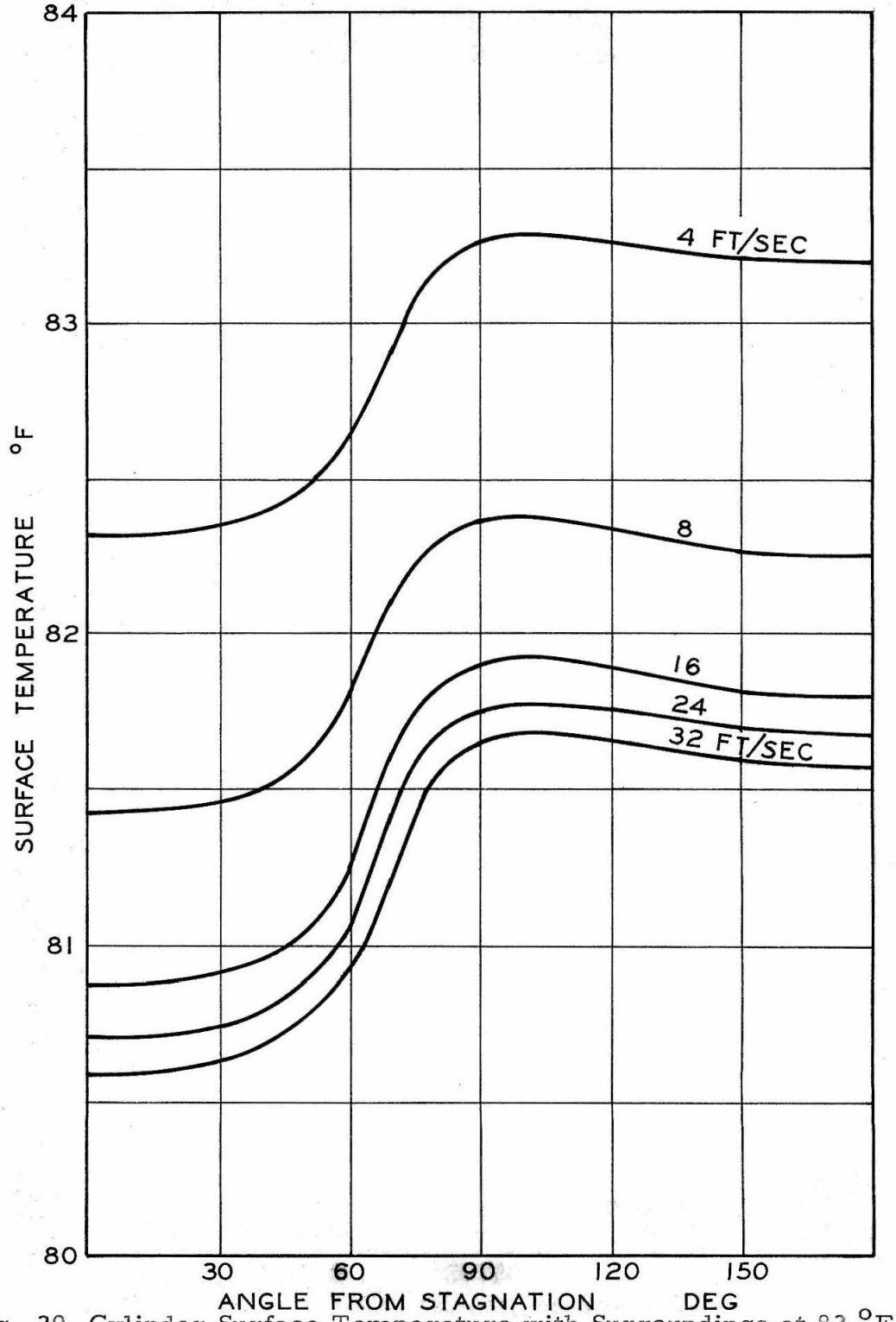

Fig. 20 Cylinder Surface Temperature with Surroundings at 82 °F; n-Octane, $Z_t = 0.013$

data for adjacent points were commonly taken hours apart. The relative stability of the laboratory temperature for runs made with n-octane is probably due to the fact that these data were taken on a priority basis with runs made every day, which was not true of the runs made using n-heptane.

Finally it is felt that the uncertainty involved in determining the mean cylinder surface temperature at which mass transfer rate measurements were made is less than 0.2 ^{o}F for n-heptane, and 0.1 ^{o}F for n-octane because mass flow rate measurements were made concurrently with cylinder surface temperature measurements. Also the trends shown by the statistically determined Fourier coefficients are felt to have comparable accuracy because whenever one data point was taken at one angle from stagnation another point 180^{o} opposed was also taken. Thus the effect of transient temperature perturbations of the cylinder temperature would tend to cancel out except for data points taken in the vicinity of separation.

D. Material Transport From Cylinders -- Comparison with the Results of Other Workers

The results of this investigation are compared in Figure 21 with data obtained by Schnautz (49) with cast napthalene cylinders, and with the data of Maisel and Sherwood (33). Maisel and Sherwood studied the evaporation of a number of liquids in air, carbon dioxide, and helium in an effort to determine the effect of the Schmidt Number on mass transfer rates. They concluded that the j_D factor for material transport (the Frössling Number considered in this study is equivalent to the Chilton Colburn j_D factor multiplied by the square root of the Reynolds Number) was best correlated by the one-third power of the Schmidt Number, but in this regard the scatter of their data was too great to allow them to distinguish between a one-third or a 0.4 power dependence. The results obtained by Maisel and Sherwood (33) corroborate the present study, again within the limitations of their data. These data were taken with several cylinders, whose diameters were somewhat greater than 0.5 inches, placed in a section of pipe with an inside diameter of 4.015 inches. With this design it would be difficult to document the two-dimensionality of the flow around the test cylinder. In addition their free stream turbulence level was inordinately high, 3.2 per cent.

The data of Schnautz (49) also scatter widely, but the experimental design was much more favorable. He took data over a range of turbulence intensities from 0.5 to 11.0 per cent, but at much higher Reynolds Numbers than those used in the present study. His data complement the present investigation very favorably by

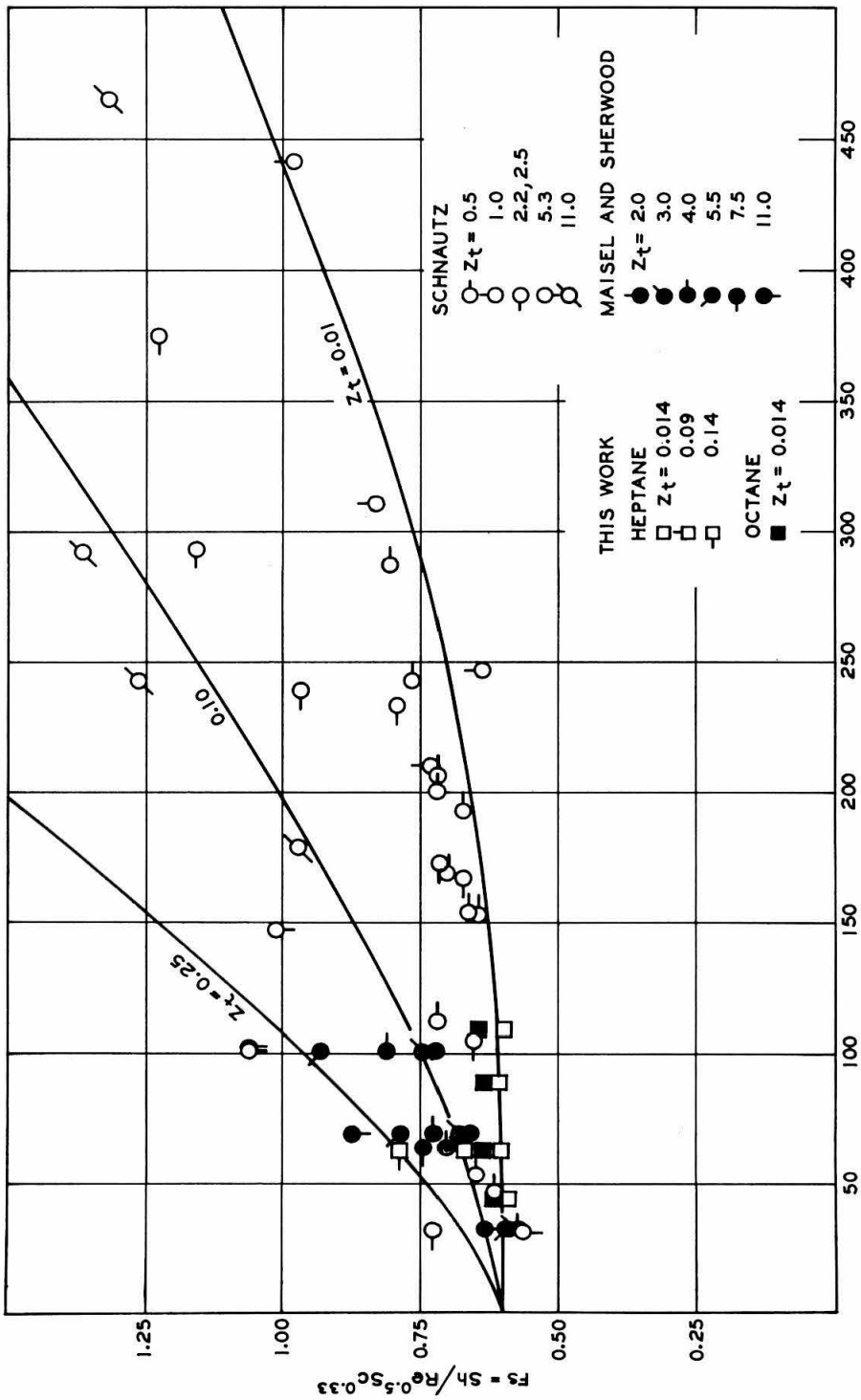

Fig. 21 Material Transport - Frössling Numbers a Comparison with Maisel and Sherwood (33) and Schnautz (49)

indicating the general trend of the Frössling Number with level of turbulence at the higher Reynolds Numbers. His scatter is disappointing, but seemingly unavoidable in view of his observation that "the cast napthalene cylinders tended to sag when left in the duct over sustained periods of time."

E. Comparison with Data for Energy Transfer

As indicated earlier, the results of the present investigation indicate that the Frössling Number for material transport from cylinders is independent of the Reynolds Number for low levels of free stream turbulence and Reynolds Numbers. This contrasts markedly with the correlation proposed by Galloway (19), which in turn was influenced by the systematic decrease in Frössling Number with decreasing Reynolds Numbers observed by Perkins and Leppert (39). However a review of the latter's work with flow of water and ethylene glycol over horizontal cylinders indicates that their results were correlated best with a Frössling Number involving the 0.4 power of the Prandtl Number over a range of Prandtl Numbers from 1 to 300. Their data, taken over a range of Reynolds Numbers from 40 to 100,000, are correlated by the expression:

$$(\Im s)_H = \frac{Nu\left(\frac{\mu_w}{\mu_b}\right)^{0.25}}{Re^{0.5}\,Pr^{0.4}} = 0.53 + 0.0015\,Re^{1/2}$$

This comparison with the present work is very favorable in terms of the indicated dependence of Nusselt Number on the 0.4 power of the Prandtl Number, but the slope of the Frössling Number with the square root of the Reynolds number is somewhat incompatible with that indicated in the present investigation. The cause of this difference is not clear, although it may be that the free stream turbulence level of Perkins and Leppert was much higher than their reported 1.08 per cent. They employed a turbulence grid to smooth out

irregularities in the flow through the test section. The test cylinder was placed 430 bar widths downstream of a grid having a solidity of 0.395. This, from a cursory glance, would indicate that the reported turbulence level is not untoward. However it is to be suspected that the level of turbulence upstream of the mesh would be very high due to flow through a long section of pipe prior to expansion into the test section, and as indicated by Dryden et al. (15), one could not expect the single grid to damp out the residual free stream turbulence. Whether or not this would prove to be an important factor is uncertain. Another possible explanation for the discrepancy would be that Perkins and Leppert performed their studies in a channel with blockage ratios ranging up to 0.3 while this investigation was conducted with a cylinder placed over a free jet with comparable blockage. As noted earlier, the effect of blockage in a free jet is opposite to that in a channel, leading to lower local velocities outside of the boundary layer in the former case. However this would lead one to anticipate lower heat or mass transfer rates with a free jet. If the difference in transport for the two cases is significant, it does not seem readily explained in terms of the different blockage effects for the two situations.

Other workers in energy transport, notably Richardson (41, 42) feel that the Frössling Number should become assymptotically independent of Reynolds Number as the Reynolds Number approaches zero. Richardson arrives at this conclusion by reasoning that laminar boundary layer theory indicates that transport rates in the

front half of the cylinder should be proportional to the square root of the free stream Reynolds Number, and that transport rates for the back half of the cylinder, in the separated flow region, should increase with the two thirds power of the Reynolds Number. He bases the latter conclusion on a correlation of heat transfer rate measurements by a variety of workers in the separated flow region behind cylinders, flat plates (placed normal to the oncoming air stream), and a few other shapes. Further, Richardson (41, 42) determines that the transport rates from the front and back halves of the cylinder become comparable at a Reynolds Number of approximately 40,000. For free stream Reynolds Numbers less than this value, according to Richardson, transport from the forward half of the cylinder predominates, and the Nusselt Number becomes asymptotically proportional to the square root of the Reynolds Number. This conclusion is in accord with the results of the present investigation. The absolute magnitude of his coefficients are not. Richardson's correlation may be expressed in terms of a Frössling Number by the formula:

$$\mathfrak{Fs}_H = c_1(Z_T) + c_2 Re^{1/6}$$

In the expression above, c_1 lies within the limits of 0.42 to 0.62, depending on the level of free stream turbulence, and c_2 between 0.064 and 0.095. However, continuing his reasoning one must conclude that the "constant," c_1 is a function of Reynolds Number as well as the turbulence level, for it does not seem reasonable to expect an

effect of turbulence level for vanishing free stream velocities.

Comings, Clapp and Taylor (10) measured heat transfer rates from a cylinder over a range of Reynolds Numbers from 400 to 20,000. Interestingly their results for the two levels of turbulance (1.0 to 3.0%) are very similar to those obtained in the present study except that their data indicate that the Frössling Number for vanishing Reynolds Numbers approaches a limiting value of 0.67 to 0.68. Their results are compared with the results of this study in Figure 22. In view of their negligible blockage, and without the non-zero normal velocity component at the cylinder surface (as is the case with material transport), it is not surprising that their results for the Frössling Number for energy transport are higher than those observed in the present study for material transport.

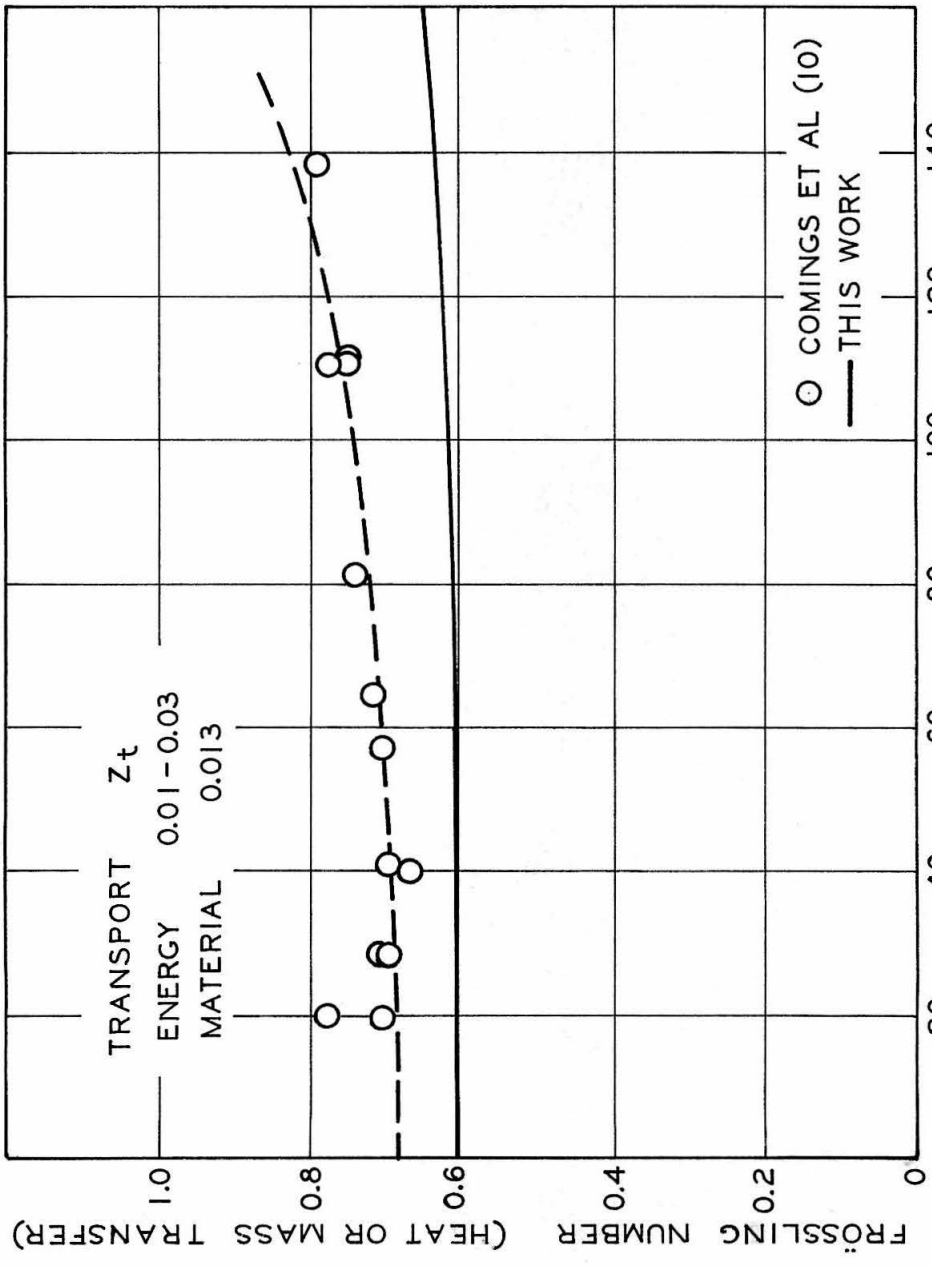

Fig. 22 Analogy between Energy and Material Transport a Comparison with Comings (10)

VI. CONCLUSIONS

Material transport rates from cylinders, at least in the range of low Reynolds Numbers, are analogous to energy transport rates. The overall transport rate at low Reynolds Numbers is nearly proportional to the square root of the free stream Reynolds Number and to the 0.4 power of the Schmidt Number. The 0.4 power dependence of material transport on the Schmidt Number suggested by this work is somewhat less certain than the Reynolds dependence because of an estimated 3% uncertainty in the Maxwell Diffusion Coefficient for n-octane.

At higher levels of free stream turbulence, 0.110 to 0.260, material transport rates increase substantially faster than the square root of the Reynolds Number. At a Reynolds Number of 3700, the overall material transport rate was increased approximately 30% by going from a free stream turbulence level of 0.013 to 0.260, and 12% by a free stream turbulence level of 0.110. Thus, to a first order approximation material transport rates at this Reynolds Number, show a percentage increase which is proportional to the per cent level of turbulence. Also it is indicated that the effects of turbulence are proportionately greater at higher Reynolds Numbers.

The data were compared with the results of Comings, Clapp and Taylor (10) concerning energy transport rates from cylinders. Comings et al. measured energy transport rates which, when compared on the basis of Frössling Numbers for heat and mass transfer, were approximately ten per cent higher than the Frössling Numbers

for material transport obtained in this study at the low levels of turbulence. However, in their work the cylinder was placed in a duct where the blockage was 12 per cent or less. In the present study the cylinder was placed in a free jet where the blockage was 33 per cent. The reader will appreciate that the effects of blockage in the two cases are diametrically opposed. In the duct, high blockage ratios restrict the flow past a cylinder causing higher local velocities than those which would be anticipated for the same cylinder placed in an infinite air stream having the same bulk velocity. For the case of the cylinder placed in a free jet, the flow diverges more than would be the case with an infinite air stream, and the local velocities are reduced.

It seems that these lower local velocities encountered by the cylinder placed in a free jet could account for a reduction in the overall transport rate (energy or material) because the laminar boundary layer thickness on the front half of the cylinder would be correspondingly increased. However, it is not known how transport in the wake region would be affected by high blockage ratios for a cylinder placed in a free jet, and it is certainly possible that an increase in transport rates from the wake region could offset any small decrease in transport rates encountered in going from stagnation up to the point of separation. Interestingly the effects of blockage do not seem to be high, for Galloway (18, 19) working with a 1.4 inch cylinder placed over a 3 inch free jet, (blockage ratio = 0.467), encountered energy transport rates comparable to those found by Perkins and Leppert (39), who studied energy transport rates from a cylinder placed in a closed

duct.

In this study the normal velocity component at the cylinder surface due to the vaporization process ranged from 0.001 to 0.004 ft/sec. The effect of a non-zero velocity component at the cylinder surface would be to increase the boundary layer thickness, thereby reducing overall transport rates. It is difficult to estimate this effect and to do so with any degree of accuracy would require a more detailed knowledge of local transport rates as a function of the angle from stagnation. It is felt though that these velocities are sufficiently small so that the effect of the non-zero surface velocities on the boundary layer thickness and transport rates outside of influencing the viscosity of the fluid in the boundary layer, would be negligible.

The effects of blockage ratio for a cylinder placed in a free jet or of a non-zero normal velocity component at the cylinder surface is not well documented. However, it is probable that these effects would act to reduce overall transport rates. It was observed that the Frössling Numbers for material transport measured in this study were approximately 10% lower than those measured by Comings et al. (10) for energy transport in a closed duct. This agreement is considered excellent and gives strong support to the analogy between energy and material transport from cylinders at low Reynolds Numbers.

It was shown that radiant energy transport from the surroundings had a significant effect on the surface temperature of the cylinder. It was not anticipated that the effect of small changes in the laboratory room temperature would have much influence on the cylinder surface

temperature, and no provisions were made to control this variable. For these reasons the results of the investigation of the cylinder surface temperature profile were somewhat disappointing and were not used in any way except to determine the mean temperature of the cylinder during the vaporization process. In future studies of material transport rates it is strongly recommended that the temperature of the radiation environment be controlled, or possibly that steps to reduce the total energy transport through radiation be taken.

VII. REFERENCES

1. Acrivos, Andreas, Snowden, D. D., Grove, A. S., and Petersen, E. E., "The Steady Separated Flow Past A Circular Cylinder at Large Reynolds Numbers," Journal of Fluid Mechanics, Vol. 21, pp. 737-760 (1964).

2. Batchelor, G. K., and Townsend, A. A., "Decay of Isotropic Turbulence in the Initial Period," Proceedings of the Royal Society of London, Vol. 193A, pp. 539-558 (1948).

3. Batchelor, G. K., and Townsend, A. A., "Decay of Turbulence in the Final Period," Proceedings of the Royal Society of London, Vol. 194A, pp. 527-543 (1948).

4. Batchelor, G. K. and Townsend, A. A., "Decay of Vorticity in Isotropic Turbulence," Proceedings of the Royal Society of London, Vol. 190A, pp. 534-550 (1947).

5. Baines, W. D. and Peterson, E. G., "An Investigation of Flow Through Screens," Transactions of the ASME, Vol. 73, pp. 467-480 (July, 1951).

6. Bird, R. G., Stewart, W. E. and Lightfoot, E. N., Transport Phenomena. New York: John Wiley and Sons (1960).

7. Chen, Shiou-Shan, Ph.D. Thesis, California Institute of Technology Pasadena, California (1966).

8. Chilton, T. H. and Colburn, A. P., "Mass Transfer (Absorption) Coefficients," Industrial and Engineering Chemistry, Vol. 26, No. 11, pp. 1183-1187 (November, 1934).

9. Collis, D. C. and Williams, M. J., "Two-Dimensional Convection from Heated Wires at Low Reynolds Numbers," Journal of Fluid Mechanics, Vol. 6, pp. 357-384 (1959).

10. Comings, E. W., Clapp, J. T., and Taylor, J. F., "Air Turbulence and Transfer Processes - Flow Normal to Cylinders," Industrial and Engineering Chemistry, Vol. 40, pp. 1076-1082 (1948).

11. Connolly, T. J., Sage, B. H., and Lacey, W. N., "Isobaric Heat Capacities at Bubble Point - n-Hexane, Methylcyclopentane, and n-Octane," Industrial and Engineering Chemistry, Vol. 43, No. 4, pp. 946-950 (April, 1951).

12. Corcoron, W. H., Page, F. Jr., Schlinger, W. G., and Sage, B. H., "Temperature Gradients in Turbulent Gas Streams, Methods and Apparatus for Flow Between Parallel Plates," Industrial and Engineering Chemistry, Vol. 44, pp. 410-419 (1952).

13. Cuffel, R. F., Ph.D. Thesis, California Institute of Technology, Pasadena, California (1964).

14. Davis, Leo, "Measurements of Turbulence Decay and Turbulent Spectra Behind Grids," Report No. 3-17, Jet Propulsion Laboratory, Pasadena, California (1952).

15. Dryden, H. L., Schubauer, G. B., Mock, W. C., and Skramstad, H. K., "Measurements of Intensity and Scale of Wind Tunnel Turbulence and Their Relation to the Critical Reynolds Number of Spheres," NACA Report No. 581 (1937).

16. Dryden, H. L. and Schubauer, G. B., "The Use of Damping Screens for the Reduction of Wind Tunnel Turbulence," Journal of Aeronautical Science, Vol. 14, pp. 221-228 (1947).

17. Frössling, N., "Evaporation, Heat Transfer, and Convective Mass Transfer for a Two-Dimensional and Rotationally-Symmetric Laminar Boundary Layer," Lunds Universitets Arsskrift, N.F. Aud. 2, Bd 36, Nr. 4 (1940).

18. Galloway, T. R. and Sage, B. H., First Semiannual Report -- Peter E. Fluor Memorial Fellowship, California Institute of Technology, Manuscript 4182 (January, 1966).

19. Galloway, T. R. and Sage, B. H., "Local and Macroscopic Transport from A 1.5 In. Cylinder in a Turbulent Air Stream," California Institute of Technology, Manuscript 5296 (to be published).

20. Geidt, W. H., "Effect of Turbulence Level of Incident Air Stream on Local Heat Transfer and Skin Friction on a Cylinder," Journal of Aeronautical Sciences, Vol. 18, 725-29, 730, 766 (1951).

21. Grove, A. S., Shair, F. H., Petersen, E. E., and Acrivos, Andreas, "An Experimental Investigation of the Steady Separated Flow Past a Circular Cylinder," Journal of Fluid Mechanics, Vol. 19, Part 1, pp. 60-80 (1964).

22. Hall, A. A., "Measurements of the Intensity and Scale of Turbulence," Aeronautical Research Comm. Reports and Memoranda, No. 1842 (1938).

23. Hinze, J. O., Turbulence. New York: McGraw-Hill Book Co., Inc. (1959).

24. Homann, F., "Der Einflus grosser Zaehigkeit bei der Stroemung um den Zylinder und um die Kugel," ZAMM, Vol. 16, pp. 153-164 (1936).

25. Hsu, N. T., Sato, K., and Sage, B. H., "Effect of Shape on Evaporation of Drops," Industrial and Engineering Chemistry, Vol. 46, pp. 870-876 (1954).

26. Hsu, N. T., Ph.D. Thesis, California Institute of Technology, Pasadena, California (1956).

27. Hsu, N. T., Reamer, H. H., and Sage, B. H., Document 4219 American Document Institute, Washington, D.C. (1954).

28. International Critical Tables, Vol. 5 (New York: McGraw-Hill Book Co., Inc, 1929). p. 63.

29. Jorissen, A. L. and Ithaca, N. Y. "Discharge Coefficients of Herschel-Type Venturi Tubes," Transactions of the ASME, Vol. 74, pp. 905-913 (August, 1952).

30. Kestin, J. and Maeder, P. F., "Influence of Turbulence on Transfer of Heat from Cylinders," NACA Technical Note 4018, (1957).

31. Korobkin, I., "Discussion of Local Laminar Heat Transfer Coefficients for Spheres and Cylinders in Incompressible Flow," Paper No. 54-F-18-Revised, The American Society of Mechanical Engineers, (1954).

32. Longwell, P. A., and Sage, B. H., "Some Molecular Transport Characteristics in Binary Homogeneous Systems," A.I.Ch.E. Journal, Vol. 11, No. 1, pp. 46-54 (1965).

33. Maisel, D. S. and Sherwood, T. K., "Effect of Air Turbulence on Rate of Evaporization of Water," Chemical Engineering Progress, Vol. 46, No. 4, pp. 172-175 (April, 1950).

34. McKay, R. A., Ph.D. Thesis, California Institute of Technology, Pasadena, California (1959).

35. Mendelson, Harvey and Yerazunis, Stephen, "Mass Transfer at High Mass Fluxes: Part I. Evaporation at the Stagnation Point of a Cylinder," A.I.Ch.E. Journal, Vol. 11, pp. 834-840 (1965).

36. Opfell, J. B., Pings, C. J., and Sage, B. H., Equations of State for Hydrocarbons, Research Project 37 (New York: American Petroleum Institute, 1959).

37. Opfell, J. B. and Sage, B. H., "Relations in Materials Transport," Industrial and Engineering Chemistry, Vol. 47, No. 5, pp. 918-923 (1955).

38. Opfell, J. B., Schlinger, W. G., and Sage, B. H., "Benedict Equation of State: Application to Methane, Ethane, n-Butane, and n-Pentane," Industrial Engineering Chemistry, Vol. 46, No. 6, pp. 1286-1291 (1954).

39. Perkins, H. C. Jr., and Leppert, G., "Forced Convection Heat Transfer from a Uniformly Heated Cylinder," Journal of Heat Transfer, Vol. 84, pp. 257-261 (August, 1962).

40. Reamer, H. H. and Sage, B. H., "Method of Control of a Predetermined Flow Rate," Review of Scientific Instruments, Vol. 24, pp. 362-366 (1953).

41. Richardson, P. D., "Estimation of the Heat Transfer from the Rear of an Immersed Body to the Region of Separated Flow," AD 290 339, ARL 62-423 (1962).

42. Richardson, P. D., "Heat and Mass Transfer in Turbulent Separated Flows," Chemical Engineering Science, Vol. 18, pp. 149-155 (1963).

43. Rossini, F. D., et al., Selected Values of Physical and Thermodynamic Properties of Hydrocarbons and Related Compounds, Pittsburg: Carnegie Press, 1953.

44. Sage, B. H., "Letter to the Editor: Sherwood Number," reprinted from Chemical Engineering Progress (July, 1953).

45. Sato, K., Ph.D. Thesis, California Institute of Technology, Pasadena, California (1955).

46. Schlichting, H., translated by Kestin, J., Boundary Layer Theory, 4th edition, New York: McGraw-Hill Book Co., Inc., 1962.

47. Schlinger, W. G., Reamer, H. H., Sage, B. H., and Lacey, W. H., "Diffusion Coefficients in Hydrocarbon Systems; n-Hexane and n-Heptane in Air," Fundamental Research on Occurrence and Recovery of Petroleium, Biennial Volume, pp. 70-114 (1952-53).

48. Schmidt, E. and Wenner, K., "Warmeabgabe uber den Umtang eines angeblasenen geheizten Zylinders," Forsch. Ing.-Wes., Vol. 12, p. 65 (1941). English translation: NACA Technical Manuscript No. 1050 (1943).

49. Schnautz, J. A., "Effect of Turbulence Intensity on Mass Transfer from Plates, Cylinders, and Spheres in Air Streams," Ph.D. Thesis (1957). Oregon State College, Corvallis (Univ. Microfilm No. 33920).

50. Schubauer, G. B., "A Turbulence Indicator Utilizing the Diffusion of Heat," NACA Report No. 524 (1935).

51. Seban, R. A., "Influence of Free Stream Turbulence on the Local Heat Transfer from Cylinders," Transactions of the ASME, Vol. 82, pp. 101-107 (1960).

52. Shair, F. H., Grove, A. S., Petersen, E. E., and Acrivos, A. A., "The Effect of Confining Walls on the Stability of the Steady Wake Behind a Circular Cylinder," Journal of Fluid Mechanics, Vol. 17, part 4, pp. 546-550 (1963).

53. Short, W. W., Ph.D. Thesis, California Institute of Technology, Pasadena, California (1958).

54. Squire, H. B., section in "Modern Developments in Fluid Dynamics," edited by Goldstein, S., Oxford II, p. 623 (1938).

55. Sutera, S. P., "Vorticity Amplification in Stagnation-Point Flow and Its Effect on Heat Transfer," Journal of Fluid Mechanics, Vol. 21, pp. 513-534 (1964).

56. Van der Hegge Zijnen, B. G., "Heat Transfer from Horizontal Cylinders to a Turbulent Air Flow," Appl. Sci. Res., Vol. 7A, pp. 205-223 (1958).

57. Van der Hegge Zijnen, G. B., "Measurements of the Intensity, Integral Scale and Microscale of Turbulence Downstream of Three Grids in a Stream of Air," Appl. Sci. Res., Vol. 7A, pp. 149-174 (1957).

58. Venezian, E. C., Ph.D. Thesis, California Institute of Technology, Pasadena, California (1962).

59. Winding, C. C. and Cheney, A. J. Jr., "Mass and Heat Transfer in Tube Banks," Industrial and Engineering Chemistry, Vol. 40, pp. 1087-1094 (1948).

60. Yuge, T., "Theory of Distributions of the Coefficients of Heat Transfer of Two Dimensional Bodies of Various Shapes," Reports of the Institute of High Speed Mechanics, Tohoku University (Sendai, Japan), Vol. 6, No. 58, pp. 153-173 (1956).

VIII. NOMENCLATURE

A. Roman Type Symbols

b	gas constant	ft, lb/lb, ^{o}R
b	grid bar width	ft
c_p	heat capacity	Btu/lb, ^{o}R
D	cylinder diameter	ft
D^*	effective diffusion coefficient	lb/lb-mole, ft, sec
D_{ckj}	Chapman-Cowling diffusion coefficient	ft^2/sec
D'_{Mk}	Modified Maxwell diffusion coefficient	lb/sec
$\mathfrak{Fs}$	Frössling Number	
f	fugacity	lb/ft^2
g_o	gravitational constant	ft/sec^2
g_x	local acceleration due to gravity	ft/sec^2
K	thermometric conductivity	ft^2/sec
K_G	mass transfer coefficient	lb/lb-mole, ft^2, sec
k	thermal conductivity	Btu/ft, sec, ^{o}R
L	cylinder length	ft
L_x	scale of turbulence	ft
M	molecular weight	
M	mesh width	ft
$\dot{m}$	weight flow rate	lb/ft^2, sec
$\dot{m}$	molal flow rate	lb-mole/ft^2, sec
n	weight fraction	
n	mole fraction	
Nu	Nusselt Number	

P	pressure	lb/ft^2
Pr	Prandtl Number	
$\vec{q}$	velocity	ft/sec
R	molal gas constant	ft, lb/lb-mole, ^oR
Re	Reynolds Number	
Sc	Schmidt Number	
Sh	Sherwood Number	
T	temperature	^oR
U	free stream velocity	ft/sec
U	bulk velocity at jet exit	ft/sec
u	velocity component in Cartesian coordinate direction x	ft/sec
u	local velocity	ft/sec
$\dot{V}$	modal volume	ft^3/lb-mole
v	velocity component in Cartesian coordinate direction y	ft/sec
w	velocity component in Cartesian coordinate direction z	ft/sec
x	Cartesian coordinate direction	ft
y	Cartesian coordinate direction	ft
Z	compressibility factor	
Z_t	turbulence level	
z	Cartesian coordinate direction	ft

B. Greek Type Symbols

η	viscosity	lb, sec/ft^2
θ	time	sec

λ_x	microscale of turbulence	ft
ν	kinematic viscosity	ft^2/sec
σ	specific weight	lb/ft^3
$\dot{\sigma}$	molal specific weight	$lb\text{-}mole/ft^3$
ϕ	frictional dissipation function	sec^{-2}
ϕ	angle from stagnation	radians

C. Operators

∇	gradient operator	ft^{-1}
$\vec{\nabla}\cdot$	divergence operator	ft^{-1}
Δ	finite difference operator	

D. Subscripts

d	pertaining to diffusion effects
j	component j
k	component k
o	external to boundary layer
s	surface
∞	undisturbed free stream

E. Superscripts

o	pure component
'	fluctuating component pertaining to turbulence

APPENDIX

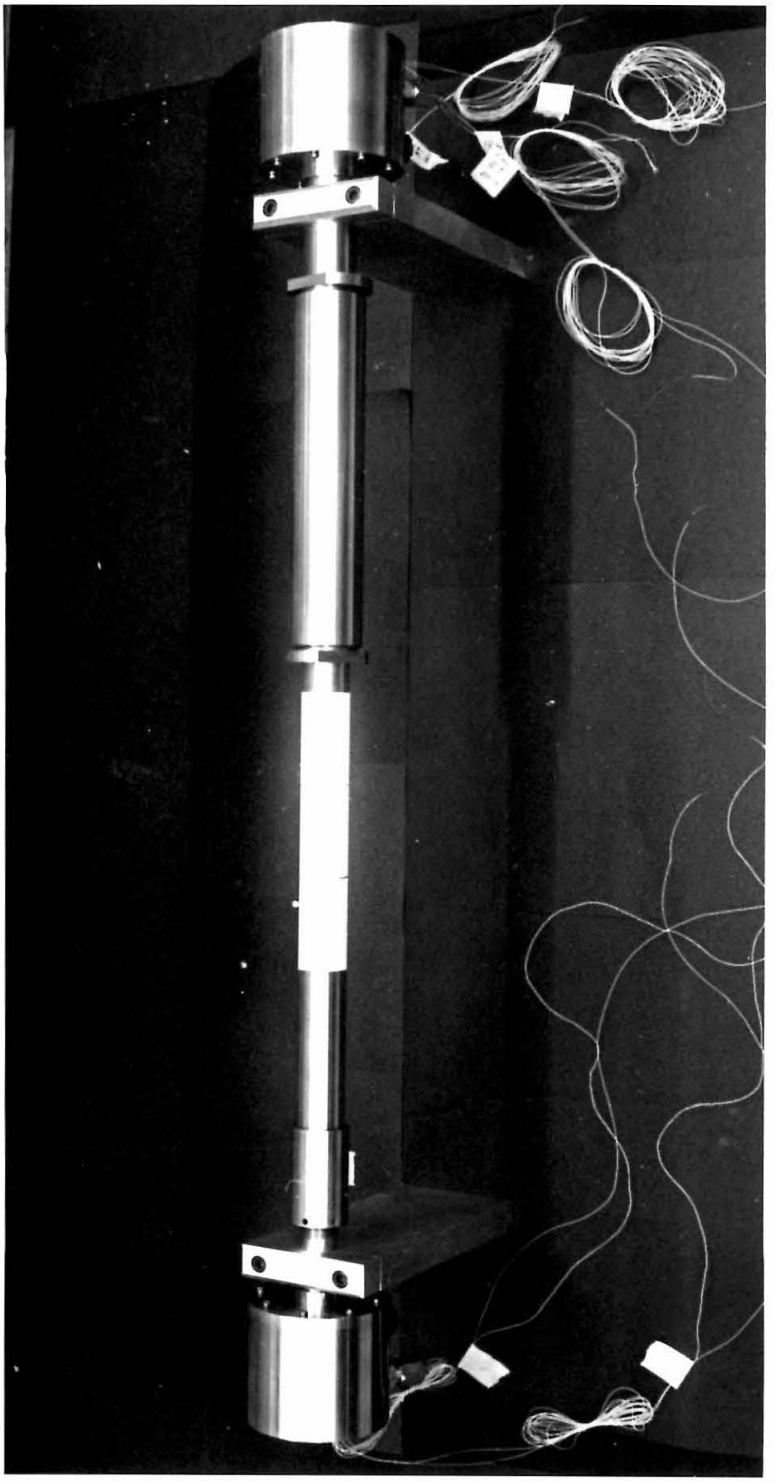

Fig. A1 Porous Cylinder in Final Stages of Construction

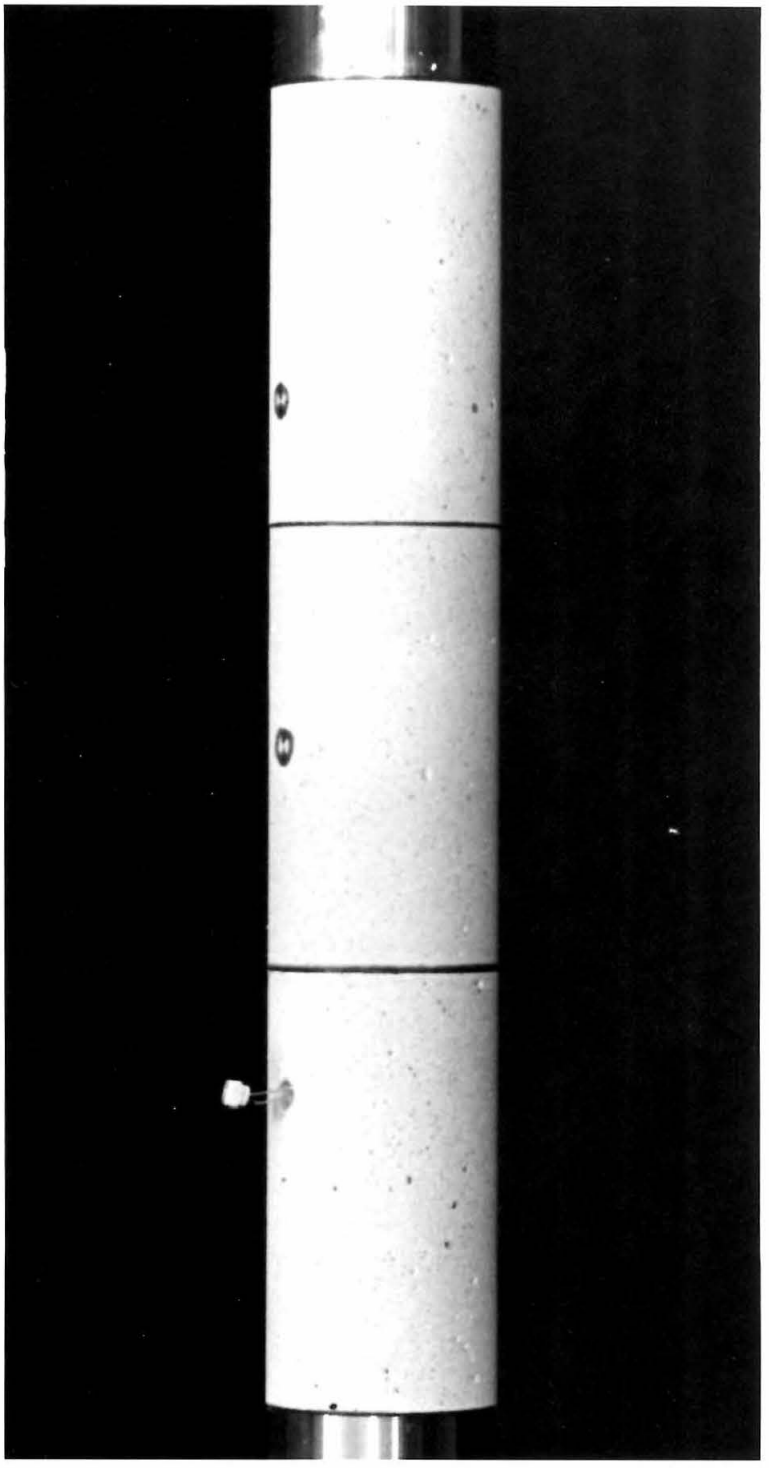

Fig. A2 Porous Cylinder - The Evaporating Sections

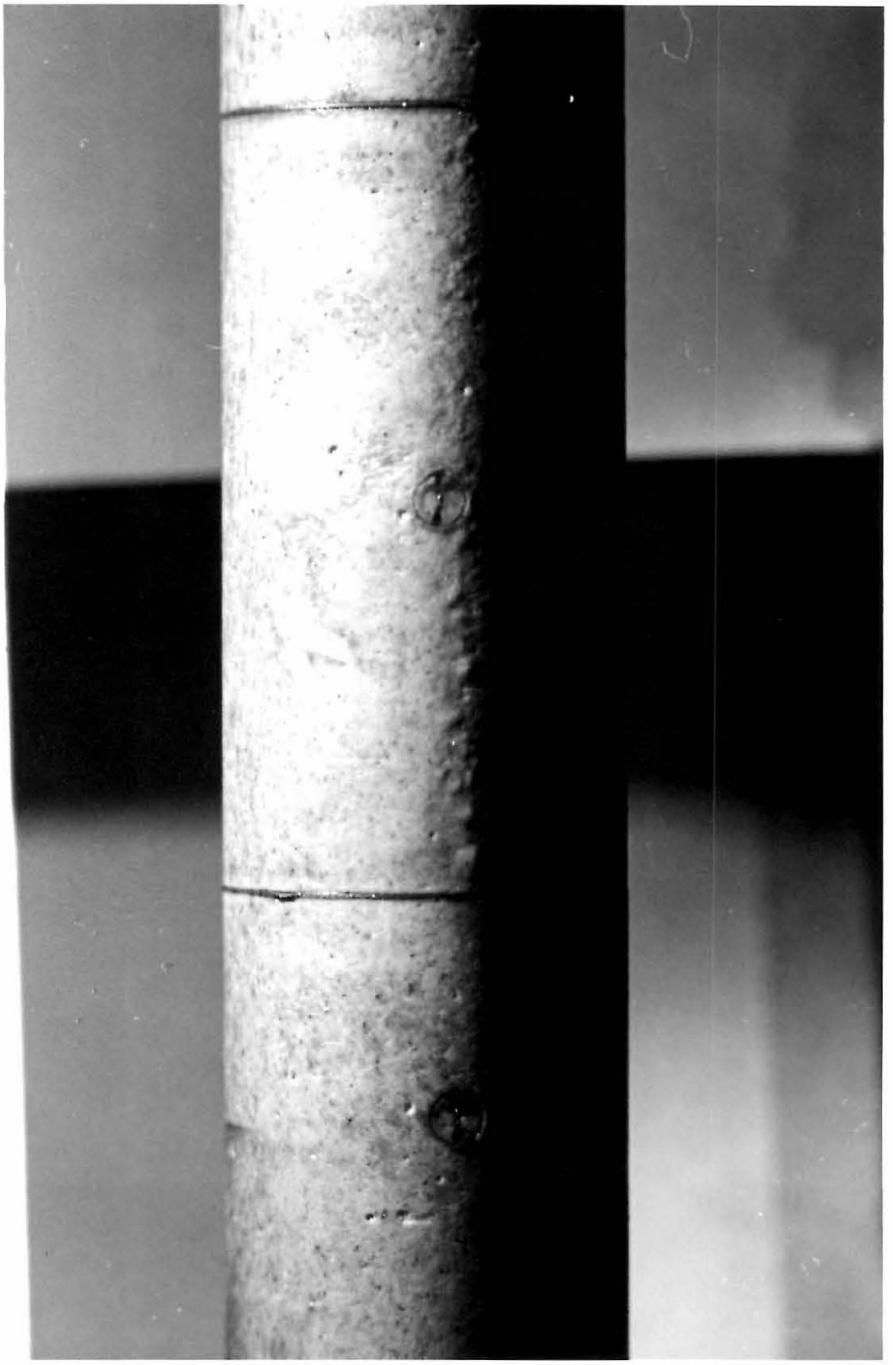

Fig. A3 Porous Cylinder - Showing Porous Sections During Experimentation

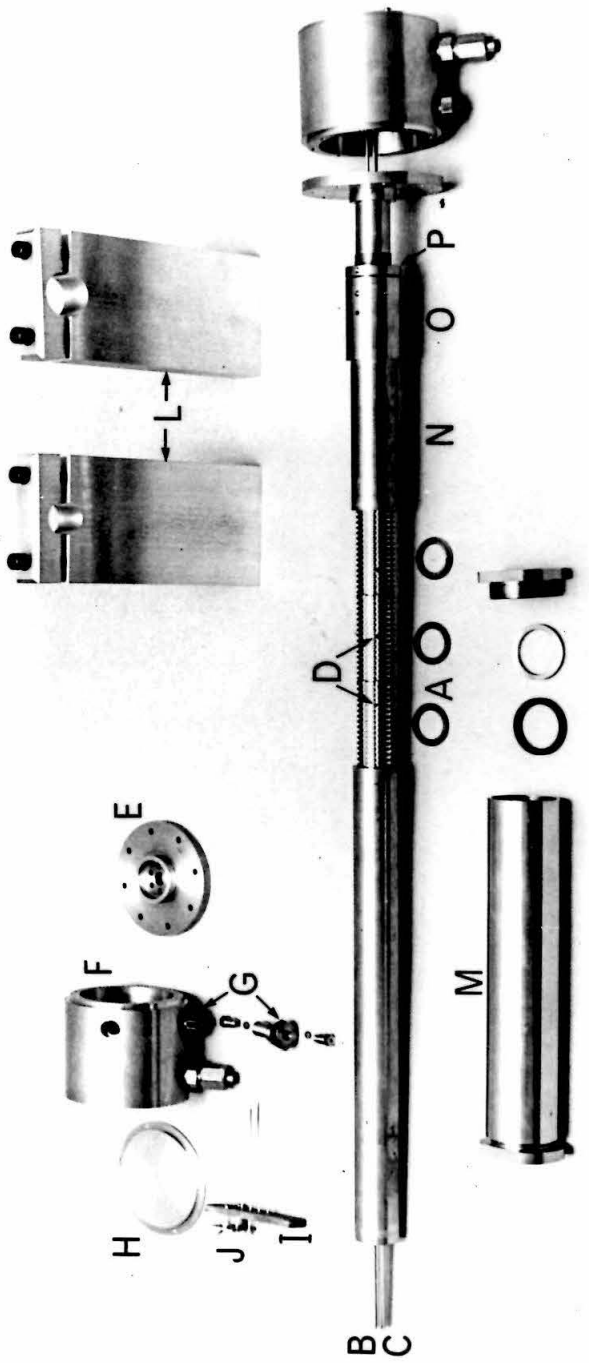

Fig A4 Porous Cylinder - Exploded View of Parts

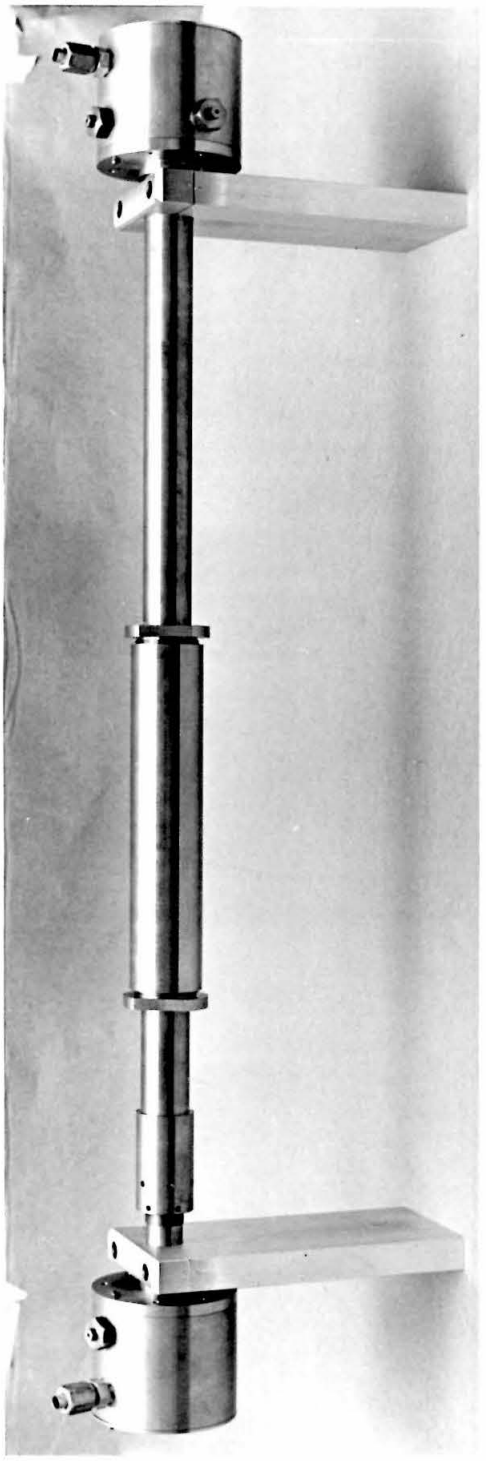

Fig. A5 Porous Cylinder Showing Operation of Vacuum Jacket

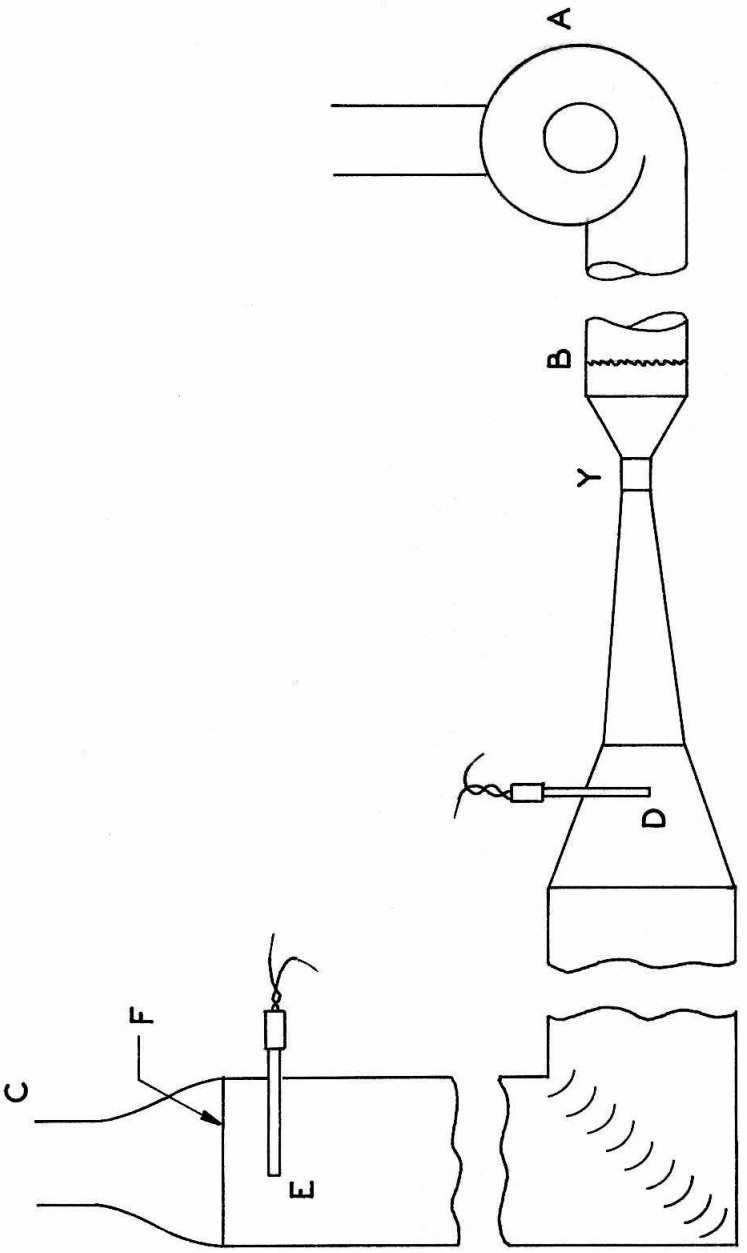

Fig. A6 Schematic Diagram of the Air Supply System

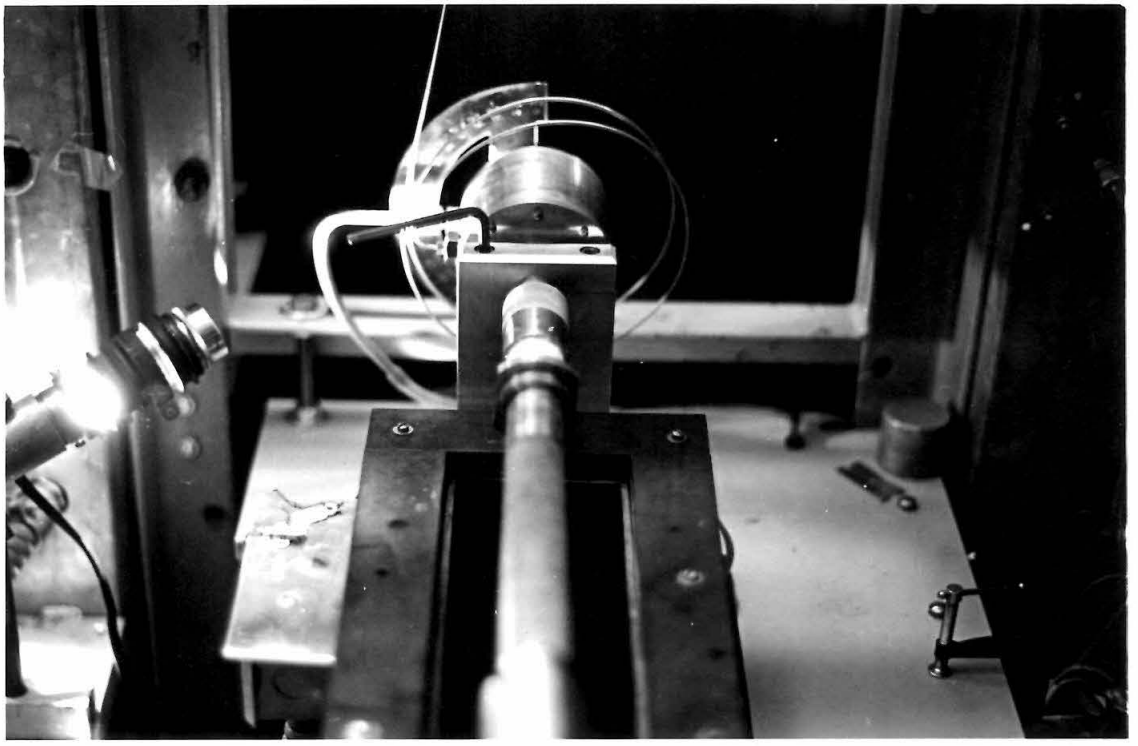

Fig. A7 Porous Cylinder - Showing Installation over Jet Exit

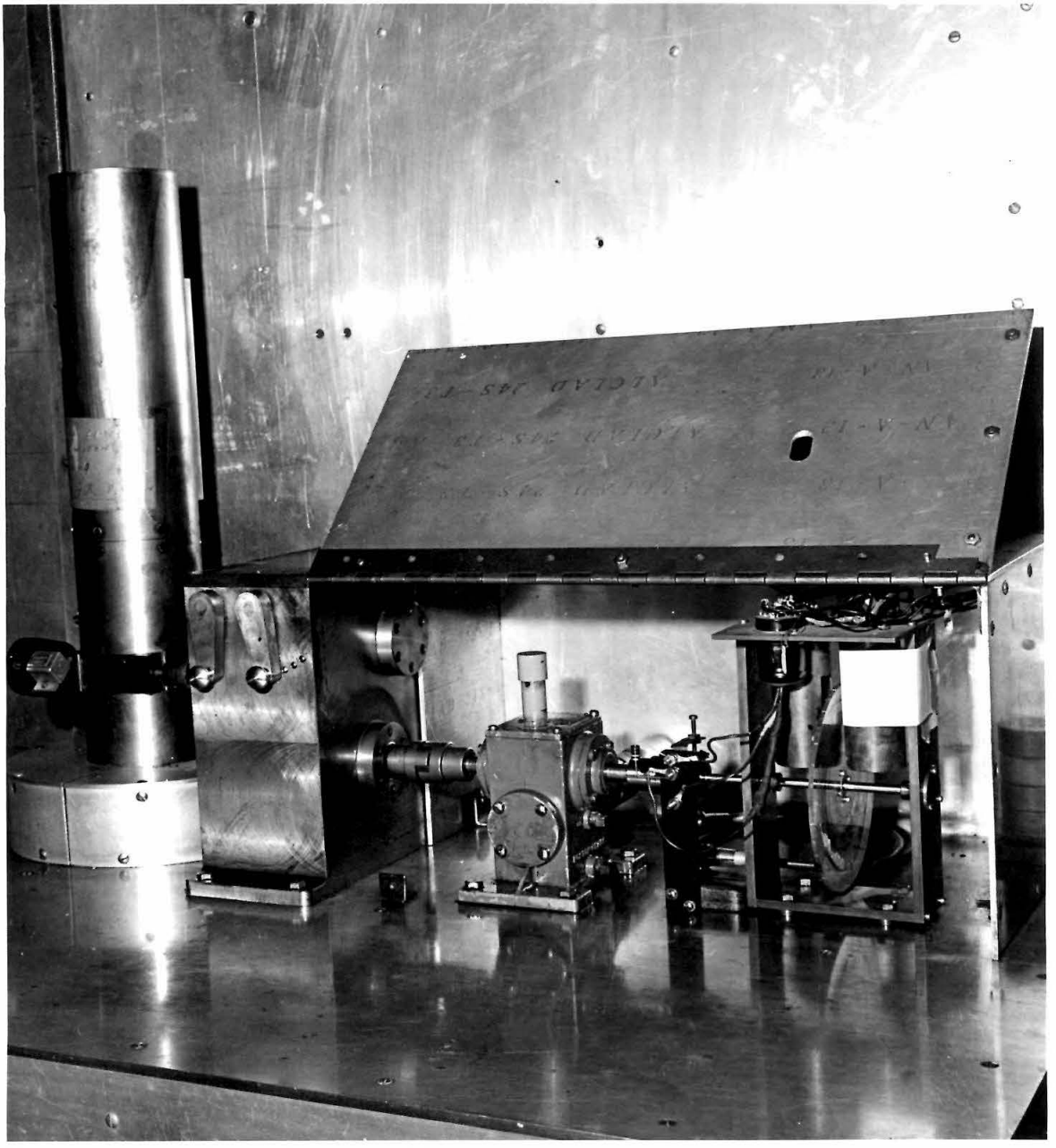

Fig. A8 The Injector and Injector Drive Mechanism

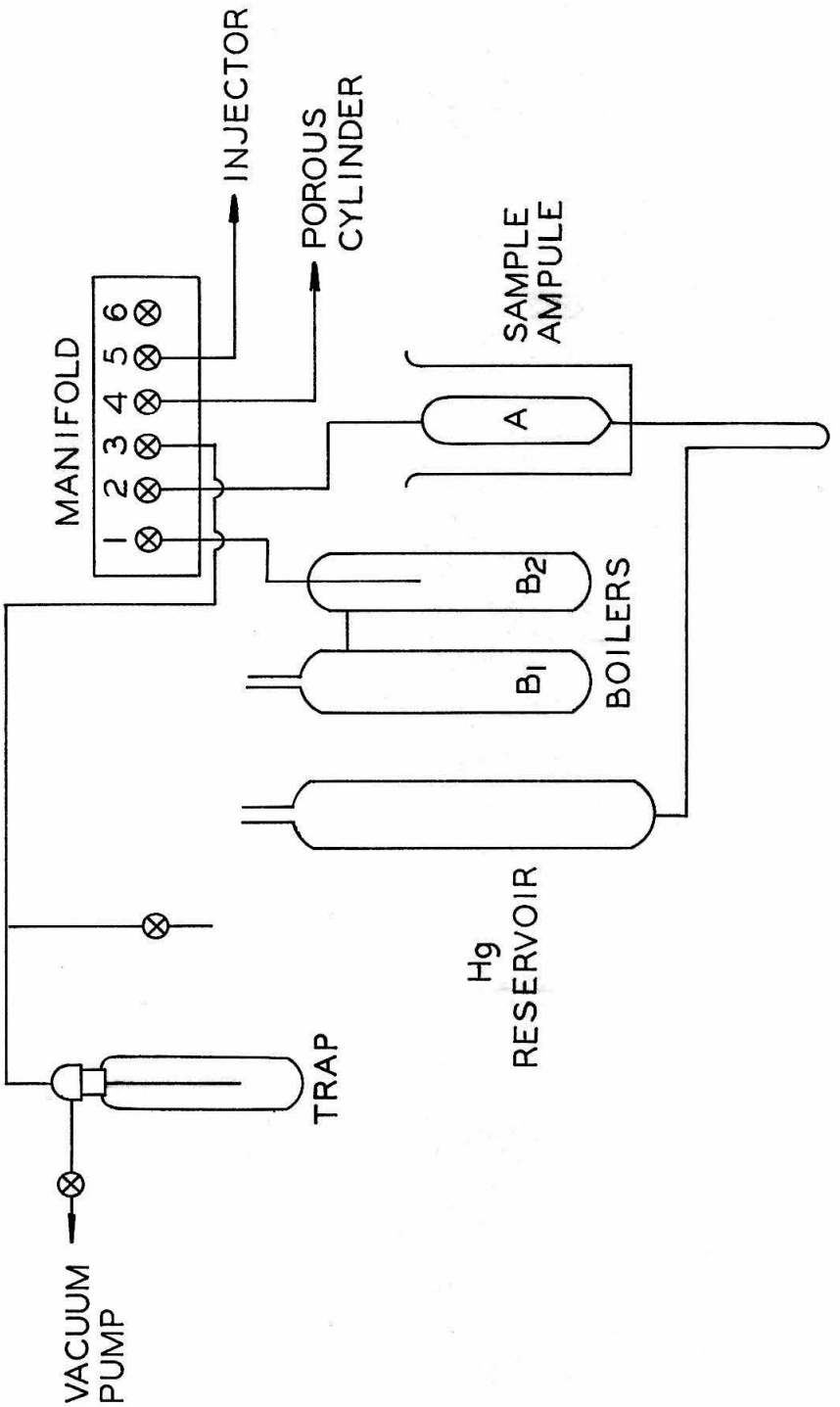

Fig. A9 Schematic Diagram of Injector Feed Circuit and Sample Purification Apparatus

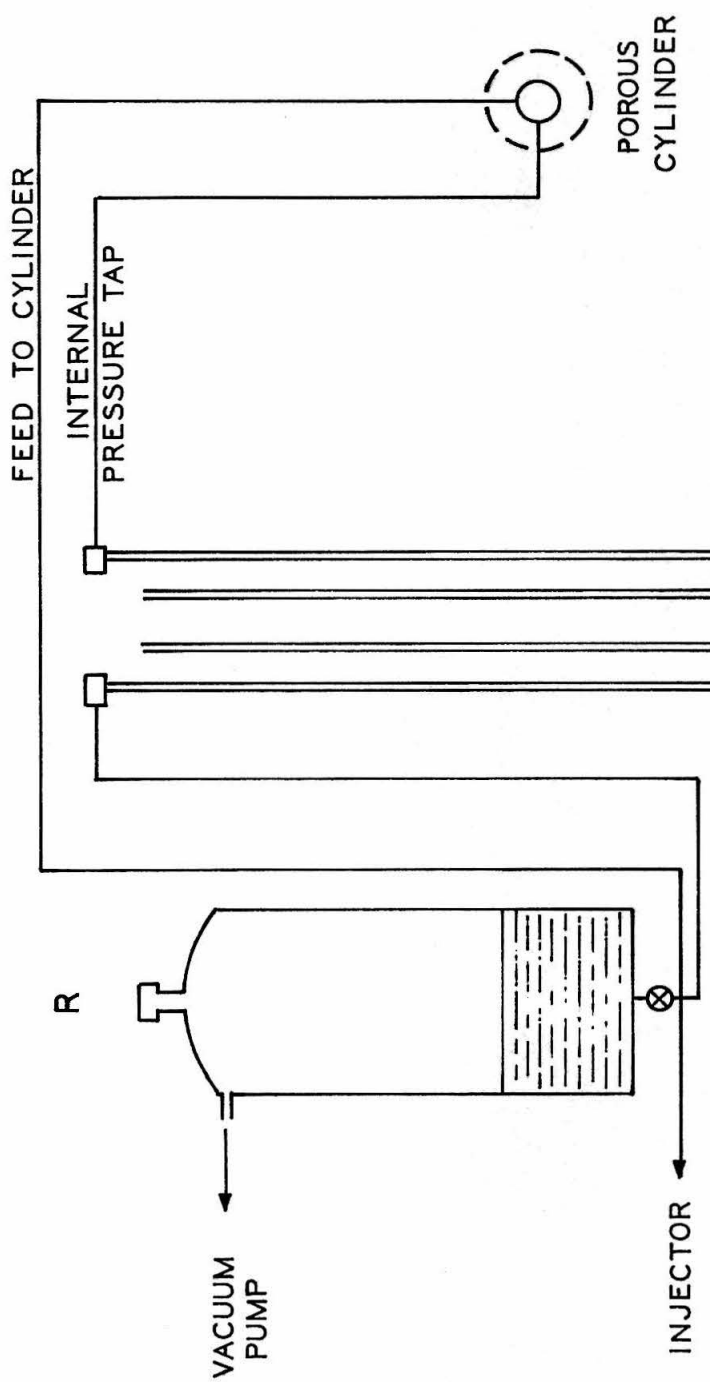

Fig. A10 Schematic Diagram of Liquid Flow to Cylinder - Relation Between Injector and Auxiliary Feed Systems

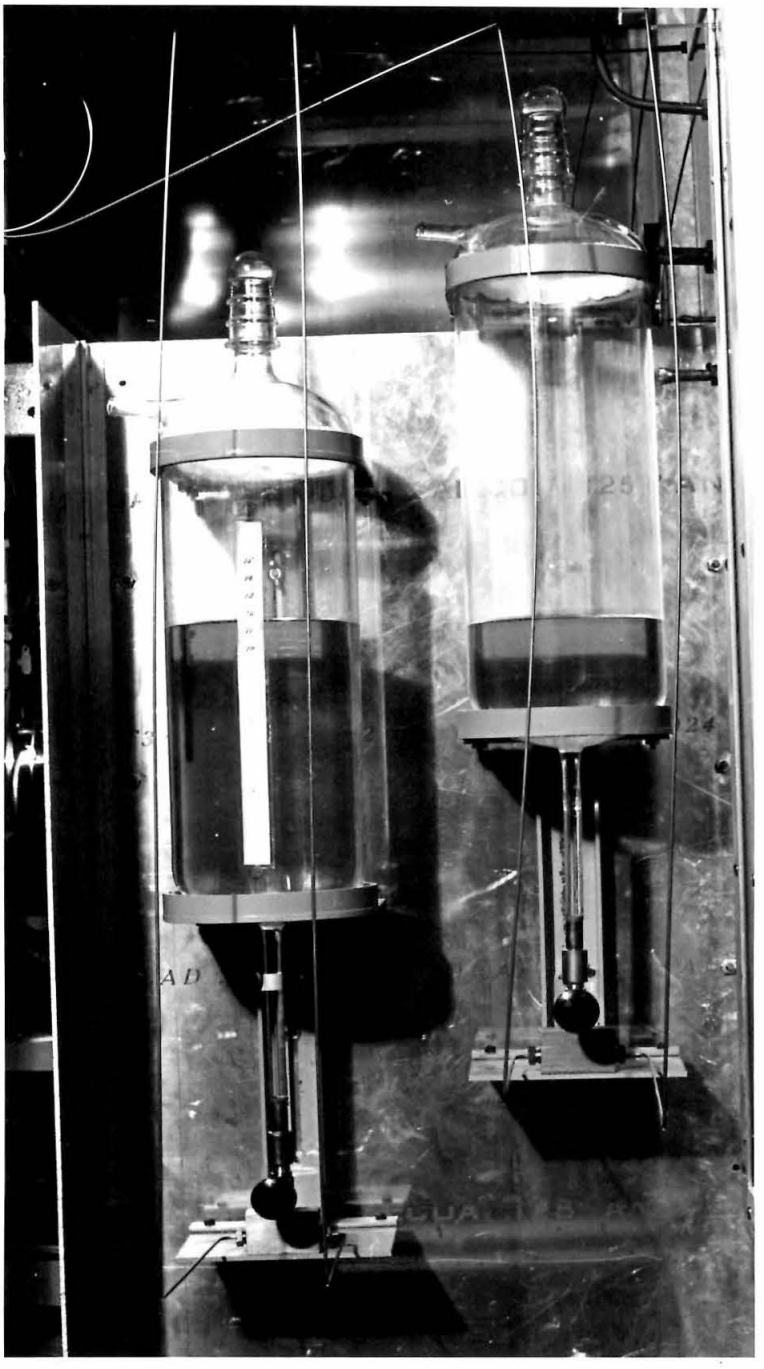

Fig. A11 Auxiliary Feed System - The Reservoir and Connections

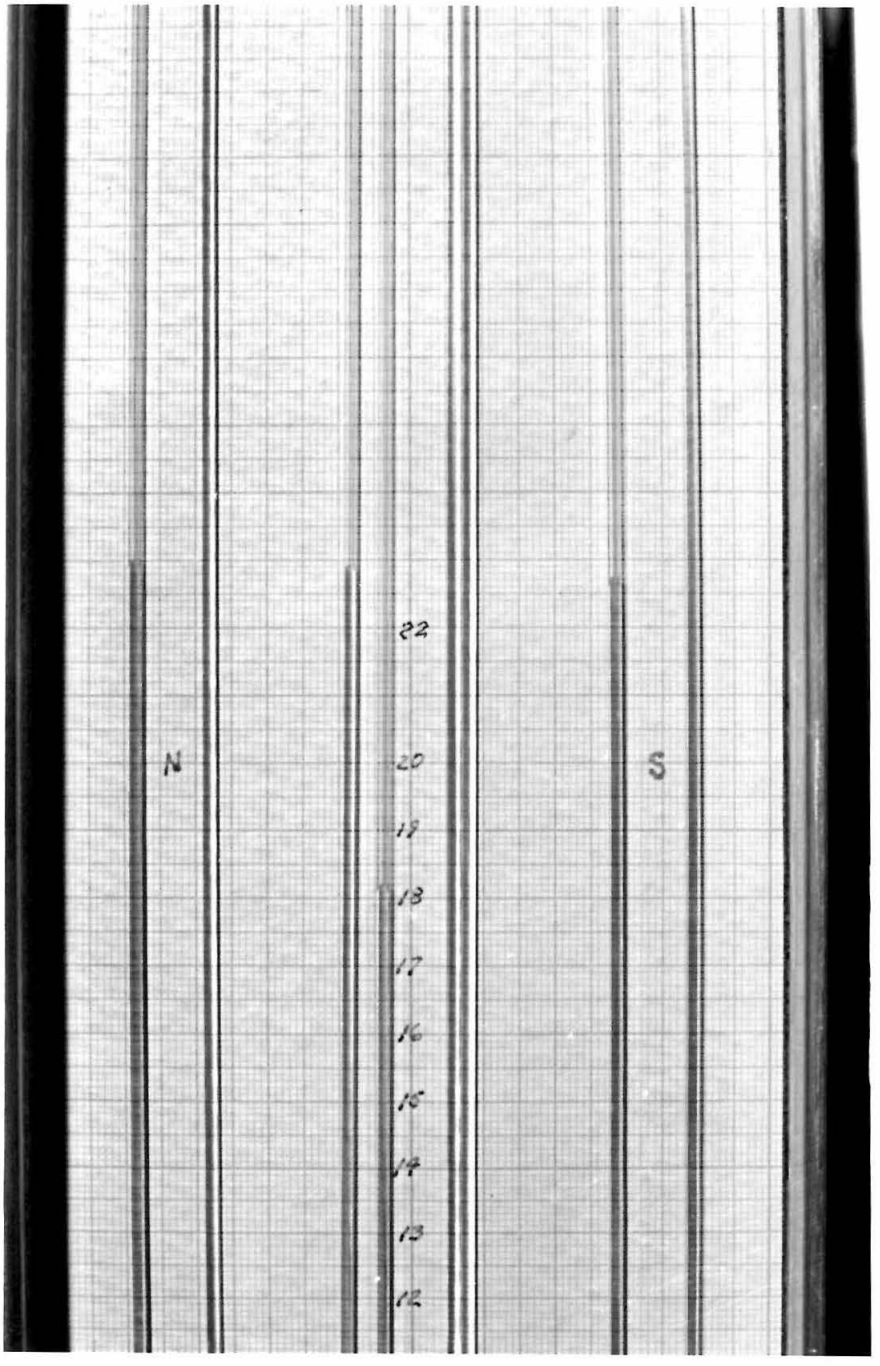

Fig. A12 Manometer System used to Monitor Liquid Feed Rates

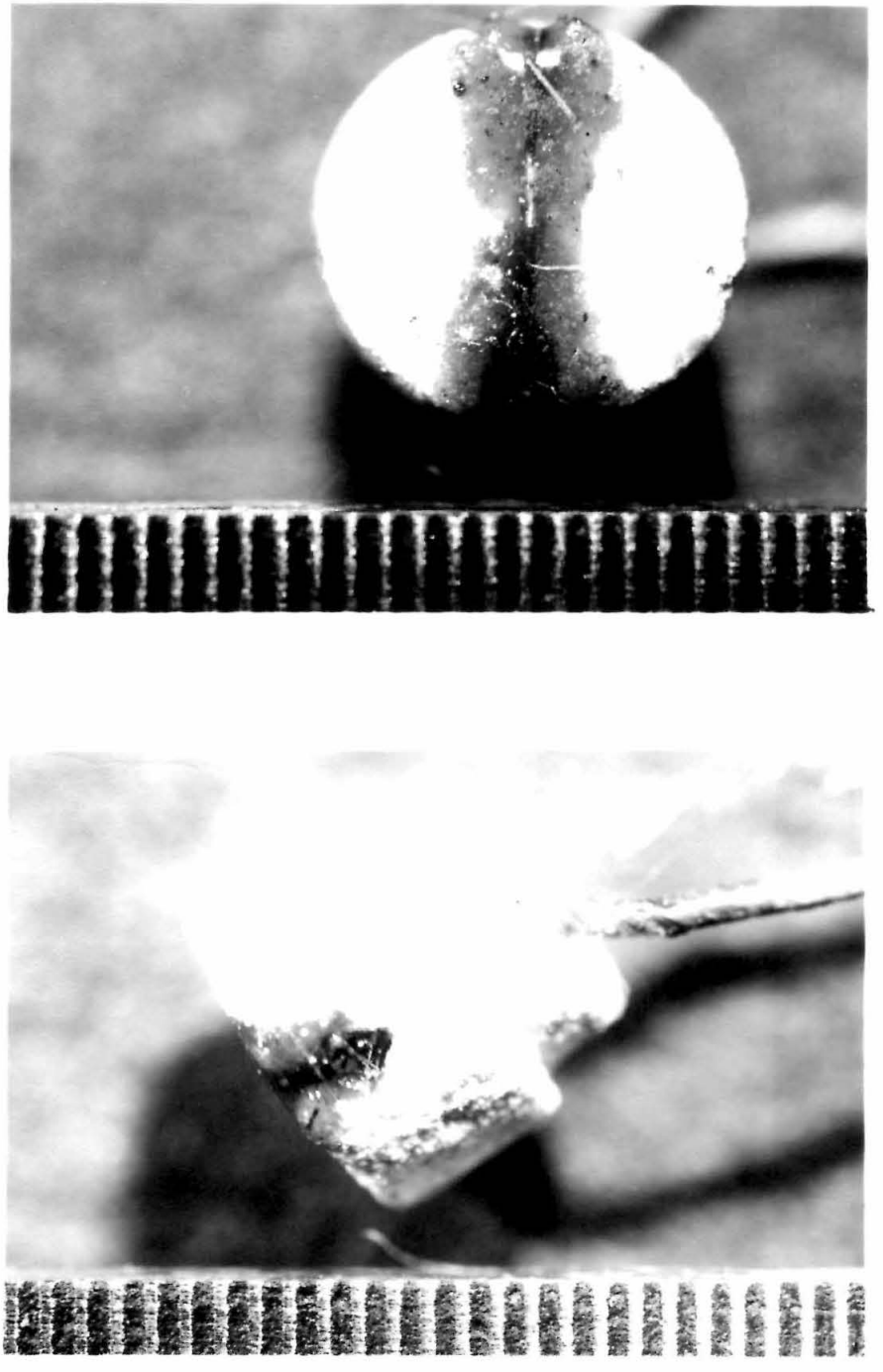

Fig. A13 Photomicrographs of Thermocouple Plug Showing Installation of Surface Thermocouple

Table I

EVAPORATION RATES OF n-HEPTANE AND n-OCTANE IN A TURBULENT AIR STREAM

Liquid Evaporation Rate lb/ft^2-sec	Mean Surface Temperature °F	Free Stream Reynolds No.	Free Stream Turbulence Level	Sherwood Number	Frössling Number
n-Heptane					
16.32×10^{-6}	69.88	1868	0.013	31.72	0.5949
23.82	69.76	3781	0.013	46.27	0.6093
32.35	66.33	7769	0.013	66.58	0.6121
40.88	68.08	11626	0.013	79.81	0.5998
26.83	68.79	3781	0.110	51.01	0.6722
30.15	67.68	3781	0.260	59.62	0.7857
n-Octane					
8.22×10^{-6}	82.65	1871	0.013	35.85	0.6198
11.98	82.20	3781	0.013	52.54	0.6386
17.04	82.29	7752	0.013	74.62	0.6334
21.23	81.88	11655	0.013	94.26	0.6525
* 28.98	81.55	15631	0.013	131.26	0.8141

*Data Point rejected because of suspected supersaturation of cylinder surface with a subsequent loss of fluid by other means than direct evaporation.

Table II

ESTIMATED UNCERTAINTIES IN THE SHERWOOD, REYNOLDS AND FRÖSSLING NUMBERS AND THE LEVEL OF TURBULENCE

A. Sherwood Number

Uncertainty	Affects	Relative Deviation		Absolute Deviation	
		n-Heptane	n-Octane	n-Heptane	n-Octane
Liquid vaporization rate	Direct	0.35%	0.35%	0.35%	0.35%
Cylinder surface temperature	Interface concentration of diffusing species calculated from P"	1.0	0.5	1.0	0.5
Maxwell diffusion coefficient	Direct	-	-	0.7	3.0
Sample Purity	Direct	0.01	0.01	0.01	0.01

Overall Uncertainty in Sherwood Number:	Relative	Absolute
n-Heptane	1.06%	1.27%
n-Octane	0.61	3.06

Table II (Continued)

B. Reynolds Number

Uncertainty	Relative Deviation	Absolute Deviation
Bulk flow rate	0.1%	0.5%
Ratio between local and bulk velocity	1.5	1.5
Kinematic viscosity of air	-	0.1

Overall Uncertainty in Reynolds Number:	Relative	Absolute
	1.50%	1.58%

C. Frössling Number

Uncertainty	Relative Deviation		Absolute Deviation	
	n-Heptane	n-Octane	n-Heptane	n-Octane
Sherwood Number	1.06%	0.61%	1.27%	3.06%
Cube Root Schmidt Number	-	-	0.23	0.99
Reynolds Number	1.50		1.58	

Overall Uncertainty in Frössling Number:	Relative	Absolute
n-Heptane	1.84%	2.04%
n-Octane	1.62	3.58

Table II (Concluded)

D. Level and Integral Scale of Turbulence with Perforated Plate Grid 7/8" Holes on 1" Centers

	Level	Uncertainty	Scale	Uncertainty
No grid	0.013	0.004	?	?
8 fps; 4-1/2" downstream	0.26	0.026	0.67"	10%
8 fps; 7-1/2" downstream	0.11	0.011	0.78"	10%

Table III

VARIATION IN CYLINDER SURFACE TEMPERATURE WITH THE REYNOLDS NUMBER, LEVEL OF TURBULENCE AND THE MEAN LABORATORY TEMPERATURE

Run	Evaporating Fluid	Reynolds No.	Turbulence Level	Mean Cylinder Temperature	First Fourier* Coefficient A	Mean Laboratory Temperature
601	n-Heptane	1868	0.013	69.72	-1.15	80.6
598-600		3787		69.77	-0.83	83.0-84.0
603		7769		66.22	-1.05	81.0
604		11626		67.98	-1.72	86.7
611	n-Heptane	3781	0.110	68.46	-1.45	85.5
610		3781	0.260	67.40	-1.16	84.0
608	n-Octane	1871	0.013	82.62	-0.44	81.5
609		3781		82.16	-0.47	82.5
605		7752		82.24	-0.73	86.0
606		11655		81.86	-0.71	86.0
607		15631		81.52	-0.51	84.5

*The cylinder surface temperature is described by a Fourier Series which was fit statistically to the many point temperature measurements available, hence:

$$T(\phi) = \overline{T} + A_1 \cos \phi + A_2 \cos 2\phi + \ldots + A_n \cos n\phi$$

the negative values for the first coefficient indicate that the back half of the cylinder is warmer than the front half.

Table IV

FOURIER COEFFICIENTS DESCRIBING THE SURFACE TEMPERATURE OF THE POROUS CYLINDER AS A FUNCTION OF FREE STREAM REYNOLDS NUMBER AND TURBULENCE LEVEL ~ LABORATORY TEMPERATURE 82 °F

Run	Reynolds Number	Turbulence Level	Mean Cylinder Temperature	A_1	A_2	A_3	A_4	A_5	A_6	A_7
n-Heptane										
601	1870	0.013	70.90	-1.27	-0.40	0.12	0.20	0.04	-0.28	-0.16
598-600	3780		68.97	-1.19	-0.45	0.13	0.18	0.10	-0.19	-0.16
603	7760		67.12	-1.15	-0.52	0.23	0.24	0.14	-0.10	-0.16
604	11640		66.26	-1.13	-0.51	0.33	0.32	0.15	-0.06	-0.16
611	3780	0.110	68.23	-1.39	-0.64	0.28	0.26	0.07	-0.15	-0.10
610	3780	0.260	66.83	-1.60	-0.74	0.37	0.28	0.02	-0.10	-0.04
n-Octane										
608	1870	0.013	82.90	-0.48	-0.16	-0.02	0.11	0.04	-0.07	-0.10
609	3780		82.00	-0.46	-0.21	-0.01	0.08	0.11	-0.02	-0.10
605	7760		81.52	-0.45	-0.24	0.13	0.11	0.14	0.0	-0.10
606	11640		81.37	-0.45	-0.24	0.26	0.16	0.15	0.0	-0.10
607	15630		81.30	-0.45	-0.20	0.36	0.21	0.15	0.0	-0.10

PROPOSITIONS

Proposition 1

The ability to estimate pressure losses for a compressible fluid flowing in a constant area duct is very important in the design of a variety of fluid systems. The pressure loss (or gain) for the flow of a compressible fluid through a constant area duct may be many times greater than that calculated from the Fanning friction factor due to the acceleration or deceleration of the fluid accompanying changes in the specific volume. A correction to the Fanning friction factor is proposed which relates the pressure loss of a compressible fluid flowing in a constant area duct to the incompressible Fanning friction factor and the volumetric behavior of the fluid.

The proposed differential expression for the steady flow of a compressible fluid in a constant area duct is:

$$\frac{dP}{dx} = \left\{1 + \frac{G^2}{g_o \overline{P}} \left[\frac{d}{d\overline{P}} (ZbT) - \left(\frac{ZbT}{P}\right)\right]\right\}^{-1} \left(\frac{dP}{dx}\right) \qquad (1)$$

where $(dP/dx)_{friction}$ denotes the frictional pressure drop calculated for an incompressible fluid having the same density, flow rate, and Reynolds Number as the compressible fluid, and the indicated derivative with respect to pressure must be evaluated along the path of flow.

Where the compressible fluid can be assumed to be an ideal gas the differential equation above reduces to the following simple expression when the flow is adiabatic:

$$\frac{dP}{dx} = \frac{1 + (\gamma - 1)M^2}{1 - M^2} \left(\frac{dP}{dx}\right)_{friction} \qquad (2)$$

whereas, if isothermal flow of an ideal gas is considered, it can be shown that the general form reduces to:

$$\frac{dP}{dx} = \frac{1}{1 - \gamma M^2} \left(\frac{dP}{dx} \right)_{friction} \qquad (3)$$

Discussion

Measurements and correlations of friction losses for compressible flow at velocities near sonic have been made by Moody (1) and Keenan et al. (2). These investigators found no significant variation in the Fanning friction factor with velocity (outside of the well known Reynolds Number dependence) for Mach numbers less than unity. Shapiro (3) and Lappell (4) substantiated these findings. Lappel states,* "For a given pipe and flow rate, f depends only upon viscosity, which in turn depends only upon temperature, (the variation with pressure generally being negligible for pressures less than 100 atmospheres)."

Since the frictional forces observed for flow through a pipe or duct are not appreciably affected by the compressibility or incompressibility of the fluid studied, as evidenced by the findings above, it seems reasonable to relate the total pressure loss for the flow of a compressible fluid to the frictional losses encountered by an incompressible fluid under the same conditions of flow. For incompressible flow the Fanning friction factor is a function of the pipe Reynolds Number and pipe roughness only, and the following equation applies:

---

*This statement is not strictly true. In the case of hydrocarbon vapors the viscosity at 100 atmospheres may be substantially different than the viscosity at atmospheric pressure.

$$\left(\frac{dP}{dx}\right)_{friction} = -\frac{4f}{D}\left(\frac{\rho U^2}{2}\right) \qquad (4)$$

It is proposed that this relation be used in conjunction with the differential forms presented previously to calculate the pressure drop (or gain) for the flow of a compressible fluid through a constant area duct.

Finally it will be appreciated that the pressure effects associated with the compressiblity of a fluid are related to rate of change of the specific volume with downstream distance. For this reason the derivative of the group (ZbT) appearing in the general expression for the pressure drop of a compressible fluid must be evaluated along the path of flow. The derived relation is applicable to the steady flow of a non-ideal gas which may be undergoing chemical reaction. The overall pressure drop is calculated from a line integration involving the evaluation of the derivatives of the variables Z, b, and T with respect to the pressure P along the actual path of flow.

Theory

For steady flow in a constant area duct the momentum equation can be written as indicated by Longwell (5):

$$u \frac{\partial u}{\partial x} = \frac{1}{\rho} \left(- \frac{dP}{dx} + \frac{F}{A} \right) \qquad \text{ft/sec}^2 \qquad (5)$$

Continuity can be expressed:

$$G = g_o \rho U = \text{const} \qquad \text{lb/ft}^2\text{sec} \qquad (6)$$

Introducing an equation of state:

$$V = \frac{ZbT}{P} \qquad \text{ft}^3\text{/lb} \qquad (7)$$

$$U = \frac{G}{g_o \rho} = GV = G\left(\frac{ZbT}{P}\right) \qquad (8)$$

$$\frac{dU}{dx} = G \frac{d}{dx}\left(\frac{ZbT}{P}\right) \qquad (9)$$

and

$$U \frac{dU}{dx} = G^2\left(\frac{ZbT}{P}\right) \frac{d}{dx}\left(\frac{ZbT}{P}\right) \qquad (10)$$

Expanding this expression, and equating it to the net forces acting on the system per unit weight, one obtains*

*Strictly speaking, this equality is not correct, as it implies U(dU/dx) = u(du/dx). However, this approximation becomes better as the Reynolds Number increases due to the relatively flat velocity profile caused by turbulence. Since situations where sonic velocity is approached will seldom be accompanied by Reynolds Numbers less than 100,000, this approximation is reasonable.

$$G^2\left(\frac{ZbT}{P}\right)\left[\frac{1}{P}\frac{d(ZbT)}{dP} - \frac{1}{P}\left(\frac{ZbT}{P}\right)\right]\frac{dP}{dx} = \frac{1}{\rho}\left(-\frac{dP}{dx} + \frac{F}{A}\right) \qquad (11)$$

Since from equation (7) $\rho = \frac{1}{g_o}\left(\frac{P}{ZbT}\right)$

$$-G^2\frac{1}{g_o}\left[\frac{1}{P}\frac{d(ZbT)}{dP} - \frac{1}{P}\left(\frac{ZbT}{P}\right)\right]\frac{dP}{dx} = \frac{dP}{dx} - \frac{F}{A} \qquad (12)$$

Rearranging this expression, and designating the frictional forces per unit area, F/A, as $-(dP/dx)_{friction}$ gives the desired expression which can be put in any of several forms.

$$\frac{dP}{dx} = \left\{1 + \frac{G^2}{g_o}\left(\frac{dV}{dP}\right)\right\}^{-1}\left(\frac{dP}{dx}\right)_{friction}$$

$$= \left\{1 + \frac{G^2}{g_o}\frac{d\left(\frac{ZbT}{P}\right)}{dP}\right\}^{-1}\left(\frac{dP}{dx}\right)_{friction}$$

$$= \left\{1 + \frac{G^2}{g_o P}\left[\frac{d}{dP}(ZbT) - \left(\frac{ZbT}{P}\right)\right]\right\}^{-1}\left(\frac{dP}{dx}\right)_{friction} \qquad (1)$$

where it is noted that the pressure differential in the bracketed quantity must be evaluated according to the path followed by the flowing fluid.

For an ideal gas with no reaction taking place:

$$\frac{d}{dP}(ZbT) = b\frac{dT}{dP} \qquad (Z = 1) \qquad (13)$$

and

$$a^2 = \left(\frac{\partial P}{\partial \rho}\right)_s = g_o \gamma bT \qquad ft^2/sec^2 \qquad (14)$$

For an ideal gas in adiabatic flow:

$$\left(\frac{dT}{dP}\right)_{adiabatic} = \left(\frac{dT}{du}\right)_{adiabatic} \times \left(\frac{du}{dP}\right)_{adiabatic} \tag{15}$$

From the energy equation:

$$H + \frac{u^2}{2g_o} = \text{const} \tag{16}$$

Again making the approximation that $u = U$, differentiating, and replacing dH by $C_P\,dT$

$$C_P\,dT + \frac{U\,dU}{g_o} = 0 = \frac{\gamma}{\gamma-1}\,b\,dT + \frac{U\,dU}{g_o} \tag{17}$$

where the second equality results from the ideal gas law, where $C_P = (\gamma/\gamma-1)b$, then:

$$\frac{dT}{dU} = -\frac{\gamma-1}{\gamma} \cdot \frac{U}{g_o b} \tag{18}$$

Also:

$$\frac{dU}{dx} = G\,\frac{d}{dx}\left(\frac{ZbT}{P}\right) \tag{9}$$

Replacing the independent variable x with P and performing the indicated operation gives:

$$\frac{dU}{dP} = G\,\frac{d}{dP}\left(\frac{ZbT}{P}\right) = \frac{Gb}{P}\left(\frac{dT}{dP}\right)_{adiabatic} - \frac{GbT}{P^2} \tag{19}$$

Substituting equations (18) and (19) into equation (15), recognizing that $G = U(P/bT)$ and that $M \cong U/a$:

$$\left(\frac{dT}{dP}\right)_{adiabatic} = -\frac{\gamma-1}{\gamma}\frac{U}{g_o}\cdot\frac{G}{P}\left\{\left(\frac{dT}{dP}\right)_{adiabatic} - \frac{T}{P}\right\}$$

or

$$\left(\frac{dT}{dP}\right)_{adiabatic} = \frac{(\gamma-1)\frac{U^2}{g_o\gamma bT}}{1+(\gamma-1)\frac{U^2}{g_o\gamma bT}} = \frac{(\gamma-1)M^2}{1+(\gamma-1)M^2}\frac{T}{P} \qquad (20)$$

Then returning to equation (1)

$$\frac{dP}{dx} = \left\{1 + \frac{PU^2}{g_o b^2 T^2}\left[b\frac{(\gamma-1)M^2}{1+(\gamma-1)M^2}\frac{T}{P} - \frac{bT}{P}\right]\right\}^{-1}\left(\frac{dP}{dx}\right)_{friction}$$

$$= \left\{1 - \frac{U^2}{g_o bT}\frac{1}{1+(\gamma-1)M^2}\right\}^{-1}\left(\frac{dP}{dx}\right)_{friction}$$

$$= \left\{1 - \frac{\gamma U^2}{a^2}\frac{1}{1+(\gamma-1)M^2}\right\}^{-1}\left(\frac{dP}{dx}\right)_{friction}$$

Finally, a rearrangement gives the desired formula relating the pressure drop for an ideal gas to the friction loss for adiabatic flow.

$$\frac{dP}{dx} = \frac{1+(\gamma-1)M^2}{1-M^2}\left(\frac{dP}{dx}\right)_{friction} \qquad (2)$$

For isothermal flow of an ideal gas with no reaction taking place

$$\frac{d}{dP}\left(\frac{ZbT}{P}\right) = -\frac{bT}{P^2}$$

and equation (1) reduces to:

$$\frac{dP}{dx} = \left\{1 - \frac{G^2 bT}{g_o P^2}\right\}^{-1} \left(\frac{dP}{dx}\right)_{friction}$$

as before

$$G^2 = U^2\left(\frac{P}{bT}\right)^2 \quad \text{and} \quad \frac{G^2 bT}{g_o P^2} = \frac{U^2}{g_o bT} = \frac{\gamma U^2}{a^2}$$

and

$$\frac{dP}{dx} = \frac{1}{1 - \gamma M^2} \left(\frac{dP}{dx}\right)_{friction} \tag{3}$$

Nomenclature:

A	cross sectional area of pipe	ft^2
a	sonic velocity	ft/sec
b	gas constant	ft lb/lb^oR
D	pipe diameter	ft
F	total frictional forces/ft	lb/ft
f	Fanning friction factor	
G	weight flow rate	lb/ft^2sec
g_o	standard gravity = 32.17	ft/sec^2
H	specific enthalpy	ft lb/lb
M	Mach number = U/a	
P	pressure	lb/ft^2
T	absolute temperature	^oR
U	bulk velocity	ft/sec
u	local velocity	ft/sec
V	specific volume	ft^3/lb
Z	compressibility factor	
γ	ratio of specific heats	
ρ	density	lb sec^2/ft^4

Note: The force-length-time system of units is employed above, where the lb is the force exerted on a lb mass (in the mass-length-time system) by a standard gravitational field.

References:

1. Moody, L. F., Trans. ASME 66 (1948), p. 671.

2. Keenan, J. H., and Neumann, E. P., Journal App. Mech., 13, No. 2, (1946), p. A-91.

3. Shapiro, Ascher H., The Dynamics and Thermodynamics of Compressible Flow, (two volumes) Copy 1953, Ronald Press Co.

4. Lappel, C. E., Fluid and Particle Mechanics, University of Delaware, (1956), pp. 51-68.

5. Longwell, P. A., Mechanics of Fluid Flow (1958), (unpublished).

Proposition 2

In the study of catalysis the Langmuir Model for the adsorption and subsequent dissociation of a diatomic gas is well known. Based on this model Hougen and Watson (1) derive a series of theoretical rate expressions for catalytic reactions involving the adsorption and subsequent dissociation of a diatomic gas on the catalyst surface. It is proposed that these expressions are fundamentally wrong because allowance was not made for the number of "active sites" occupied by the inert diatomic species, which under some circumstances can amount to an appreciable fraction of the total available "active sites."

Introduction

In their analysis of catalytic reaction rates Hougen and Watson obtain the following "general" expression for the concentration of an adsorbed atomic species A:

$$c_A = \frac{\left(K_A a_{A_{2i}}\right)^{\frac{1}{2}} L}{1 + \left(K_A a_{A_{2i}}\right)^{\frac{1}{2}} + K_B a_{B_i} + K_I a_{I_i}} \qquad \text{XIX, eq. (22)}$$

where B and I are other chemical species, assumed to be adsorbed without dissociation. Since it is assumed that A must first dissociate before reacting to form products, and (implicitly), that the activation energy for the surface reaction is independent of the concentration of adsorbants, the catalytic reaction rate between two adsorbed species becomes proportional to the product of their concentrations.

Much work has been done (2) to indicate that the heat of adsorption of an adsorbed species is not a constant; hence, the adsorption rate constant in the Langmuir expression would not be constant. These considerations led to other forms for the adsorption isotherm (3).

However, it is proposed that the Langmuir derivation for the concentration of adsorbed atomic A presented by Hougen and Watson (1) is fundamentally wrong, and that the magnitude of other effects may be masked by a comparison with an improper model.

Theory

Hougen and Watson (1) present Langmuir's derivation by postulating the following two reactions:

$$A_2 + \ell_2 \rightleftarrows A_2 \cdot \ell_2 \qquad \text{rate controlling step}$$

$$A_2 \cdot \ell_2 + 2\ell \rightleftarrows 2A \cdot \ell + \ell_2 \qquad \text{equilibrium step}$$

where A_2 represents a diatomic gas, ℓ an active site, and ℓ_2 two adjacent active sites. Hence $A_2 \cdot \ell_2$ and $A \cdot \ell$ represent the adsorbed diatomic gas and adsorbed atom respectively. From the second step an expression for the quantity of adsorbed diatomic A_2 was found in terms of the surface dissociation equilibrium constant.

$$c_{A_2} = \frac{s}{2L} \frac{1}{K_{A_d}} c_A^2 \qquad \text{sites/gram}$$

It is conceivable that an appreciable quantity of adsorbed diatomic A_2

might be present on the catalyst surface, thereby reducing the sites available for atomic A. In this case the adsorption of the diatomic form must be taken into account, which Hougen and Watson (1) failed to do.

Again, if the reaction rate of a system involving the participation of dissociated A_2 is proportional to the surface concentration of the atomic form, a rate expression which does not take into account the competitive adsorbed diatomic form could be quite erroneous for systems where the ratio of adsorbed diatomic to monatomic reactant is high. Hence, a new form for the concentration of monatomic A on the catalyst surface is proposed:

$$c_A = \frac{\left(K_A a_{A_{2i}}\right)^{\frac{1}{2}} L}{1 + \left(K_A a_{A_{2i}}\right)^{\frac{1}{2}} + K'_A a_{A_{2i}} \theta_\ell + \cdots} \qquad (1)$$

where

K_A = adsorption equilibrium constant for gaseous A_2

K'_A = equilibrium constant relating adsorbed A_2 to adsorbed A

L = total active sites/gram

c_A = total sites with adsorbed A/gram

θ_ℓ = c_ℓ / L = fraction sites which are unoccupied, and must be evaluated with due consideration to all adsorbed species

and

$$\theta_\ell = \frac{\left[\left\{\sum_i \left(K_A a_{A_{2i}}\right)^{\frac{1}{2}} + \sum_j K_B a_{B_i} + 1\right\}^2 + 4\sum_i K'_A a_{A_{2i}}\right]^{\frac{1}{2}} - \sum_i K_A a_{A_{2i}} + \sum_j K_B a_{B_i} + 1}{\frac{1}{2}\sum_i K'_A a_{A_{2i}}} \tag{2}$$

Using the nomenclature, and following the derivation of Hougen and Watson (1), the rate of adsorption of A_2 can be expressed:

$$r = k_A a_{A_{2i}} c_{\ell_2} - k'_A c_{A_2} \tag{3}$$

From the equilibrium step for dissociation on the catalyst surface;

$$K_{A,d} = \frac{c_A^2 c_{\ell_2}}{c_{A_2} c_\ell^2} \tag{4}$$

Now considering the geometry of an active site, which is surrounded on the average by s nearest equidistant neighbors, it is evident "that the concentration of adjacent vacant active sites is" (1):

$$c_{\ell_2} = \frac{s c_\ell}{2}\theta_\ell = \frac{s c_\ell^2}{2L} \tag{5}$$

Then

$$c_{A_2} = \frac{c_A^2 c_{\ell_2}}{K_{A,d} c_\ell^2} = \frac{s}{2L}\frac{c_A^2}{K_{A,d}} \tag{6}$$

Now L, the number of active sites/gram of catalyst, is the sum of a) the vacant sites, b) the sites with adsorbed A, c) twice the number

of dual sites with adsorbed A_2, plus d) the number of sites occupied by other reacting species. Hence,

$$L = c_\ell + c_A + 2c_{A_2} + \ldots \tag{7}$$

a form which differs from that of Hougen and Watson. Furthermore, if we consider that the adsorption of the diatomic form is in equilibrium as well (this assumption is tantamount to assuming that the rate of the surface chemical reaction, e.g., $aA + bB \rightarrow cC + dD$ is slow relative to the rate of adsorption of A_2 and the rate of dissociation of A_2):

$$r = 0 = k_A a_{A_{2i}} c_{\ell_2} - k'_A c_{A_2} \tag{3a}$$

$$k_A a_{A_{2i}} \frac{s c_\ell^2}{2L} - k'_A \frac{s}{2L} \frac{c_A^2}{K_{A,d}} = 0$$

$$\frac{s}{2L}\left(k_A a_{A_{2i}} c_\ell^2 - k'_A \frac{1}{K_{A,d}} c_A^2\right) = 0 \tag{8}$$

Define the adsorption equilibrium constant as:

$$K_A = \frac{k_A K_{A,d}}{k'_A} = \frac{c_A^2}{a_{A_{2i}} c_\ell^2} \tag{9}$$

Then

$$c_A = c_\ell \left(K_A a_{A_{2i}}\right)^{\frac{1}{2}} \tag{10}$$

and

$$c_{A_2} = \frac{s}{2L} \frac{c_A^2}{K_{A,d}} = \frac{s}{2LK_{A,d}} c_\ell^2 K_A a_{A_{2i}} \tag{11}$$

Then returning to equation (7);

$$L = c_\ell + c_\ell \left(K_A a_{A_{2i}}\right)^{\frac{1}{2}} + \frac{s}{LK_{A,d}} c_\ell^2 K_A a_{A_{2i}} + \cdots \tag{12}$$

and the concentration of adsorbed atomic A is, contrary to formula XIX (22) in Hougen and Watson, the following

$$c_A = \frac{c_A L}{L} = \frac{c_\ell \left(K_A a_{A_{2i}}\right)^{\frac{1}{2}} L}{c_\ell + c_\ell \left(K_A a_{A_{2i}}\right)^{\frac{1}{2}} + \frac{s}{LK_{A,d}} c_\ell^2 K_A a_{A_{2i}} + \cdots} \tag{13}$$

Reducing

$$c_A = \frac{\left(K_A a_{A_{2i}}\right)^{\frac{1}{2}} L}{1 + \left(K_A a_{A_{2i}}\right)^{\frac{1}{2}} + \frac{s}{LK_{A,d}} c_\ell K_A a_{A_{2i}} + \cdots} \tag{14}$$

It is apparent that the other terms in the denominator are of the form $K_B a_{B_i}$ for species adsorbed without dissociation, and

$\left(K_C a_{C_{2i}}\right)^{\frac{1}{2}} + \frac{s}{LK_{C,d}} c_\ell K_C a_{C_{2i}}$ for species adsorbed with dissociation.

This follows since the concentration of all other adsorbed species can be related to the concentration of vacant sites, as was done here, for

component A, independent of the other components.

As it stands, this formula is not yet useful, since it includes the unknown variable c_ℓ in the denominator. However, the quantity c_ℓ/L is the proportion of vacant sites to total sites, which makes evaluation feasible. Then

$$c_A = \frac{\left(K_A a_{A_{2i}}\right)^{\frac{1}{2}} L}{+\left(K_A a_{A_{2i}}\right)^{\frac{1}{2}} + \frac{s}{K_{A,d}} a_{A_{2i}} \theta_\ell + \ldots} \qquad (1)$$

Noting again that the other terms in the denominator are of the form:

$k_B a_{B_i}$ for adsorption without dissociation

and

$\left(K_C a_{C_{2i}}\right)^{\frac{1}{2}} + \frac{s}{K_{C,d}} K_C a_{C_{2i}} \theta_\ell$ for adsorption and dissociation

The expression for the sum of the catalyst sites is again introduced, but is simplified by the substitution of θ_ℓ for c_ℓ / L and the further substitution

$$K'_A = \frac{sK_A}{K_{A,d}} \; ; \qquad K'_C = \frac{sK_C}{K_{C,d}}$$

Then

$$L = c_\ell + c_\ell \left(K_A a_{A_{2i}}\right)^{\frac{1}{2}} + c_\ell K'_A a_{A_{2i}} \theta_\ell + \ldots \qquad (15)$$

Dividing by L

$$1 = \theta_\ell + \theta_\ell \left(K_A a_{A_{2i}}\right)^{\frac{1}{2}} + \theta_\ell^2 K'_A a_{A_{2i}} + \ldots$$

$$+ \theta_\ell K_B a_{B_i} \qquad \text{for non-dissociating species}$$

$$+ \theta_\ell \left(K_C a_{C_{2i}}\right)^{\frac{1}{2}} + \theta_\ell^2 K'_C a_{C_{2i}} \qquad \text{for dissociating species} \quad (16)$$

Hence

$$\theta_\ell^2 \sum_i K'_A a_{A_{2i}} + \theta_\ell \sum_i \left(K_A a_{A_{2i}}\right)^{\frac{1}{2}} + \sum_j K_B a_{B_i} + 1 - 1 = 0 \qquad (17)$$

where the index i denotes a summation of the dissociating species, and j, a summation of the inerts. Then

$$\theta_\ell = \frac{\left\{\left[\sum_i \left(K_A a_{A_{2i}}\right)^{\frac{1}{2}} + \sum_j K_B a_{B_i} + 1\right]^2 + 4\sum_i K'_A a_{A_{2i}}\right\}^{\frac{1}{2}} - \left\{\sum_i \left(K_A a_{A_{2i}}\right)^{\frac{1}{2}} + \sum_j K_B a_{B_i} + 1\right\}}{2 \sum_i K'_A a_{A_{2i}}} \qquad (18),(2)$$

and substituting θ_ℓ into the derived expression for c_A equation (1) gives

$$c_A = \frac{2\left(K_A a_{A_{2i}}\right)^{\frac{1}{2}} L}{\left\{\left[\sum_i \left(K_A a_{A_{2i}}\right)^{\frac{1}{2}} + \sum_j K_B a_{B_i} + 1\right]^2 + 4\sum_i K'_A a_{A_{2i}}\right\}^{\frac{1}{2}} + \sum_i \left(K_A a_{A_{2i}}\right)^{\frac{1}{2}} + \sum_j K_B a_{B_i} + 1} \qquad (19)$$

This expression will now be used to determine the form of a rate equation for two reacting diatomic gases. It will be assumed that adsorbed atomic A and adsorbed atomic C can react only when the two species are adsorbed on adjacent sites:

$$c_{A.C} = c_A \frac{s c_C}{L} = \frac{s}{L} c_A c_C \tag{20}$$

and the rate of reaction is then proportional to this quantity, or by incorporating the constants s and L into the rate constant

$$\text{rate} = k(T) \frac{1}{sL} c_{A.B} = k(T) \frac{c_A c_B}{L^2} \tag{21}$$

Hence the forward rate of reaction between the two adsorbed species A and C is:

$$\text{rate} = \frac{4k(T) \left(K_A a_{A_{2i}}\right)^{\frac{1}{2}} \left(K_C a_{C_{2i}}\right)^{\frac{1}{2}}}{\left\{\left[\sum_i \left(K_A a_{A_{2i}}\right)^{\frac{1}{2}} + \sum_j K_B a_{B_i} + 1\right]^2 + 4\sum_i K'_A a_{A_{2i}}\right\}^{\frac{1}{2}} + \left[\sum_i \left(K_A a_{A_{2i}}\right)^{\frac{1}{2}} + \sum_j K_B a_{B_i} + 1\right]^2} \tag{22}$$

where

$k(T)$ = reaction rate constant/unit wt. catalyst

K_A = adsorption equilibrium constant for A_2

K_B = adsorption equilibrium constant for B_2 (where B is a non-dissociating species)

K'_A = equilibrium constant for surface dissociation of species A

$a_{A_{2i}}$ = gas phase activity for A_2 at the catalyst surface

Discussion

An example for the catalytic reaction of two diatomic gases will now be worked and compared with the formula from Hougen and Watson for the same conditions. The following assumptions are made:

1. A_2 and C_2 adsorbed in appreciable quantities.
2. The surface reaction is the rate controlling step.
3. The reverse reaction rate is negligible.
4. Only adjacently adsorbed atomic A and C can undergo reaction.
5. The rate of diffusion of reactants to the catalyst surface and products away from the surface is much greater than the surface reaction rate.
6. The activities are defined as $a_{A_2} = f/f^o$, where f^o = fugacity at 1 atm.

The comparable formula from Hougen and Watson, which is to be compared with equation (22) is the following:

$$\text{rate} = \frac{k(T)\left(K_A a_{A_2}\right)^{\frac{1}{2}}\left(K_C a_{C_2}\right)^{\frac{1}{2}}}{\left[1 + \left(K_A a_{A_2}\right)^{\frac{1}{2}} + \left(K_C a_{C_2}\right)^{\frac{1}{2}} + K_{AC} a_{AC}\right]^2}$$

These formulas will be compared using the following constants:

$$K_C a_{C_2} = 1 = \text{constant}$$

$$K_A = K'_A = K'_C = 1$$

$$K_{AC} a_{AC} \ll 1$$

while the activity of A_2 will be allowed to vary from 10^{-3} to 10^3. As shown in the table below, at values for the activity of A_2, greater than unity, the form which does not consider the adsorbed diatomic form becomes a very poor approximation. For this particular case the rate expression becomes

$$\text{rate} = \frac{k(T)\left(a_{A_2}\right)^{\frac{1}{2}}}{\left\{1 + \frac{1}{2}\left(a_{A_2}\right)^{\frac{1}{2}} + \left[2 + \left(a_{A_2}\right)^{\frac{1}{2}} + \frac{5}{4} a_{A_2}\right]^{\frac{1}{2}}\right\}^2} \tag{23}$$

For the same conditions, the Hougen and Watson formula becomes:

$$\text{rate} = \frac{k(T)\left(a_{A_2}\right)^{\frac{1}{2}}}{\left[2 + \left(a_{A_2}\right)^{\frac{1}{2}}\right]^2} \tag{24}$$

A plot can be made of rate/K(T) for these two expressions as a function of the change in the partial pressure of A_2.

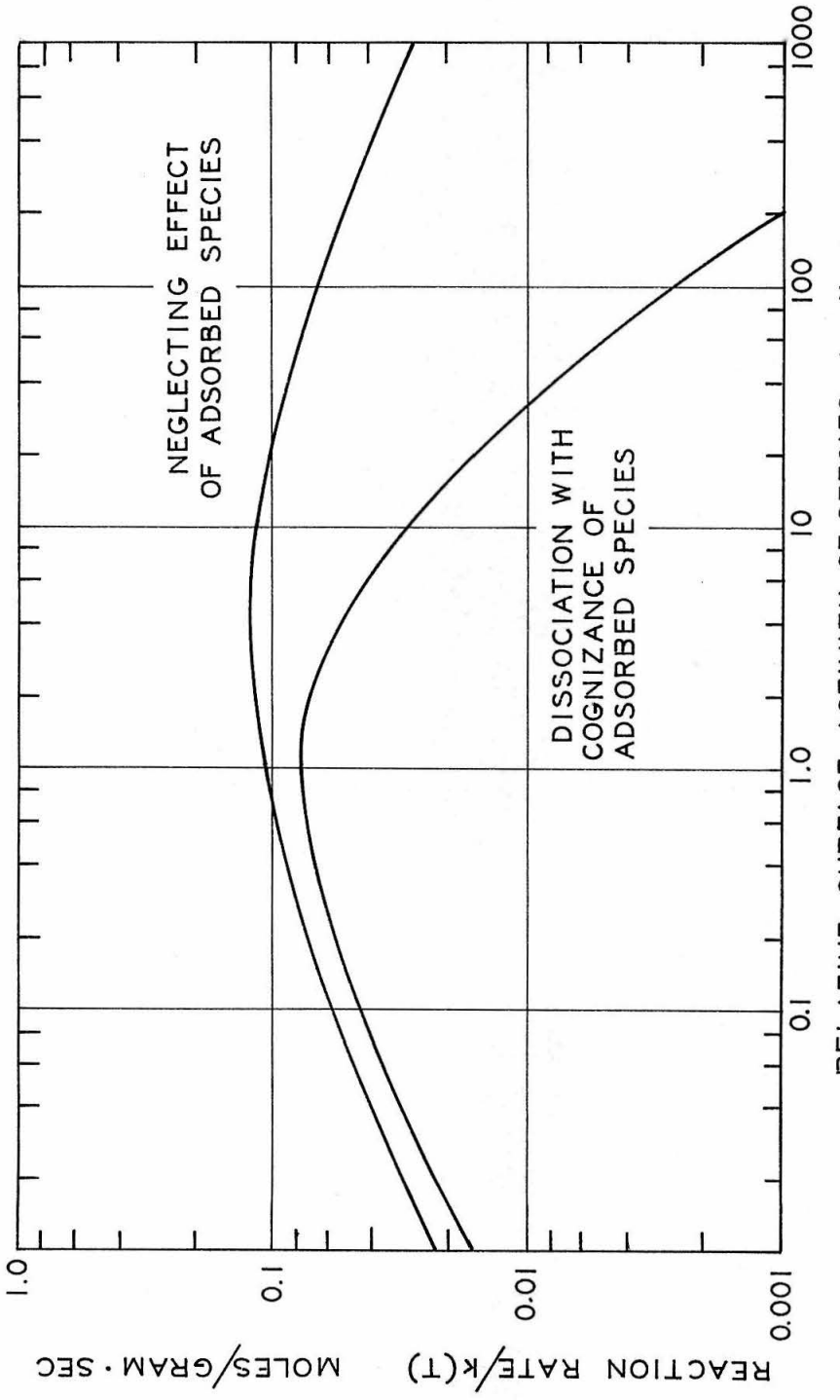

Fig. 1 Relative Catalytic Reaction Rates for the Reaction of two Diatomic Gases - Calculated With and Without Considering Presence of Adsorbed Diatomic Species

Activity in A_2	Normalized Reaction Rate	
	Hougen and Watson	Proposed
0.001	0.00765	0.00537
0.01	0.0227	0.0166
0.05	0.0452	0.0347
0.10	0.0589	0.0463
0.20	0.0747	0.0595
0.50	0.0965	0.0748
1.00	0.1111	0.0788
2.00	0.1213	0.0720
5.00	0.1246	0.0493
10.00	0.1186	0.0304
100.00	0.0694	0.00254
1000.00	0.0280	0.00011

References

1. Hougen, Olaf A., and Watson, Kenneth M., Chemical Process Principles: Part Two - Thermodynamics, John Wiley and Sons, Inc., New York (1955).

2. Trapnell, B. M. W., Chemisorption, Academic Press, New York (1955).

3. Halsey, G., Advances in Calalysis, Vol. 4, 259 (1952).

Nomenclature:

$a_{A_{2i}}$	activity of diatomic gas A at catalyst surface
a_{B_i}	activity of inert gas B at catalyst surface
c_A	concentration adsorbed atomic A per gram catalyst
c_{A_2}	concentration adsorbed diatomic A per gram catalyst
c_ℓ	concentration vacant sites per gram catalyst
c_{ℓ_2}	concentration "dual" or adjacent vacant sites per gram catalyst
$K_{A,d}$	dissociation constant for adsorbed species A
$K_A = \frac{c_A^2}{a_{A_{2i}} c_\ell^2}$	adsorption equilibrium constant for adsorbed atomic A
$K_A' = \frac{sK_A}{K_{A,d}}$	adsorption equilibrium constant for adsorbed diatomic A
k_A	forward rate constant for adsorption of A_2
k_A'	reverse rate constant for desorption of A_2
$k(T)$	reaction rate constant for reaction between adsorbed atomic A and adsorbed atomic C
L	total active sites per gram catalyst
s	average number of nearest adjacent sites, a property of the catalyst surface
$\theta_\ell = c_\ell / L$	fraction vacant catalytic sites

Proposition 3

In many of the studies of material and energy transport conducted in this laboratory, it is necessary to maintain a constant mass flow rate of air. A graphical technique is proposed for the rapid calculation of weight flow rates of air through a Herschel type venturi. This technique allows the graphical determination of weight flow rates directly from measured laboratory data with a relative accuracy of ± 0.1%. The advantage of this technique over the direct longhand computation using the standard venturi formula is its speed. The direct computation of weight flow rates using the standard laboratory procedure (1) requires between twenty and thirty minutes of computation, and is impractical for use by the operator in the laboratory to maintain desired air flow rates.

Introduction

For a given venturi the pressure drop (difference between upstream and throat pressure) is a function of the air density, flow rate, and venturi Reynolds Number, the latter parameter affecting the magnitude of the correction for viscous effects. In addition, for a compressible fluid the pressure drop is also a function of the relative pressure drop, $\Delta P/P_A$, (1, 2). For this case, the venturi formula becomes:

$$\dot{\underline{m}} = \phi\lambda \left\{ \frac{P_A \Delta P}{bT_A \left[1 + \theta\left(\frac{\Delta P}{P_A}\right)\right]} \right\}^{1/2} \qquad (1)$$

where ϕ is the discharge coefficient, a function of venturi Reynolds Number, θ is a function of the compressibility of the fluid ($\theta = 0$ for an incompressible fluid), and the subscript "A" refers to conditions immediately upstream of the venturi.

The complexity of the direct computation of the weight flow rate is due to the many steps required in the evaluation of the pressure terms in equation (1) from the laboratory manometer readings. This process requires several corrections for differences in elevation between the manometer levels and the centerline of the venturi, and also a search through tabulated values of the density of the various manometer fluids as a function of laboratory room temperature. Furthermore, the compressibility coefficient, θ, is a function of the ratio $\Delta P/P$ and temperature and is tabulated as a function of these variables for each of the several venturis. Finally, the discharge coefficient, ϕ, is tabulated as a function of Reynolds Number.

In this laboratory the air flow is provided by a series of blowers which are controlled automatically at a predetermined speed. Before reaching the experimental system the air is heated to the desired temperature and then flows through a Herschel type venturi used to measure the flow rate (3). The venturi and its relation to the manometer system is shown schematically in Figure 1.

Because the air supply system normally operates close to atmospheric pressure, and the influence of the variables other than the difference between upstream and throat pressures is small, it is possible to determine weight flow rates from the measured laboratory

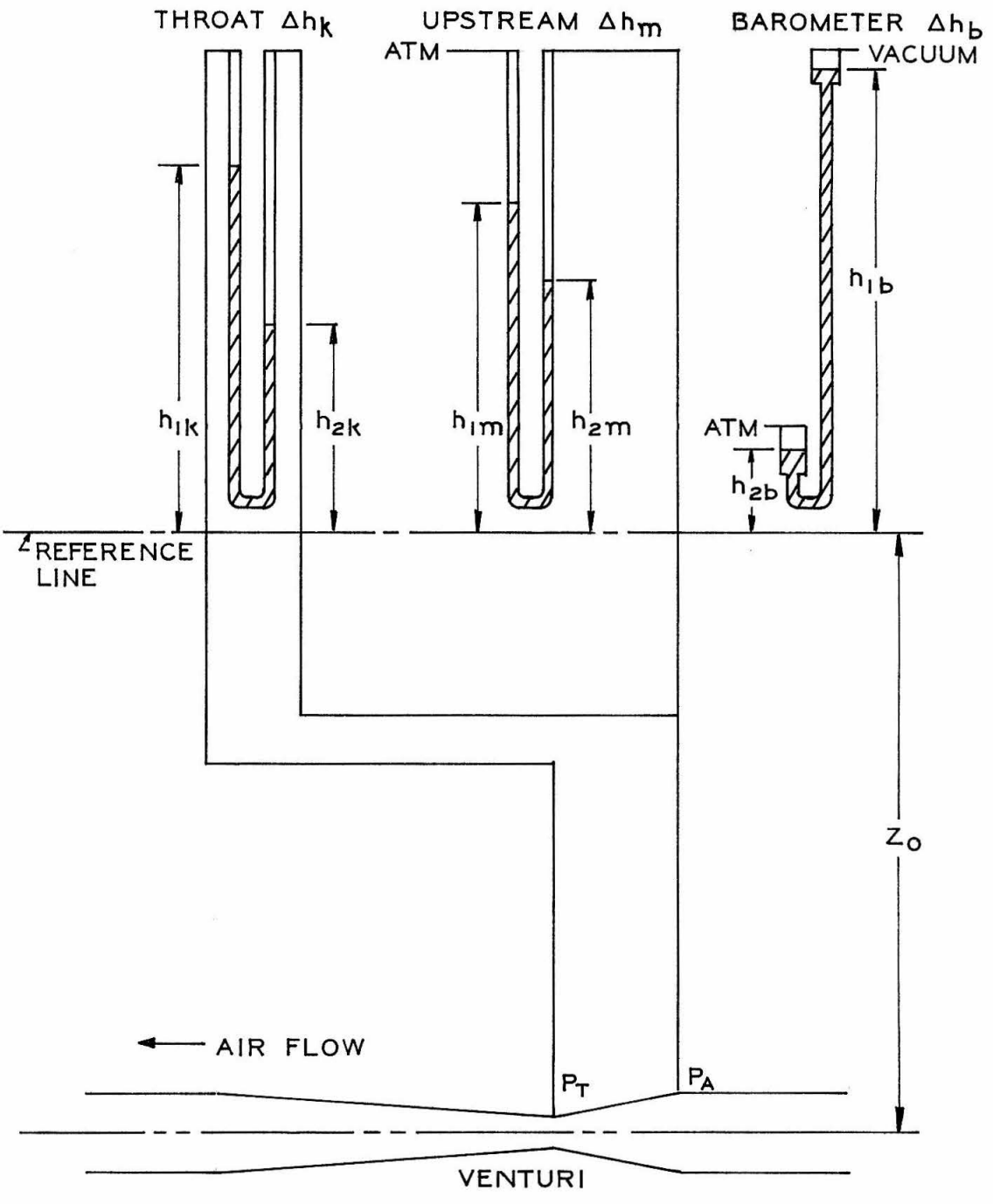

Fig. 1. Schematic Diagram of Venturi and Associated Manometer System

variables with great accuracy using the proposed graphical technique.

Theory

A dimensional analysis approach was used to separate the influence of the five independent variables in equation (1) above. From this equation it was apparent that the weight flow rate of air is a function of the inlet air temperature T_A, pressure P_A, and gas constant b. It is also a function of the manometer reading Δh_k and laboratory temperature T_m, which together determine the pressure drop, or difference between upstream and throat pressures. In this approach it is recognized that the discharge coefficient ϕ is a function of Reynolds Number, and can therefore be expressed in terms of the weight flow rate $\dot{m}$ and T_A (viscosity being nearly independent of pressure). The compressibility coefficient θ is principally a function of the pressure ratio $\Delta P/P$ (for a thermally perfect gas where the isentropic exponent, $\gamma = c_p/c_v$, is constant, θ is a unique function of the pressure ratio). In the case of air θ exhibits only a slight dependence on temperature and this dependence was neglected in the present analysis.

Equation (1) can be rearranged to separate those terms which are functions of air temperature T_A and/or the weight flow rate, $\dot{m}$, as follows:

$$\frac{1}{T_A}\left(\frac{\phi\lambda}{\dot{m}}\right)^2 = \frac{b\left[1 + \theta\left(\frac{\Delta P}{P_A}\right)\right]}{P_A \Delta P} \qquad (2)$$

where the left-hand side of equation (2) is a function of the air temperature T_A or flow rate $\dot{m}$, and the right-hand side of equation (2) is a function of the air inlet pressure P_A, gas constant b, or the pressure drop ΔP. This equality is the heart of the graphical technique presented, for it is easily seen how the function $1/T_A(\phi\lambda/\dot{m})^2$ can be plotted against the weight flow rate, $\dot{m}$, producing a family of curves each for different temperatures.

The second step is to separate the dependence of the right hand of equation (2) on the gas constant b. This is done by plotting the function:

$$\frac{1}{T_A}\left(\frac{\phi\lambda}{\dot{m}}\right)^2 \quad \text{vs.} \quad \frac{1}{bT_A}\left(\frac{\phi\lambda}{\dot{m}}\right)^2$$

thereby producing another family of curves each for a different value of the gas constant b, which for the case of air is a function of the absolute humidity.

After continuing through the first two steps we have the equality which is the counterpart of equation (2):

$$\frac{1}{bT_A}\left(\frac{\phi\lambda}{\dot{m}}\right)^2 = \frac{1 + \theta\left(\frac{\Delta P}{P_A}\right)}{P_A \Delta P} \tag{3}$$

where the right-hand side of equation (3) is now a function only of the inlet pressure P_A and the pressure difference ΔP. The third step consists of plotting the right-hand side of equation (3) against the pressure drop ΔP, thereby obtaining a third family of curves each

for a different pressure P_A, neglecting the very slight variation of the compressibility coefficient, θ, with temperature. In this regard the numerical values of θ used were those tabulated against the ratio $\Delta P/P_A$ for a constant air temperature $T_A = 100\ ^oF$ (1).

In the last step the "pressure drop" ΔP was plotted against the manometer reading Δh_k obtaining a family of curves for different prevailing laboratory temperatures since the specific weight of the manometer fluid is a function of this parameter. In this regard it was also desired to take into consideration the effect of the "air legs" on the manometer readings which tend to offset the pressure indicated by the manometer pressure head. A first order correction for weight flow rates of air in the vicinity of 0.1340 lb/sec through a 3 inch Herschel type venturi tube is formulated by the relation:

$$\Delta P = 0.99899\ \sigma_k \Delta h_k \qquad (4)$$

the indicated factor is an average value correlating a number of test runs made in this laboratory at or close to the weight flow rate cited above. It is noteworthy that the indicated factor never varied by more than six units in the last significant figure for the many test runs correlated. It is also anticipated that this coefficient is a function of Δh_k for different air velocities with the same venturi, and would be subject to some change for greatly different flow rates.

It is evident that each of the fundamental relationships above is not changed if it is desired to go from an observed manometer differential, Δh_k, back through the four graphs to obtain the current

air flow rate, so the four plots were combined on each graph. A simple graphical method of determining weight flow rates of air from an observed manometer differential which allows for the effects of changes in air density and viscosity in terms of measured laboratory variables is thereby obtained.

In practice, the inlet pressure, P_A, is not measured directly, but was determined graphically from the readings of the upstream manometer and barometer with a family of curves allowing for the effect of laboratory temperature on the density of the manometer fluids. All these relations are shown in Figure 2. The effect of the air legs in determining the venturi entrance pressure P_A is correlated by the factors 1.00036 and 1.00041 where:

$$P_A = 1.00036\ \sigma_b\ \Delta h_b + 1.00041\ \sigma_m\ \Delta h_m \qquad (5)$$

The error introduced by this correlation is comparable to the uncertainty introduced into the expression for ΔP above (equation 4) and is entirely negligible.

Discussion

In seeking a graphical technique to be used as an aid to the operator interested in maintaining constant air flow rates in the laboratory it was necessary to account for the not insignificant effects of small variations in the air density due to changes in the pressure P_A and gas constant b and in the laboratory temperature, T_m, which affects the density of the various manometer fluids.

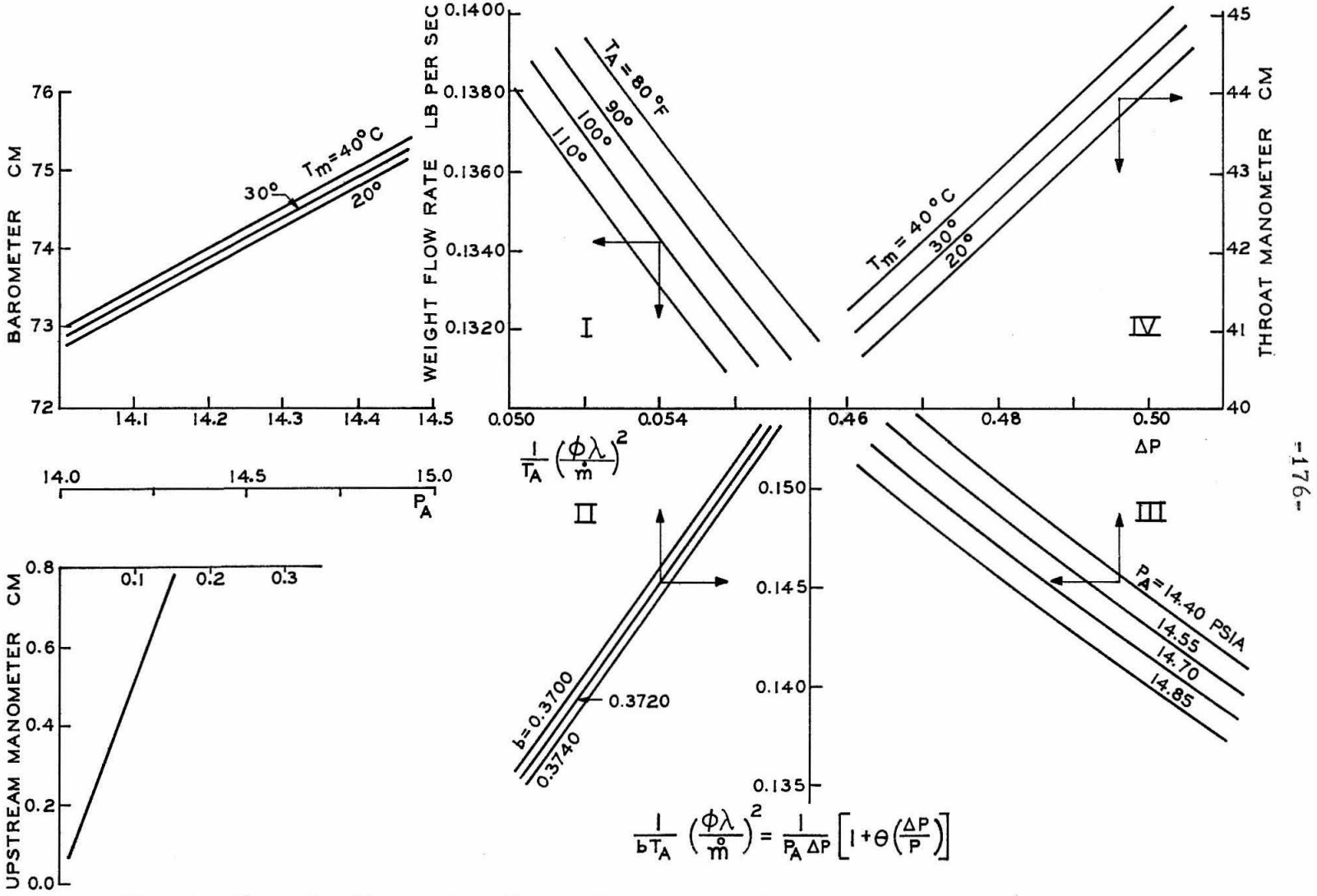

Fig. 2. Chart for Predicting Weight Flow Rates With Air From Measured Laboratory Data.

The proposed chart shown in Figure 2 is a smaller sized version of the one used in the laboratory for a nominal air velocity of 8 feet per second ($\dot{m}$ = 0.1341 lb/sec). With the larger sized laboratory version, it was found possible to predict laboratory mass flow rates with a relative certainty of better than ± 0.1% from a given set of laboratory data, or to select the necessary blower speed to obtain a desired mass flux with comparable certainty. The chart shown, as with the laboratory version, extends over a limited range only (to improve the accuracy with which the charts could be read) and different charts were made for several of the nominal air flow rates used in this laboratory.

To use the chart, one selects the desired mass flow rate $\dot{m}$ on the left, crosses over to the appropriate inlet air temperature, T_A, then travels down to the appropriate value of the gas constant, b; across to the inlet pressure, P_A, and up to the laboratory temperature T_m. The desired manometer head, Δh_k, is then read on the right-hand side of the chart. The process is reversed to go from a measured manometer head Δh_k to obtain the corresponding mass flow rate of air. On the far left-hand side of the figure the inlet pressure P_A is obtained by adding the pressures corresponding to the readings of the barometer b, and the manometer m. This is done graphically by determining the intersection of a straight line from the pressures sensed by the barometer and manometer (the abscissas of the charts shown at the far left of Figure 2) with the additive scale line P_A.

References

1. Laboratory Standards, Chemical Engineering Laboratory, California Institute of Technology, Pasadena, California (October, 1953).

2. Lacey, W. N., and Sage, B. H., Thermodynamics of One-Component Systems, Academic Press, New York (1957).

3. Jorissen, A. L., and Ithaca, N.Y., "Discharge Coefficients of Herschel-Type Venturi Tubes," Transactions of the ASME, Vol. 74, pp. 905-913 (1952).

Nomenclature:

A. Roman Type Symbols

b	gas constant	$ft^3/in^2 \cdot {}^oR$
h	elevation	ft
$\dot{m}$	weight flow rate	lb/sec
P	pressure	lb/in^2
T	temperature	${}^oR$
Z_o	elevation of manometer reference point above venturi centerline	ft

B. Greek Type Symbols

Δ	difference operator	
θ	compressibility coefficient	
λ	venturi coefficient (a function of venturi size and shape)	$ft^{3/2} \cdot$ in/sec
σ	specific weight	lb/ft^3
ϕ	venturi discharge coefficient	

C. Subscripts

b	barometer
k	manometer between venturi inlet and throat
m	manometer between venturi inlet and atmospheric

Proposition 4

The possibility of measuring small distances electrically by establishing the point of electrical contact was investigated using a 30 volt potential. It is proposed that the point of contact can be established to within ±0.0001 inch in this manner with a probe contacting either a metal or weak electrolyte surface.

Introduction

A number of experimental programs have been conducted in this laboratory to investigate local temperatures and Nusselt Numbers sensed by a small wire in the vicinity of a cylinder (1, 2) or sphere (3, 4). These workers used various techniques to determine the separation between the wire and the cylinder (or sphere), but their results indicate that their measurements of relative distance were uncertain to the extent of ± 0.001 inch.

To investigate the possibility of improving distance measurements should future studies of this nature arise preliminary tests of the proposed electrical contact method were made. A 30 volt source was selected for this investigation. With this choice of potential difference it was hoped that thin layers of surface oxide (in the case of a metal surface) would be penetrated, but that appreciable errors due to "sparking" would not be encountered.

Discussion

The contact "probe" selected for this study was a 0.01 inch

platinum wire. Distances were monitored through the use of a standard Micrometer acting against the tip of a spring loaded lever. The wire probe was located one-fifth of the way from the fulcrum to the lever end, thereby increasing the resolution of the distance measurements by a factor of five.

The electrical circuit employed consisted of a standard Leeds and Northrup Galvanometer in series with a 30 volt source and a 4 megohm resistance. The purpose of the 4 megohm resistor was to limit the current through the system to 7.5 micro-amps which was somewhat greater than that required to obtain a full scale deflection of the galvanometer. To balance the circuit a small resistance was connected in parallel with the galvanometer both to protect it against induced voltages when the circuit was opened and closed, and also to reduce the current through the galvanometer to a level so that a full scale deflection would be produced when the circuit was closed. The resistance selected for this purpose was 70 ohms.

The electrical circuit described above was closed when the platinum probe made contact with the metal or electrolyte surface. In the latter case an electrolyte "surface" was maintained by allowing a flat diatomaceous earth surface to become saturated with distilled water. In this regard the capillary action of the diatomaceous earth sample was sufficient to provide a saturated surface against an adverse pressure gradient of 13 inches of water. It was discovered that reproducible results were not obtained unless the porous material was made to lift water to the surface against some adverse pressure

gradient, which is to be expected. The diatomaceous earth used in this study is available commercially under the trade name Allen Filter Material.

Several possible situations which might be encountered were tested. The platinum probe was tested against polished and partially oxidized brass surfaces. In addition, tests were made on the wet diatomaceous earth surface where the fluid was raised 0.0, 9.5, and 13.25 inches by capillary action. The data indicate that for other than very clean metal surfaces, the point at which electrical contact is broken gives a more consistent indication of the point of contact than the point at which electrical contact is made. This effect is apparent in Figure 1. It is concluded that this phenomenon is due to the presence of an insulating oxide film which required a certain force to rupture, but did not interfere with the reverse process.*

For a porous surface impregnated with a liquid electrolyte the point at which contact is made is the best indicator of position because of an observed tendency for the probe to pull a meniscus of liquid with it as it is drawn back. This effect was very prominent when back pressures of 0 and -4.5 inches** of H_2O were employed, but was negligible at the highest back pressure used (-13.25 inches

---

*On one traverse out, the galvanometer current dropped sharply and then recovered before contact was finally broken, which is an exception to the statement above.

**Because of the capillary effect of the porous surface, it is necessary to have a small vacuum on the liquid on the inside of the test specimen to prevent the formation of a liquid film on the surface.

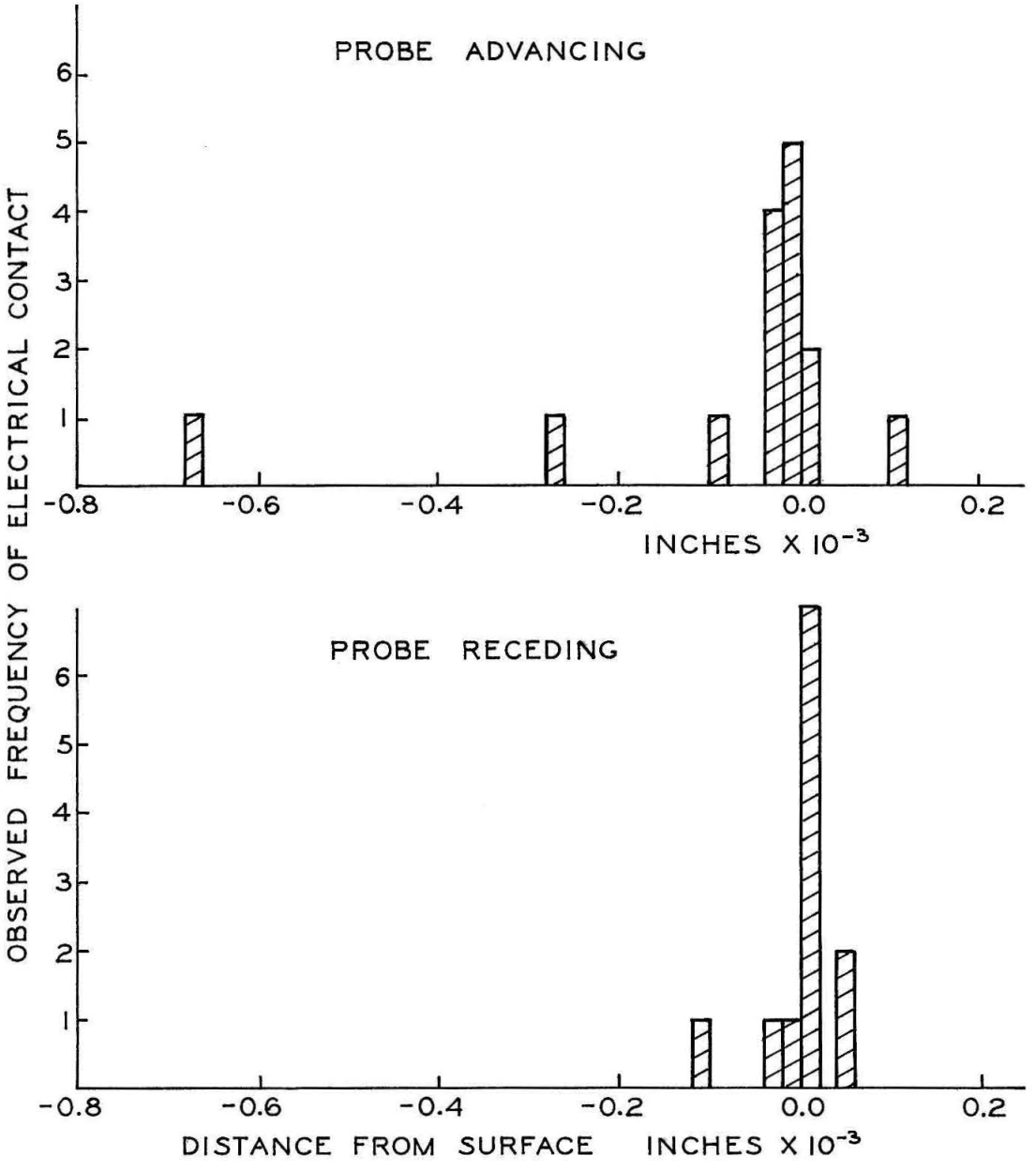

Fig. 1. Electrical Determination of Contact - Brass Surface

of H_2O). Only the results of the data taken with a back pressure of -13.25 in. H_2O appear here in Figure 2, as data taken with lower hydrostatic back pressures showed a much greater variance.

Using the point at which electrical contact is broken as representative of contact for a metal surface, the standard deviation from the mean was 0.00007 inch.

Using the point at which electrical contact is made as representative of contact for a porous surface saturated with a conducting fluid, the standard deviation of the measurements was 0.00005 inch for a back pressure of -13.25 in. H_2O, and 0.00030 and 0.00060 for a back pressure of -4.5 and 0.0 in. H_2O respectively.

All data were taken with the electrical circuit shown, using a 30 volt source. While it would be interesting to know how different voltages would affect the precision of distance measurements, the effect of this variable was not investigated.

References

1. Cuffel, R. F., Ph.D. Thesis, California Institute of Technology, Pasadena, California (1964).

2. Venezian, E. C., Ph.D. Thesis, California Institute of Technology, Pasadena, California (1962).

3. Hsu, N. T., Ph.D. Thesis, California Institute of Technology, Pasadena, California (1956).

4. Short, W. W., Ph.D. Thesis, California Institute of Technology, Pasadena, California (1958).

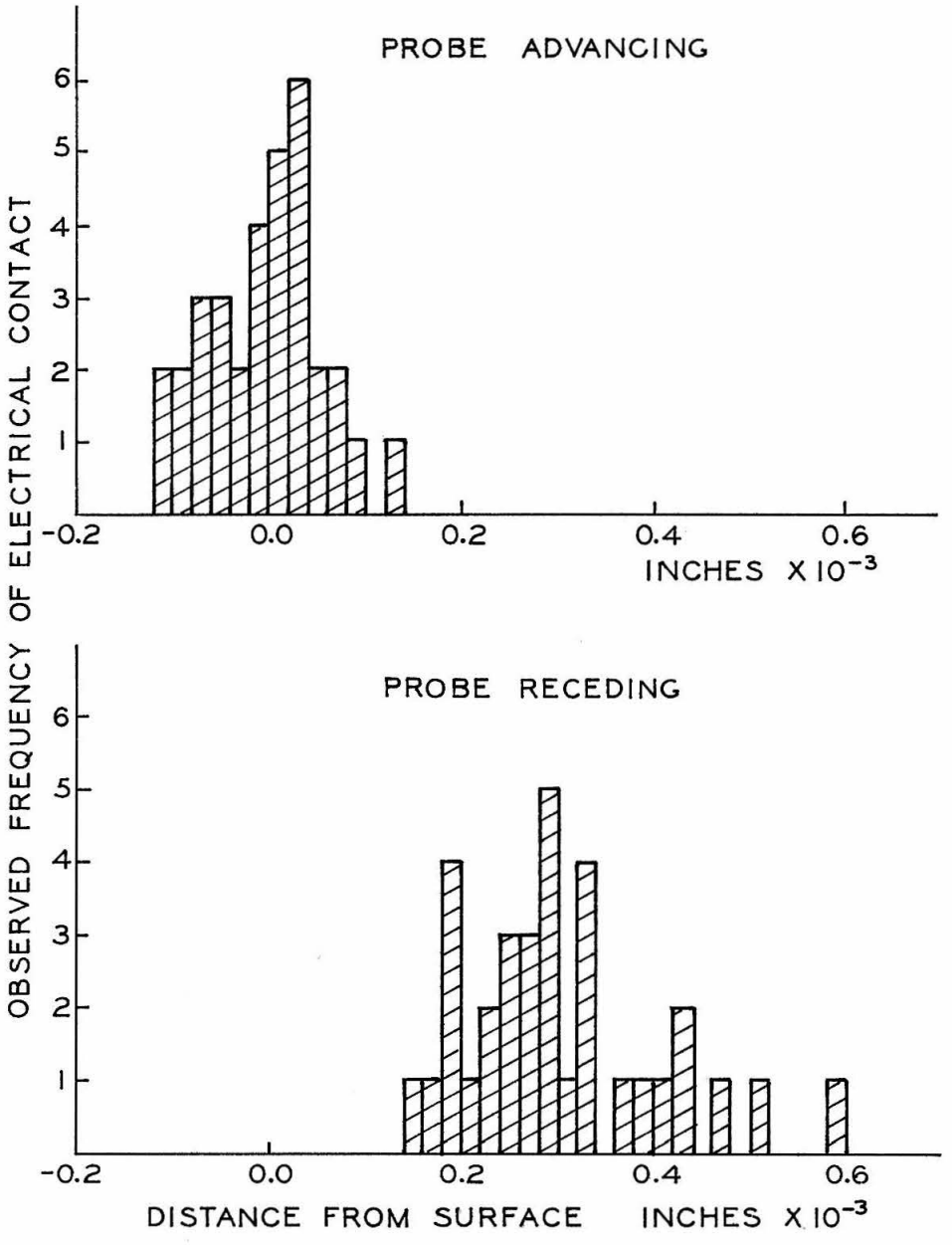

Fig. 2. Electrical Determination of Contact - Wet Diatomaceous Earth Surface

Proposition 5

Turbulence grids are frequently placed in wind tunnels and at free jet exits to control the prevailing free stream turbulence encountered in studies of transport rates from solid bodies. A quantitative knowledge of the apparent level and scale of turbulence prevailing downstream of a turbulence grid is important because transport rates of material and energy from bodies placed in an otherwise uniform air stream are very sensitive to these parameters. Both of these properties of free stream turbulence have been measured by many workers, but there is great disagreement in the results obtained by these investigators.

It is proposed that beyond the point of maximum turbulence, (two to four meshwidths downstream of the turbulence grid), the apparent level of turbulence is correlated in terms of the ratio of downstream distance to the turbulence grid bar width. Correlations for the scale and microscale of turbulence relative to grid bar width showing the additional dependence on a Reynolds Number based on mesh width, (as the distance parameter), are also proposed.

Introduction

The turbulence produced by perforated plate and square mesh type turbulence grids has received a great deal of attention from many investigators principally because of the large and still not well documented effect of free stream turbulence on transport rates from cylinders, spheres, and other common body shapes. In this regard,

even low turbulence levels significantly affect heat and mass transport rates in flow situations involving a local pressure gradient (5, 10).

Of the parameters characterizing turbulence, the intensity or level of turbulence has received the most attention. Batchelor and Townsend (2, 3, 4) made a theoretical study of turbulent decay rates based on a two-dimensional model and the assumption of isotropy. They concluded that two distinct decay laws should apply, one for the limiting case where the viscous forces are negligible relative to inertial forces, and another, for the other extreme case where viscous forces are predominant. Their data taken to verify the theory conform approximately to the first decay law, but the agreement is not good. The Reynolds Number range of its general applicability was not determined, and the low turbulent energy law was not verified experimentally. Clearly, their theory in its present form is severely limited in its general utility.

Baines and Peterson (1) conducted an extensive investigation of the turbulence levels prevailing behind both perforated plate and square mesh type grids. They did not measure the microscale or the approach to isotropy for distances close to the grid relative to the mesh dimensions; however, their work has great merit because they were the only investigators who took data through the point of maximum turbulence and they obtained consistent results with a great variety of grid sizes and geometries. Their failure to document the flow Reynolds Number does not substantially affect the application of their results concerning the turbulence level, as will be appreciated later.

Dryden (7) measured the turbulence level for flow through a

mesh type grid. His data confirm the work of Baines and Peterson (1) over a limited range. He also did not measure the scale or microscale of turbulence. Hall (9) and Davis (6) took measurements over a limited range of downstream distances from the grid. Their data lie almost 50 per cent below the measurements of Baines (1) and Dryden (7) over a range of distances downstream of the grid from 20 to 1000 bar widths. However, the point of maximum turbulence intensity lies outside of this range, and most of the data is taken at low turbulence levels where the possibility of competition from residual wind tunnel turbulence is high. Davis (6) did measure the scale of turbulence and is the only investigator to measure the approach to isotropy.

Van der Hegge Zijnen (13) considered grid generated turbulence in some detail and took measurements which conform to the average of the above workers over most of his range of investigation. He also measured the scale and microscale of turbulence and is the only investigator, other than Batchelor and Townsend, to measure the latter parameter. In this regard, the microscale is important since it is indicative of the smallest eddy sizes and, along with the integral scale, serves to give some definition to the spectrum of eddy sizes.

There are other methods besides hot wire anemometry suggested for determining the turbulence level. One such method (8) correlates the turbulence level with the critical Reynolds Number for a sphere, which is determined by observing the trend of the drag coefficient with increasing Reynolds Number. Maisel and Sherwood (11) used the wake angle technique for determining the turbulence level for their studies on mass transfer rates. Thus far, however, these

approaches have proven to be of little value in studying the character of flow behind screens. Undoubtedly one of the inherent liabilities in using the observed critical Reynolds Number for a sphere to correlate turbulence intensity is that the flow around a solid object is affected by eddy size as well as by the intensity. Van der Hegge Zijnen (14) studied heat transfer from cylinders as a function of turbulence intensity and scale. His interpretation is included here as Figure 1, where the fraction increase in energy transport rates is shown as a function of these parameters. It suggests an inherent liability when a critical Reynolds Number approach is used to measure turbulence intensity without regard to the integral scale of turbulence.

Obviously much more work must be done to enable workers to predict the nature of turbulence generated behind turbulence grids. It is certainly a necessary step towards understanding and sometimes anomalous results obtained by different workers in different laboratories concerning the effects of turbulence on transport from spheres and cylinders, as well as from other more complex bodies (5, 10, 11, 12). In this work the best available data is used to deduce the effects of the many parameters influencing the character of grid generated turbulence. Correlations are proposed for the intensity, integral scale, microscale, and approach to isotropy as a function of distance downstream of the grid, the bar width, mesh width, and mesh Reynolds Number for both perforated plate and square mesh type grids.

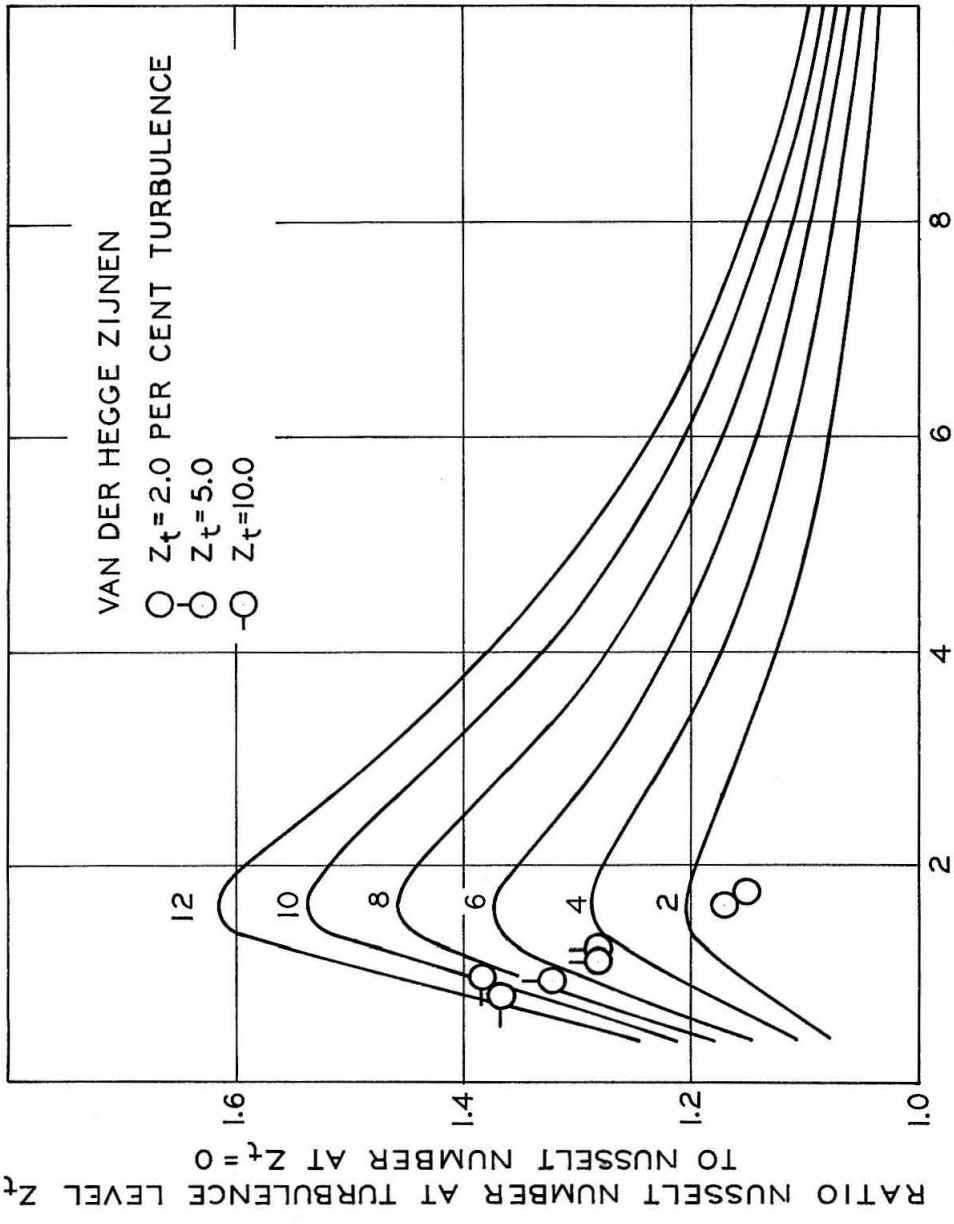

Fig. 1 Effect of Free Stream Turbulence Level and Turbulence Scale on Energy Transport from Cylinder

Discussion

In reviewing the various data available concerning grid generated turbulence it is immediately apparent that the relative intensity of turbulence produced by a perforated plate grid is substantially greater than the turbulence produced by a square Mesh grid having the same grid solidity (1, 6). The results of those investigations involving perforated plate grids are shown in Figure 2. It is seen that when the level of turbulence is plotted against the relative downstream distance referred to the mean "bar width," the curves for the various ratios of mesh width to bar width tend to coalesce as one proceeds downstream. In the case of perforated plate grids the "bar width" is equal to the bar width of a square mesh grid having the same mesh size and grid solidity.

Baines and Peterson (1) used a number of grids in their research ranging from 1.33 inches to 12 inches in mesh size and having solidities ranging from 0.23 to 0.89. They do not cite the Mesh Reynolds Numbers for their work, but it is probable that the Mesh Reynolds Number ranged from 15,000 to 135,000 since their wind tunnel was designed for work with free stream velocities up to 25 fps. Apparently they did not believe the effect of Mesh Reynolds Number on the free stream turbulence intensity was important, for this parameter was not documented. However, this parameter has a significant effect on the scale and microscale of grid produced turbulence, even though its effect on the turbulence level is minimal.

The results of various workers using a square mesh type

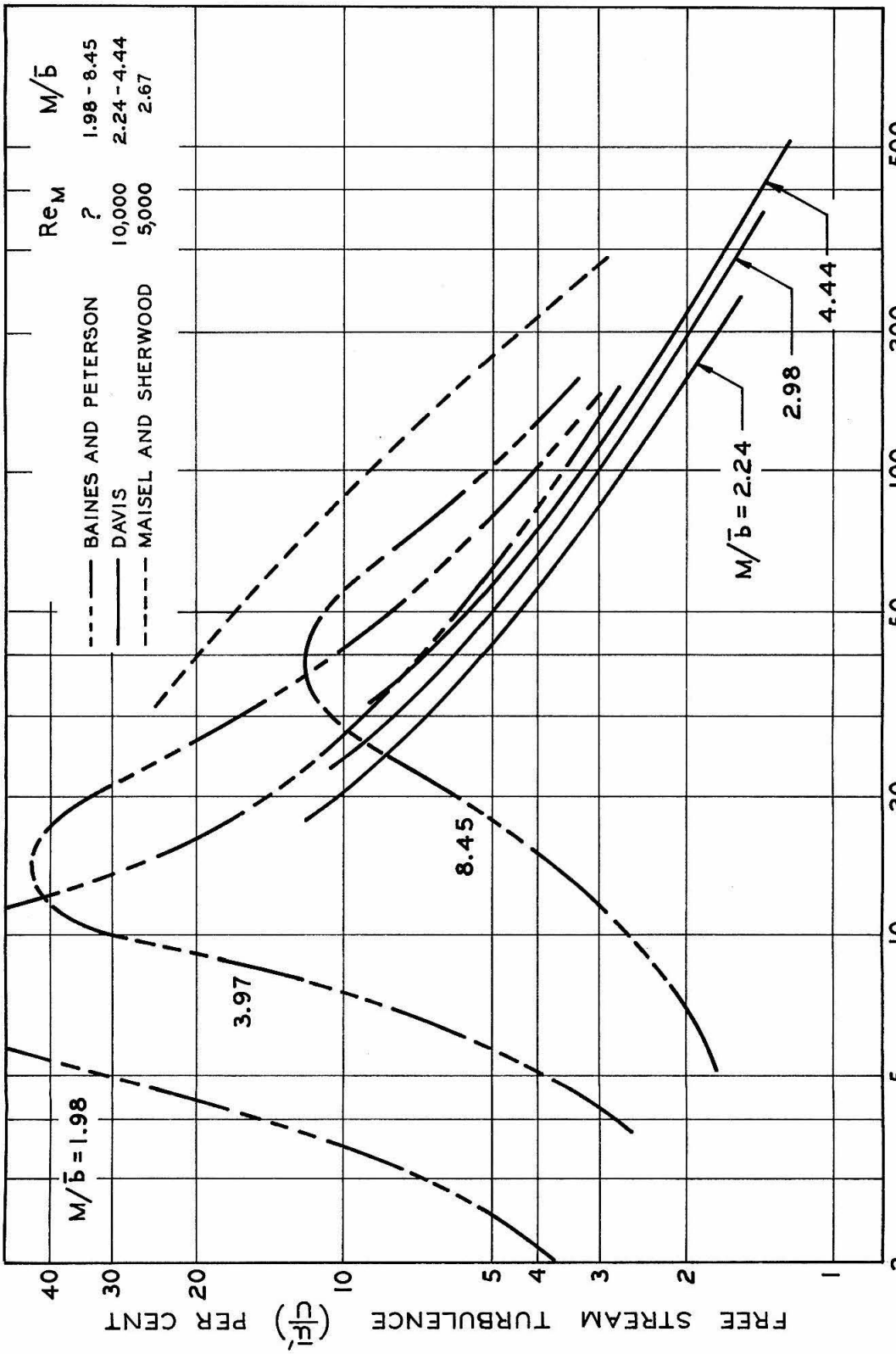

Fig. 2 Free Stream Turbulence Level Downstream of Perforated Plate Type Grid

turbulence grid are shown here in Figure 3. Representative data taken at a Mesh Reynolds Number of 10,000 were selected for this plot except for that of Baines, et al., (loc. cit.). It was desired to see how the results of the various workers compared on this common basis.

The effect of Mesh Reynolds Numbers on the intensity of grid produced turbulence appears to be negligible. The results of Davis (6) for both perforated plate and square mesh grids are shown in Figure 4, and a slight decrease in intensity with increasing Mesh Reynolds Number is indicated. The results of Batchelor and Townsend (2, 3, 4) appear in Figure 5, and their findings, except for the crossover at a Mesh Reynolds Number of 656, are similar. Van der Hegge Zijnen (13) also determined that the intensity of turbulence tended to decrease with increasing Mesh Reynolds Number. However Dryden (8) states that the intensity of turbulence over a range of Mesh Reynolds Numbers from 2,400 to 175,000 does not depend upon either U or Re_M, and Hall (9) determined that the intensity of turbulence increases with Re_M. Further Baines and Peterson (loc. cit.) find that their data taken using similar grids over a ninefold range of sizes are well correlated by a single curve downstream of the point of maximum turbulence intensity.

In view of the above uncertainty between various workers, it can be asserted that the effect of Mesh Reynolds Numbers on grid produced turbulence is small, and with this in mind Figure 6 and Figure 7 are proposed, correlating the turbulence level prevailing

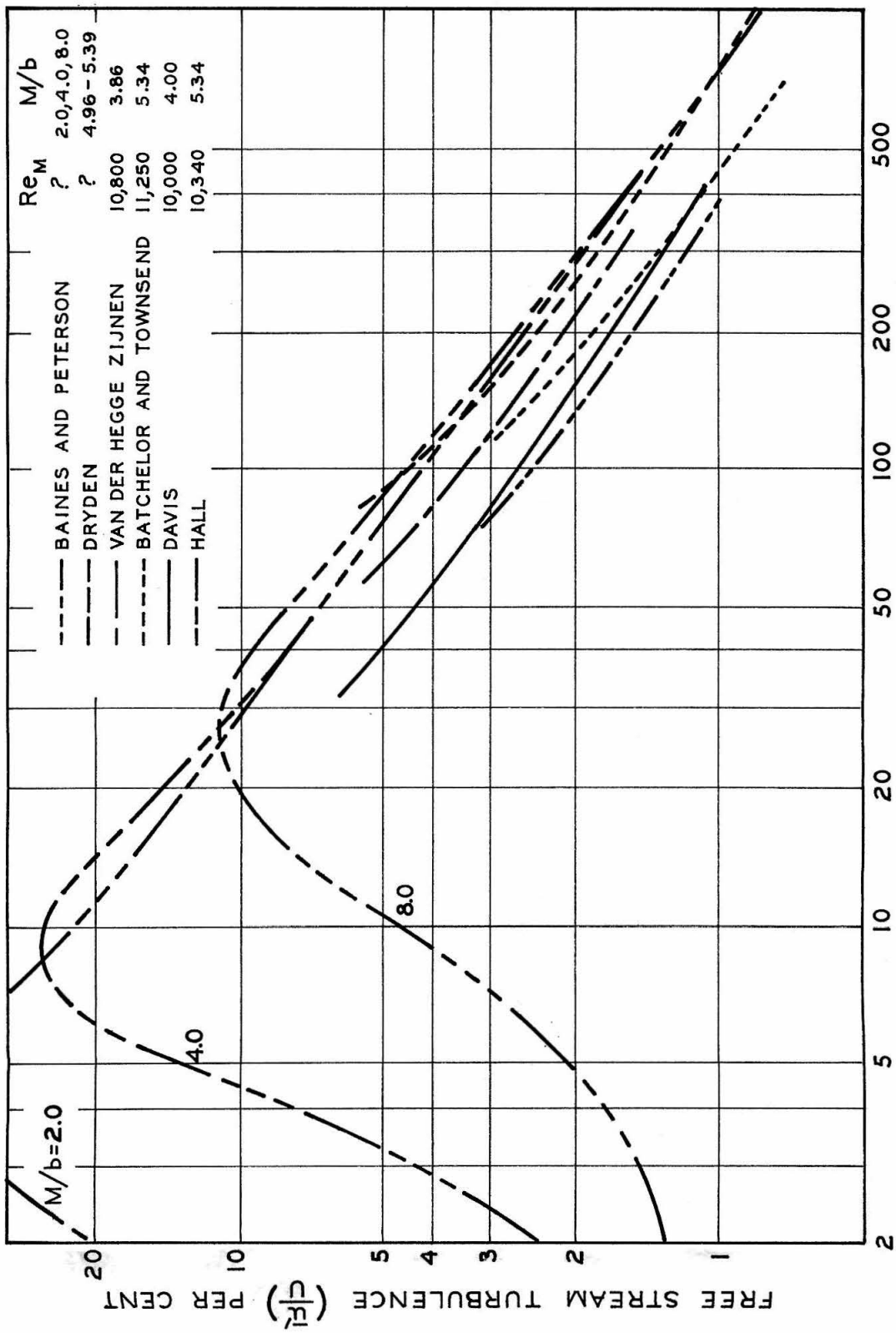

Fig. 3 Free Stream Turbulence Level Downstream of Square Mesh Type Grids

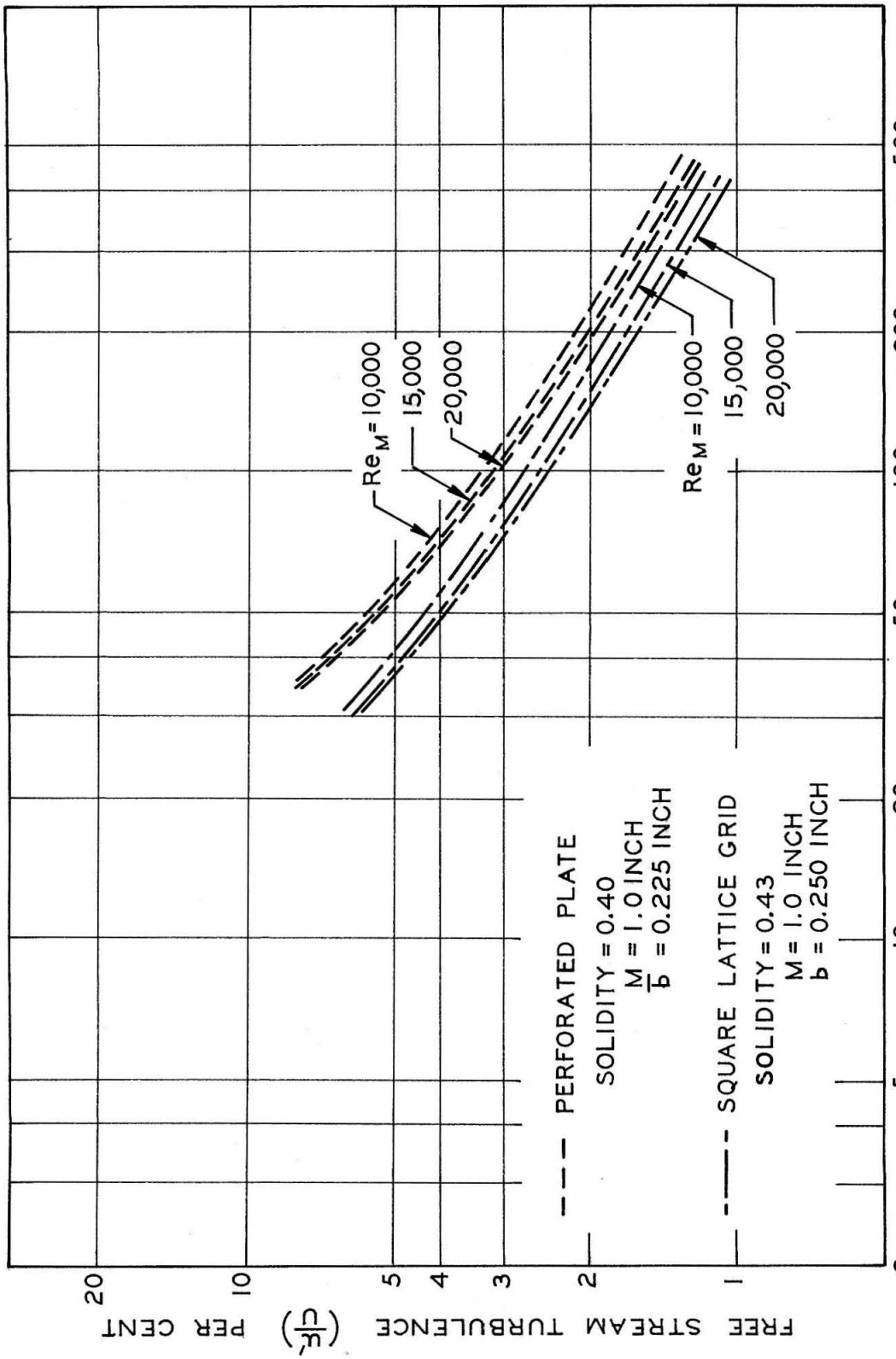

Fig. 4 Effect of Mesh Reynolds Number on Level of Turbulence Generated Downstream of Turbulence Grids - Davis (6)

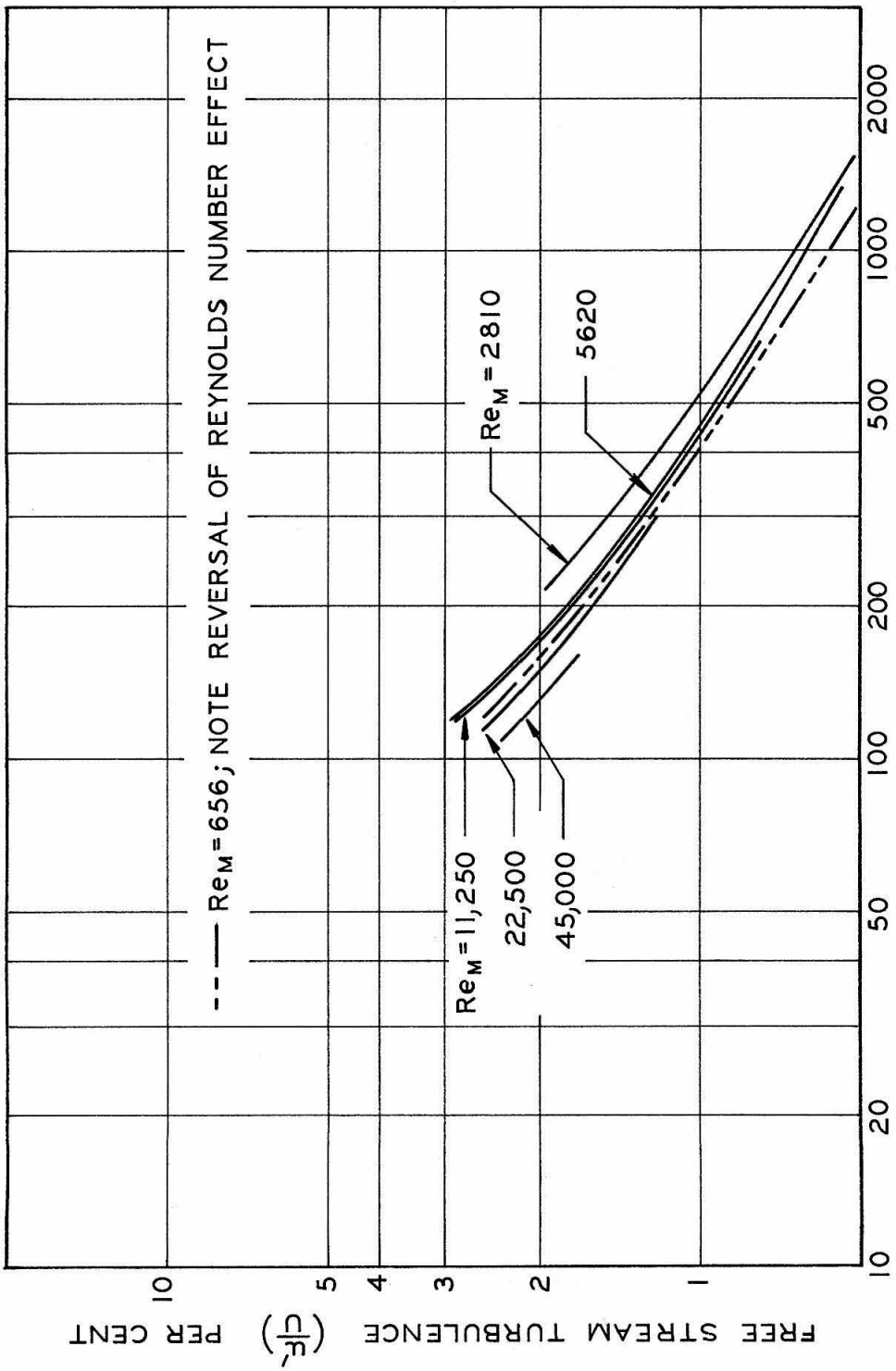

Fig. 5 Effect of Mesh Reynolds Number on Level of Turbulence Generated Downstream of Turbulence Grids - Batchelor and Townsend (2, 3, 4)

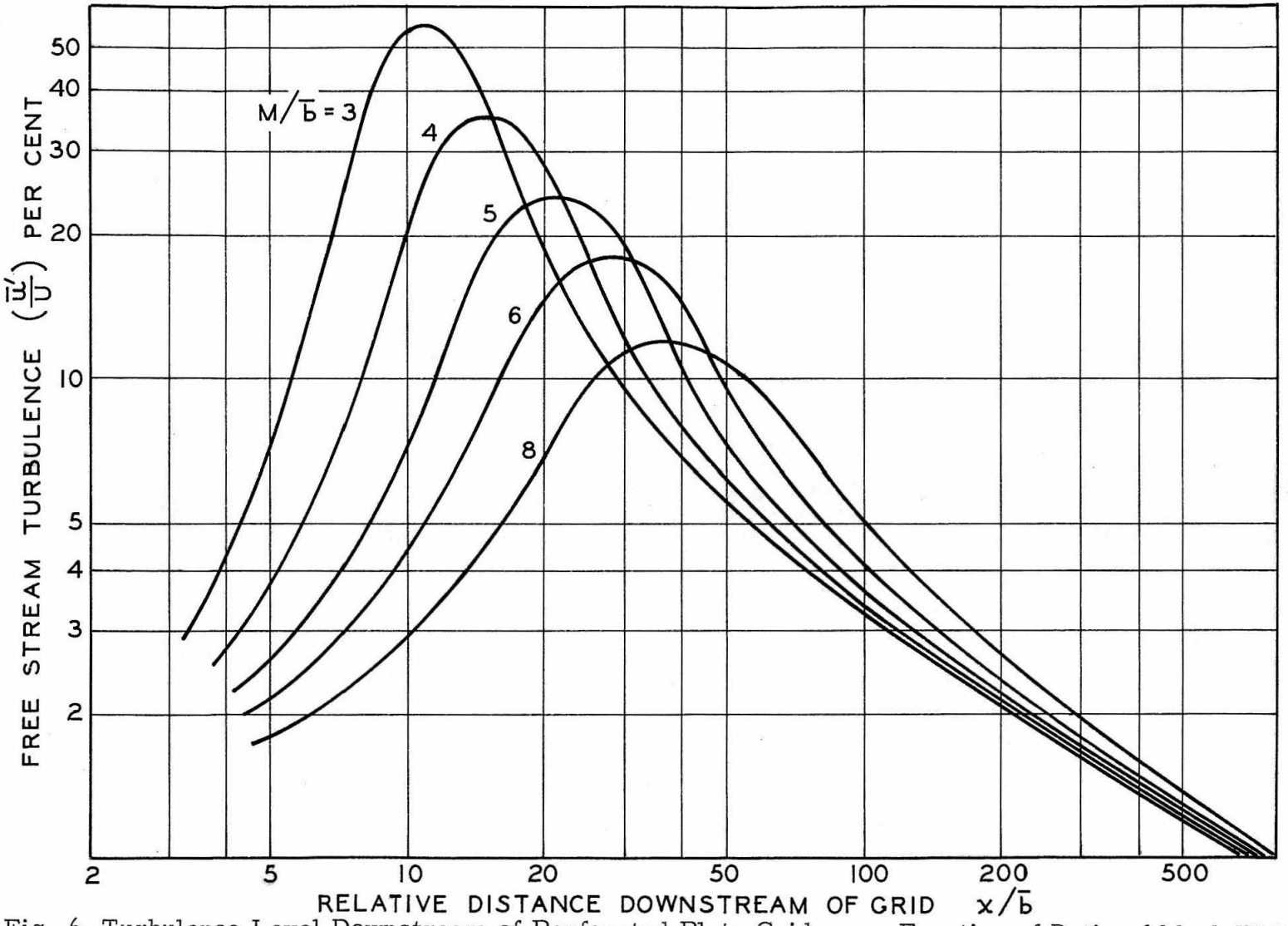

Fig. 6 Turbulence Level Downstream of Perforated Plate Grids as a Function of Ratio of Mesh Width to Bar Width

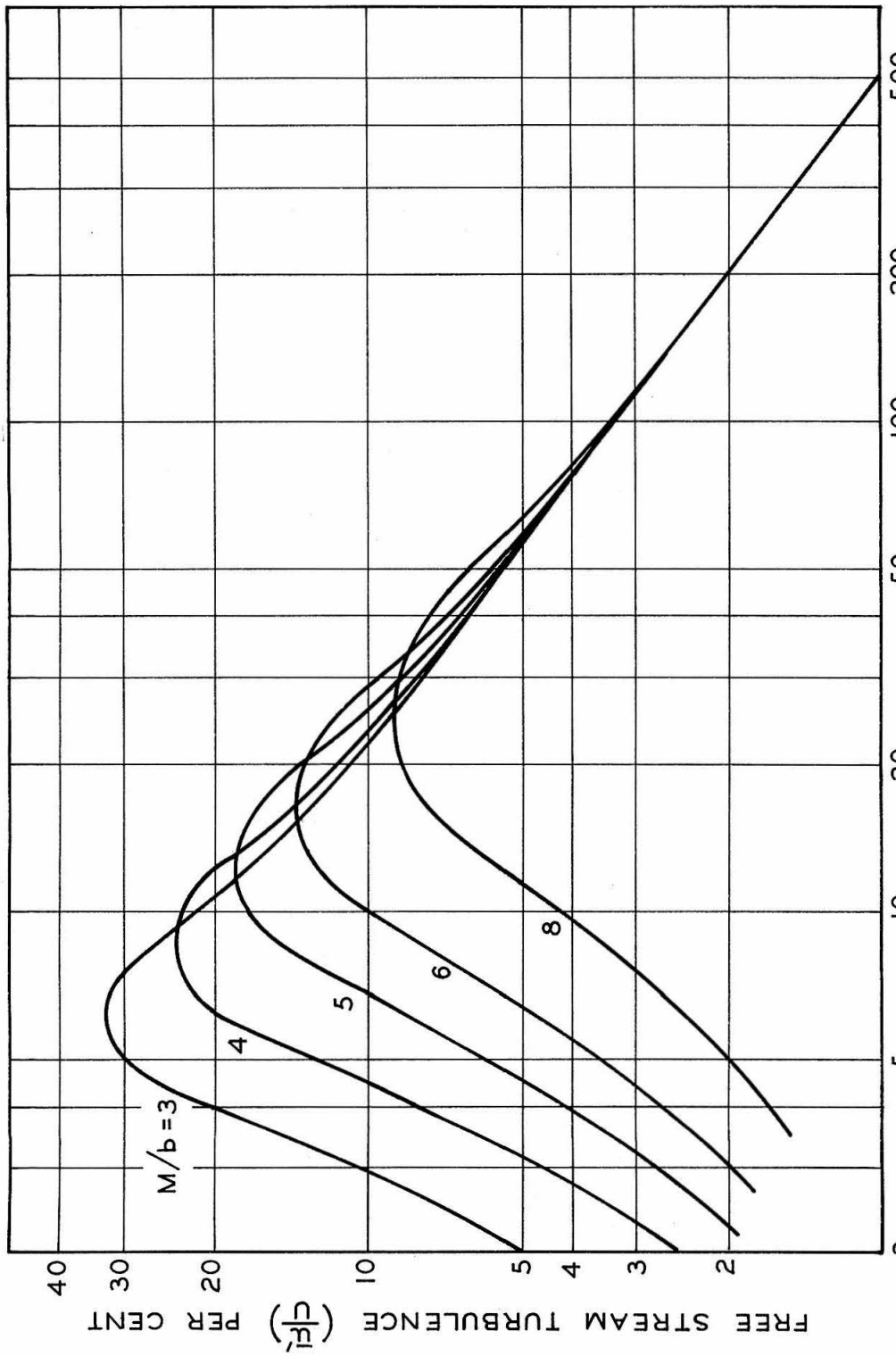

Fig. 7 Turbulence Level Downstream of Square Mesh Type Grids as a Function of Ratio of Mesh Width to Bar Width

downstream of perforated plate and square mesh type grids respectively as a function of downstream distance and the ratio of mesh width to bar width.

In arriving at these curves the work of Baines and Peterson (loc. cit.) was relied on heavily for distances close to the grid because of the absence of other data in this region. In Figure 6 for the perforated plate grids the curves were brought into the data of Davis for relative distances downstream of the grid greater than 100. In Figure 7 the curves were drawn through a mean of the other workers data further from the grid. Preference was given to the data of Baines and Peterson in the region of the onset of "isotropic decay" because of the great size of their grids. In this regard it will subsequently be shown that the microscale of the turbulence, (a dimension roughly proportional to the size of the smallest eddies), increases with the square root of distance downstream of the grid. This is significant because as one approaches the grid the resolution of individual eddies with a hot wire anemometer becomes increasingly difficult due to the decreasing mean eddy size. Hence the data which would be most reliable in this region would be those where the ratio of wire size to mesh size is smallest. Referring again to Figure 3 it will be appreciated that the only other investigator working with comparable sized grids, Dryden (8), obtained data which is more in agreement with Baines et al., than with the results of other workers. Finally, because the effect of the Mesh Reynolds Number above is certainly small, Figures 6 and 7 are

recommended as being independent of this parameter, although it will be subsequently demonstrated that this independence of Mesh Reynolds Number cannot be expected to apply for Reynolds Numbers much less than 5,000.

Pertinent data on the size of the wires used by various investigators are presented in Table I. In this Table can be found the wire length, L, the wire diameter, D, the length to diameter ratio, L/D, and the ratio of mesh size to wire length, which is mentioned above as being one possible criterion in assessing the relative merit of the various data available for distances close to the turbulence grid.

In reviewing the trend of intensity of turbulence with increasing Reynolds Number, as illustrated in Figures 4 and 5, the effect of this parameter appears more pronounced at the lower levels of turbulence. However, at these relatively low levels of intensity, one may question the validity of the trends found because of the possible effect of residual free stream turbulence on these data. Certainly it is unlikely that the residual turbulence, (that which would be present without the turbulence grid in place), would remain unchanged with increasing bulk flow through the test duct, but the direction and magnitude of this change is uncertain. Van der Hegge Zijnen (loc. cit.) points out that the two turbulent motions would not maintain their individual character, and hence the effects of residual free stream turbulence cannot easily be separated out. Because of this additional complication the observations of

Table I

Wire Sizes Employed by Various Investigators in Turbulence Measurements Downstream of Turbulence Generating Grids

Author	Wire Size			Ratio of Wire Length to Mesh Size
	Length inches	Diameter inches	L/D	
Baines and Peterson (1)	0.10	0.00031	300	13.3 - 120.0
Batchelor and Townsend (2,3,4)	~0.04	0.0001	~400	~6.3 - 50.0
Davis (6)	0.1 ?	0.0001	1000	10
Dryden et al. (8)	0.2	0.0002	1000	1.2 - 25.0
Hall (9)	0.05	0.0001	500	10.0 - 40.0
Maisel and Sherwood (11)	0.1 ?	0.0001	1000 ?	1.7 - 7.0
Van der Hegge Zijnen (13)	0.05	0.00012	430	20.7 - 62.0

Batchelor and Townsend (2, 3, 4), and Davis (6) regarding the effect of Mesh Reynolds Number at low levels of turbulence are viewed with some skepticism. In the absence of additional data it would be difficult to establish a minimum Reynolds Number above which one could expect turbulence level to be independent of this parameter.

Scale of Turbulence

The scale of turbulence is not so easily correlated by a single series of curves. Referring to the data of various workers appearing here in Figure 8 it is apparent that the relative scale of turbulence, referred to bar width, is not only a rather strong function of distance downstream of the grid, but is influenced by the ratio of Mesh width to bar width. At the same time the relative scale of turbulence for constant grid solidity, varies somewhat less rapidly than the inverse square root of the Mesh Reynolds Number. Inspection of these data reveal that the scale of turbulence for a constant mesh size decrease approximately as the 0.4 power of the Mesh Reynolds Number. Figure 9 is obtained by separating out the Reynolds Number dependence of the integral scale, and interpolating from the various data to obtain the dependence on the ratio of mesh size to bar width.

Of the referenced work, only Baines and Peterson have measured the integral scale of turbulence behind perforated plate grids. A review of their data indicates that there is no essential difference in the scale of turbulence derived from a perforated

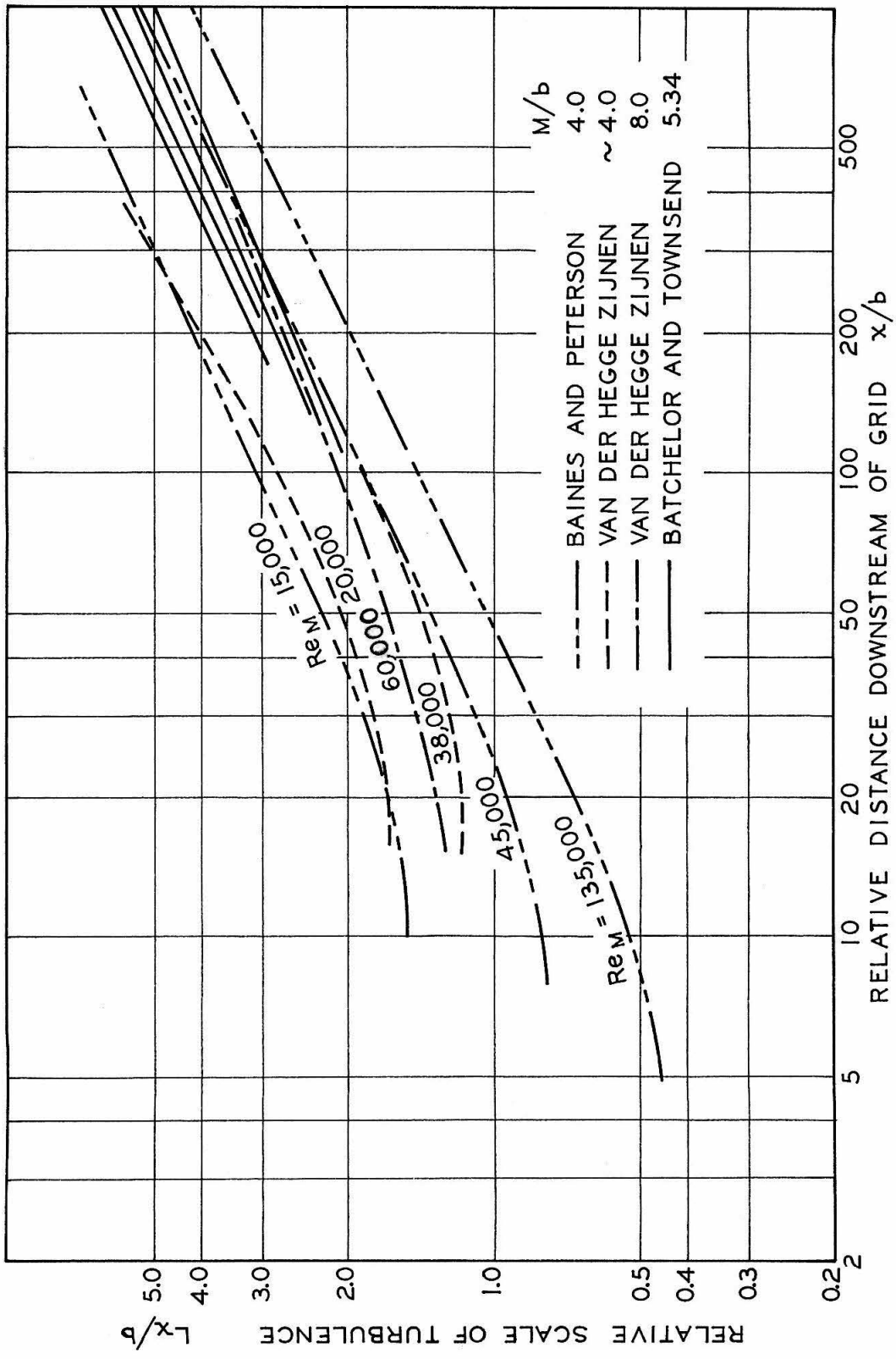

Fig. 8 Scale of Turbulence Downstream of Turbulence Grids

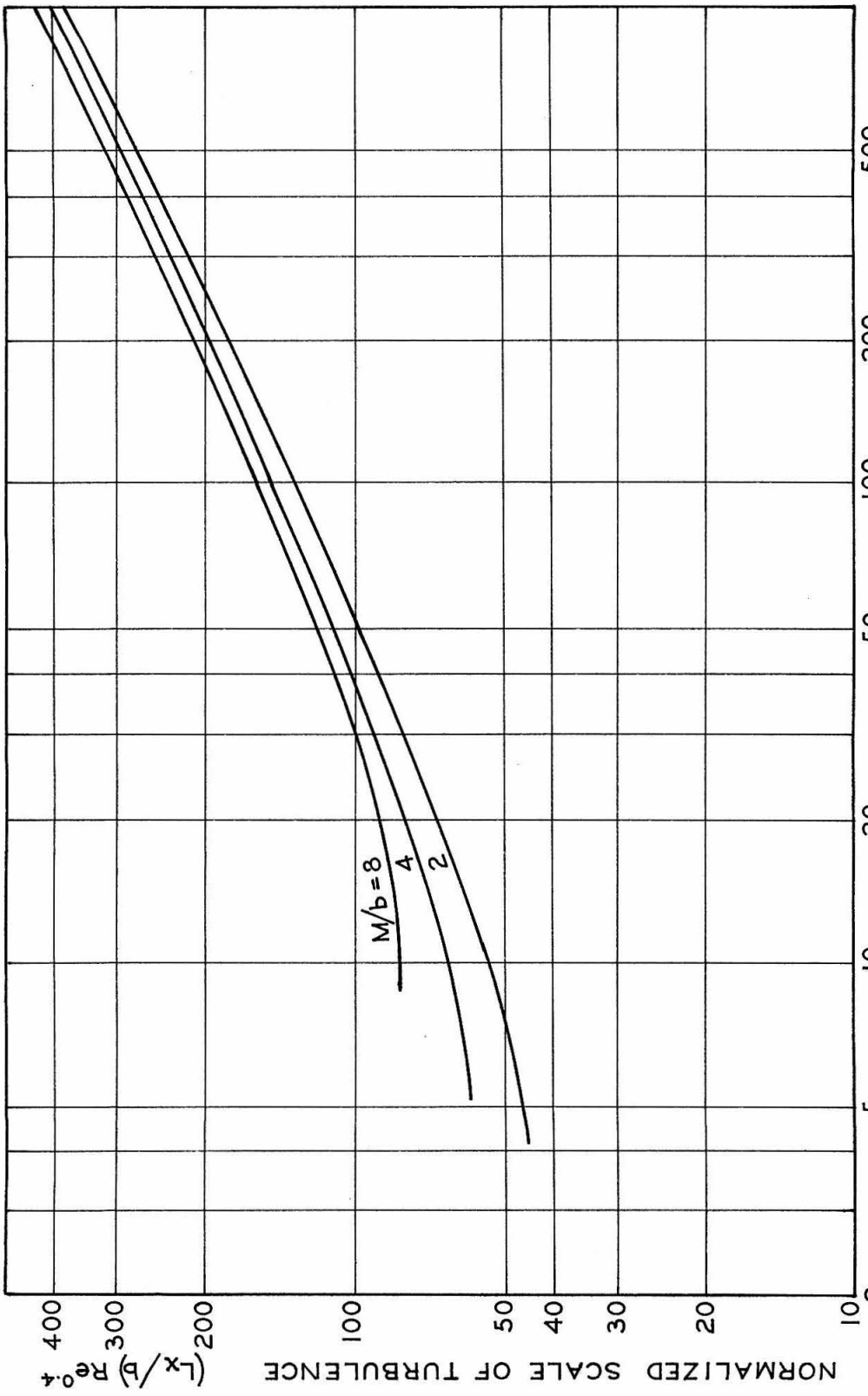

Fig. 9 Scale of Turbulence - Correlation With 0.4 Power Reynolds Number

plate grid as opposed to a square mesh grid. In view of these findings Figure 9 is presented for both types of grids.

The correlation proposed in Figure 9 can be viewed with some uncertainty concerning the effect of the ratio M/b, but the Reynolds Number dependency appears quite reliable. Certainly the exponent is much closer to 0.4 than to either 0.3 or 0.5 based on the work of Baines and Peterson (loc. cit.) and Van der Hegge Zijnen (13). The data of Batchelor and Townsend taken at a Reynolds Number of 22,000 fit the proposed correlation remarkably well, but fall 30 and 50 per cent below the proposed curve for Reynolds Numbers of 11,000 and 5,500 respectively. This may be an indication of the minimum Reynolds Number below which the proposed correlations fail, but more probably arises from the competition of residual turbulence caused by flow through the duct. In this regard it will be noted the microscale of turbulence is well correlated by an inverse square root Mesh Reynolds Number dependency, and that the data of Batchelor and Townsend (2, 3, 4) for the microscale continue to conform to this correlation down to a Mesh Reynolds Number of 2,800. Since it is anticipated that the smallest eddies, as represented by the microscale, would be the first ones to be affected by the viscous decay law, and that this type of decay is not apparent from their measurements of the microscale, it is doubtful that the deviation of their measurements of the integral scale at the lower Reynolds Numbers from the data of others carries any real significance.

Finally bearing on the possibility of competition from residual tunnel turbulence it is noted that Maisel and Sherwood (11) investigated the intensity and scale turbulence produced behind two perforated plate grids. Their data on the intensity of turbulence appear in Figure 3, but were omitted from Figure 8 because their measurements indicated that the relative scale of turbulence decreased with increasing downstream distance, a trend which is not only contrary to the results of the other workers cited above, but which is also contrary to all practical considerations, (for the scale to decrease with increasing distance downstream of the turbulence grid it would be required that the larger eddies decay before the smallest eddies). Equally in Figure 3 their data appear somewhat untoward. These anomalies can be explained by reference to their experimental design. Their data were taken in a pipe whose inside diameter is 10.2 cm., causing a free stream turbulence level (without the grids) as indicated by their measurements of 3.2 per cent. It seems evident that the effects of the grid produced turbulence in their work were obscured by the normal pipe turbulence caused by friction at the walls, and hence their data were not used in this work. This observation indicates that the measured trends of the turbulent scale appearing in Figure 8 would become less reliable with increasing downstream distance, and in particular that this same effect might be the cause of the relatively low scale of turbulence observed by Batchelor and Townsend at the lower Reynolds Numbers.

Microscale of Turbulence

The microscale of turbulence is a parameter which is related to the size of the smallest eddies. The microscale of turbulence is important in that it along with the scale of turbulence gives definition to the spectrum of eddy sizes.

Apparently the microscale of grid produced turbulence has thus far been measured only by Batchelor and Townsend (2, 3, 4) and by Van der Hegge Zijnan (13). Their data appear here in Figure 10. In Figure 11 the microscale of turbulence is correlated against downstream distance by forming its product with the square root of the Mesh Reynolds Number. Perhaps this Reynolds Number is the wrong parameter for correlating microscale, since one would expect the size of the smallest eddies to be much more dependent on bar size than on mesh size, but the correlation becomes worse with this approach. In any case the microscale of turbulence is not well documented, and the extrapolation is obtained by noting its dependence on the inverse one-half power of velocity, (for constant mesh size), and hence of decay time, which is, in turn, also proportional to downstream distance. With the available data there is no way of knowing how much the correlation of microscale would be affected by conditions of non-isotropy which become increasingly pronounced as one approaches the grid. Also it is assumed here that the microscale of turbulence produced by perforated plate grids is the same as for square mesh grids of similar mesh size; such may not be the case.

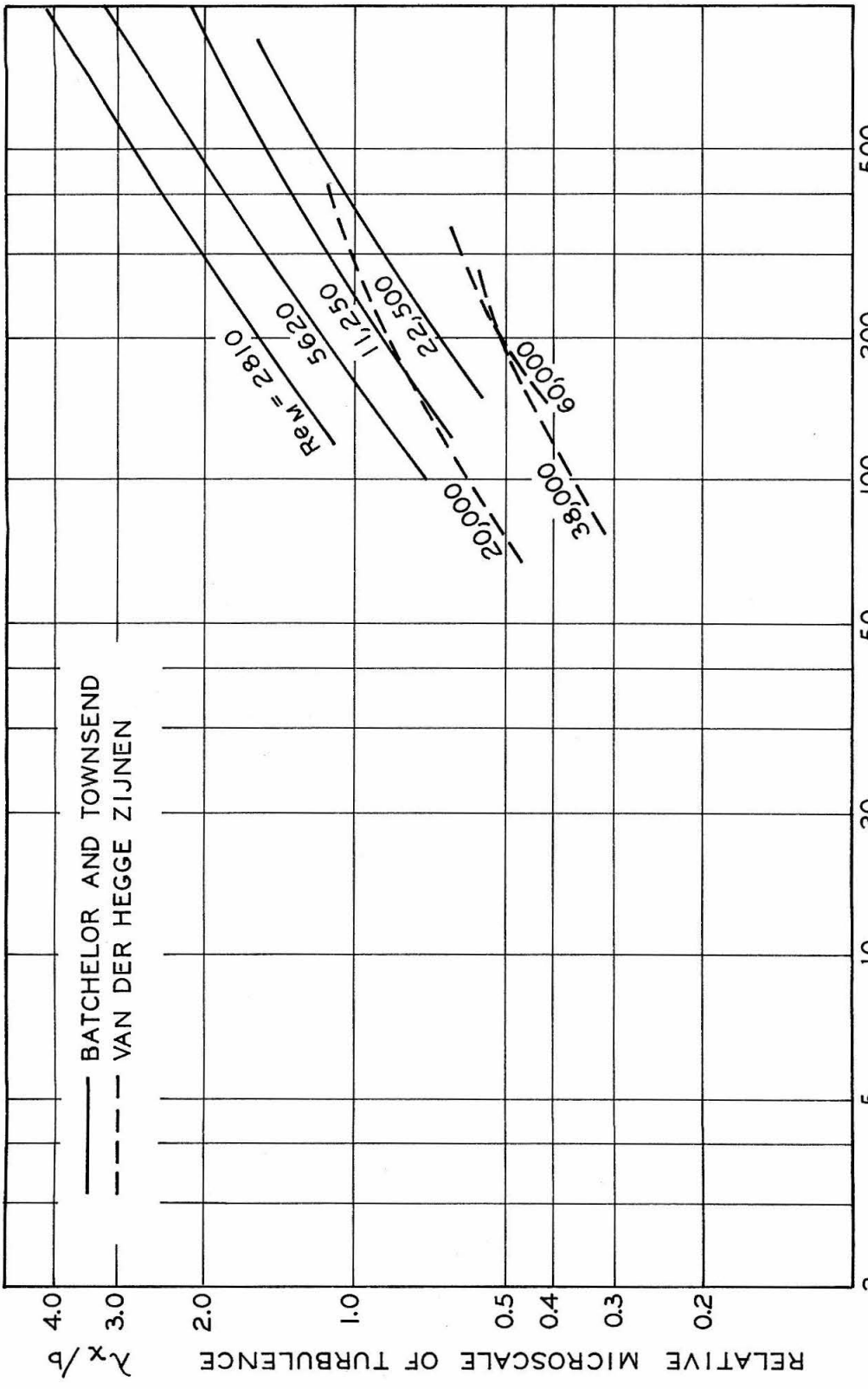

Fig. 10 Microscale of Turbulence Downstream of Turbulence Grids

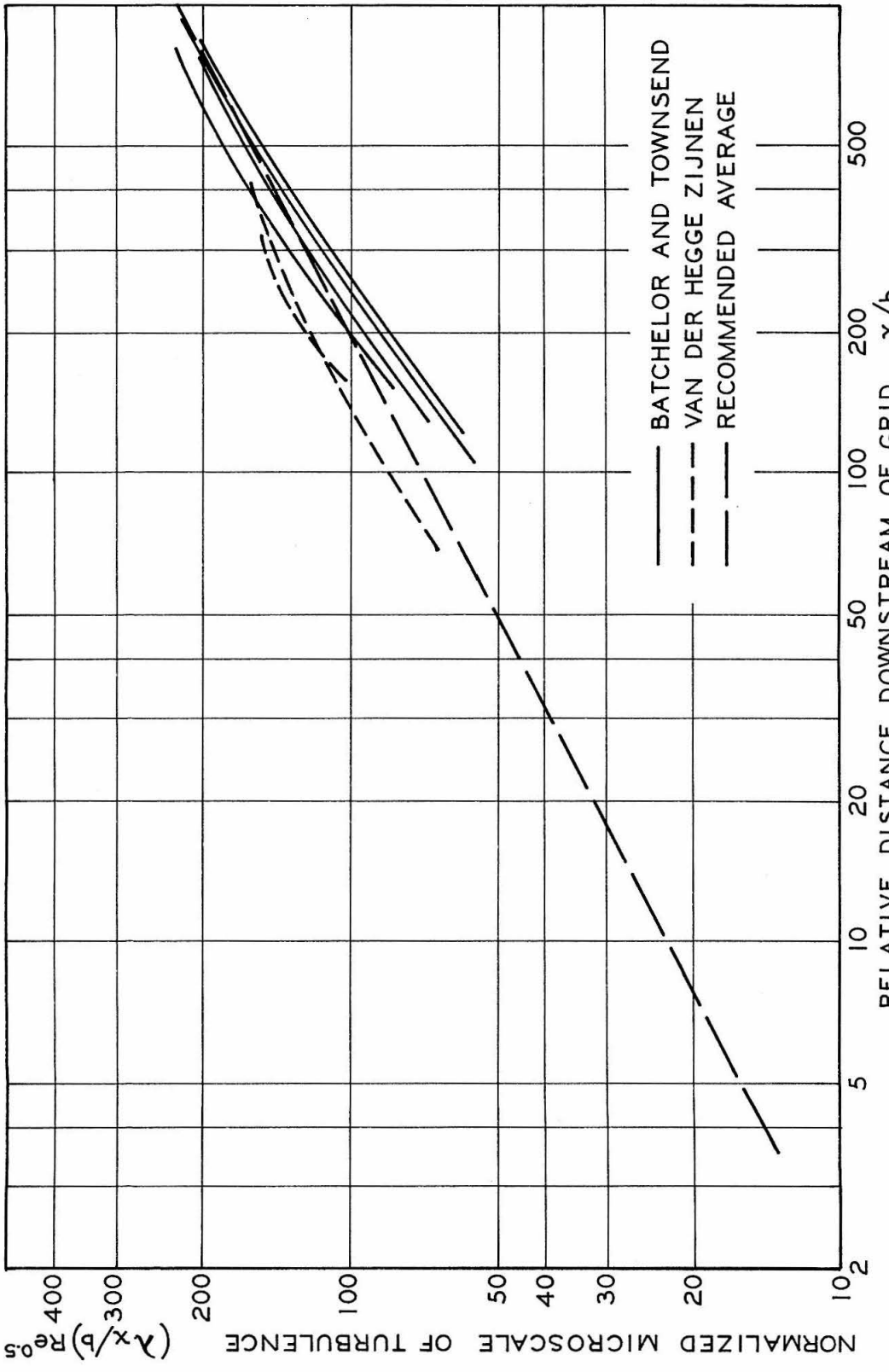

Fig. 11 Microscale of Turbulence - Correlation With 0.5 Power Reynolds Number

Approach to Isotropy

Davis (6) is the only worker who investigated the magnitude of the normal fluctuating velocity component, v' turbulence, relative to the tangential fluctuating velocity component. His data indicate that the two fluctuating velocity components are within 3 per cent of each other 100 bar widths downstream of the grid, although the normal component was always less for both perforated plate and square mesh grids. Unfortunately his data do not cover a range of grid solidities nor do they extend far enough upstream to establish the degree of non-isotropy close to the grid. His data do indicate however that turbulence conditions which are very nearly isotropic are established 100 bar widths downstream of either a perforated plate or square mesh type grid.

Conclusions

Correlations are proposed and presented in graphical form for the level of turbulence, scale and microscale of turbulence, and the approach to isotropy for turbulence generated by perforated plate and square mesh type turbulence grids. The following conclusions concerning the nature of grid generated turbulence can be drawn:

1) For Reynolds Numbers based on mesh width greater than 5,000, the intensity of turbulence produced downstream of a turbulence grid is independent of the Mesh Reynolds Number. Moreover the intensity or level of turbulence is well correlated in terms of downstream distance referred to bar size, and once complete jet mixing is established, 100 bar widths downstream, the intensity for both perforated plate and square mesh grids is relatively independent of grid solidity.

2) The maximum intensity of turbulence occurs from two to four mesh widths downstream of the grid and is roughly proportional, in magnitude, to the ratio of bar width to mesh width.

3) Work with grids having solidities greater than 0.5 is not recommended because of the tendency for uneveness and time dependency of the mean flow through individual meshes. This uneveness is certified by Baines et al., (1) and Davis (6).

4) Turbulence levels attained from perforated plate grids are higher than those achieved with mesh type grids of comparable grid solidity because of the "vena contracta" effect associated with

flow through the individual orifices leading to higher local velocities and a more intense mixing process.

5) The scale and microscale of turbulence both decrease rapidly with increasing Mesh Reynolds Number. The integral scale of turbulence downstream of a turbulence grid decreases approximately as the 0.4 power of the Reynolds Number, while for the microscale the decrease is proportional to the 0.5 power of the Mesh Reynolds group. The integral scale of turbulence, referred to bar width, is a mild function of grid solidity or of the ratio of mesh width to bar widths, while the microscale seems to be independent of this parameter. Finally both integral scale and microscale increase approximately as the square root of downstream distance.

6) The approach to isotropy has been measured only by Davis (6). His results indicate that the turbulence prevailing more than 100 bar widths downstream of a turbulent grid is very nearly isotropic. Unfortunately his results do not reveal how far from isotropy the turbulence is at the point of maximum intensity.

7) Displacements in the mean velocity profile(due to the incomplete mixing of individual jets with the wakes formed behind solid portions of the turbulence grid)persist up to somewhere between 5 and 8 mesh widths downstream of the turbulence grids. The maximum turbulence level is attained somewhat upstream of this region, and for all practical purposes an investigator operating downstream of the point of maximum intensity of turbulence will encounter a substantially uniform mean velocity profile.

Literature Cited

1. Baines, W. D., and Peterson, E. G., "An Investigation of Flow Through Screens," Transactions of the ASME, Vol. 73, p. 467-480 (1951).

2. Batchelor, G. K., and Townsend, A. A., "Decay of Vorticity in Isotropic Turbulence," Proceedings of the Royal Society of London, Series A, Vol. 190, pp. 534-550 (1947).

3. Batchelor, G. K. and Townsend, A. A., "Decay of Isotropic Turbulence in the Initial Period," Proceedings of the Royal Society of London, Series A, Vol. 193, pp. 539-558 (1948).

4. Batchelor, G. K., and Townsend, A. A., "Decay of Turbulence in the Final Period," Proceedings of the Royal Society of London, Series A, Vol. 194, pp. 527-543 (1948).

5. Büyüktür, A. R., Kestin, J., and Maechr, P. F., "Influence of Combined Pressure Gradient and Turbulence on the Transfer of Heat from a Plate," International Journal of Heat and Mass Transfer, Vol. 7, pp. 1175-1185 (1946).

6. Davis, L., "Measurements of Turbulence Decay and Turbulent Spectra Behind Grids," Jet Propulsion Laboratory Report 3-17, California Institute of Technology, Pasadena, Calif., June 5 (1962).

7. Dryden, H. L., and Schubauer, G. B., "The Use of Damping Screens for the Reduction of Wind Tunnel Turbulence," Journal of the Aeronautical Sciences, Vol. 14, No. 4, pp. 221-228 (1947).

8. Dryden, H. L., Schubauer, G. B., Mock, W. C., and Scramstad, H. K., "Measurements of Intensity and Scale of Wind Tunnel Turbulence and Their Relation to the Critical Reynolds Number of Spheres," NACA Rep. No. 581 (1937).

9. Hall, A. A., "Measurements of the Intensity and Scale of Turbulence," Aeronautical Research Comm. Rep. and Memoranda, No. 1842, London (1938).

10. Kestin, J., and Maeder, P. F., "Influence of Turbulence on Transfer of Heat from Cylinders," NACA TN 4018 (1954).

11. Maisel, D. S. and Sherwood, T. K., "Effect of Air Turbulence on Rate of Evaporation of Water," Chemical Engineering Progress, Vol. 46, pp. 172-175 (April 31, 1950).

12. Schliching, H., Boundary Layer Theory, 4th Ed., McGraw-Hill, New York, (1960).

13. Van der Hegge Zijnen, B. G., "Measurements of the Intensity, Integral Scale, and Microscale of Turbulence Downstream of Three Grids in a Stream of Air," Applied Science Research, Section A Vol. 7, pp. 149-174 (1957).

14. Van der Hegge Zijnen, B. G., "Heat Transfer from Horizontal Cylinders to a Turbulent Air Flow," Applied Science Research, Section A Vol. 7, pp. 205-222 (1958).